Negative Modes in Vacuum Decay

Hak Joon Lee

Submitted in partial fulfillment of the
requirements for the degree
of Doctor of Philosophy
in the Graduate School of Arts and Sciences

COLUMBIA UNIVERSITY

2014

ABSTRACT

Negative Modes in Vacuum Decay

Hak Joon Lee

A vacuum, a classically stable state, can decay to another vacuum by virtue of quantum tunneling. Although vacuum decay is an interesting topic itself in field theory, when it combines with gravity, it has wider applications and plays an essential role to understand the very early universe. The semi-classical solution of vacuum decay is well-described by the WKB approximation both in flat space and in curved space. Meanwhile, if we consider the configuration space of fields, we encounter many kinds of problems related with gravitational fields since the mode spectrum in curved space turns out to have an infinite number of negative modes in a de Sitter background. Despite of infinitely many negative modes, the regime in the weak gravity limit can be smoothly connected to flat space. To understand this, I discuss the nature of vacuum decay and various topics about negative modes in this thesis.

Table of Contents

List of Figures

List of Tables

Acknowledgments

First of all, I deeply thank to my advisor Professor Erick J. Weinberg for his advice, mentorship, support, inspiration and friendship. He has constantly encouraged and supported me during my whole PhD program. I can hardly imagine that I could complete this thesis without his helps. It is hard to describe his enormous works in field theory and cosmology with a few words. Nevertheless, what impresses me most about him is his perfect personality. I truly respect him not only as a physicist but also as a person.

I am grateful to Professor Robert Mahwhinney, Alfred Mueller, Alberto Nicolas and Eduardo Ponton for the classes that helped me get into various topics in theoretical high energy physics, and I thank to Professor Norman Christ for advising Lattice QCD in the first summer at Columbia. I am thankful to Professor Piljin Yi and Kimyeong Lee for their hospitality at KIAS when I visited my hometown every summer.

I thank to Lalla Grimes and Randy Torres for their essential helps.

I thank to Ali Masoumi, Xiao Xiao and Adam Brown for their friendships and discussions as academic brothers. I also want to thank to Kiyohito Iigaya, Taehyun Yoon and Seyoung Park for their friendships in the department. Outside Columbia physics department, I am thankful to my old friends, Hongsik Kim, Sanggeol Koh, Andrew Ahn and Jaehyun Cho, who have shared with all the satisfactions and have overcome together all the difficulties in PhD progress.

I thank to the most important people in my life, my father Yongsik Lee, my mother Minjung Kim, my brother Hakseung Lee and my sister-in-law Sunyoung Choi. They have never tired of advising and cheering me up. It is really hard to express their endless love and support in this short acknowledgement. I also thank to my lovely little cousin, Minkyung Kim, who studies at the same campus. Last but not least, I even don't know who she is and whether I ever met her or not. I would like to thank to my future wife already and I hope to share with her all the experiences in my PhD program when I recognize her. This thesis is dedicated to all my family.

To All My Family

Chapter 1

Introduction

Quantum tunneling is one of the most significant phenomena predicted by quantum physics. It has enormous numbers of applications to many areas and it has been one of the keystones in building up modern science and technology. In theoretical physics, quantum tunneling is a somewhat old-fashioned subject but, by virtue of quantum field theory, it can be turned into the vacuum decay problem and it has been studied over the last few decades. The vacuum decay problem in the presence of gravity has to be described in terms of quantum gravity which still has not been understood completely. Furthermore, the vacuum decay in gravity becomes more interesting and has wider applications in cosmology because it helps us to understand the very early universe and is related to inflationary models[1–3].

The vacuum decay process was first studied by Coleman[4]. In field theory, a vacuum is a classically stable state on a potential. If a field is located on a stable point, it stays there forever. On the contrary, it may not be stable anymore in quantum mechanics and may decay to another vacuum. This unstable vacuum is a so-called 'false vacuum' and the vacuum that the field on the false vacuum tunnels to is called 'true vacuum', as shown in Figure 1.1. As a consequence of vacuum tunneling, a bubble of the true vacuum is formed in the background of the false vacuum. The size of the bubble is determined by the ratio of the tension of the wall and the energy difference between two vacua.

To describe vacuum decay, we need to find a classical path from the false vacuum to the true vacuum on the potential. At a glance, there are no well-defined paths on the region where the potential is larger than the energy of the system because this is a classically forbidden region

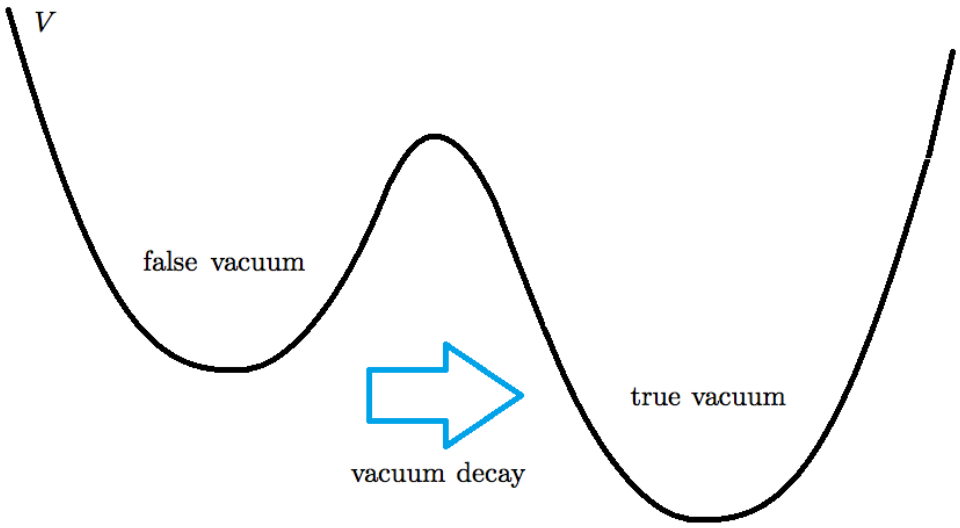

Figure 1.1: A false vacuum and a true vacuum.

because of energy conservation. However, if we can define a negative kinetic energy or reverse the potential 'V' to '$-V$', it is possible to find a classical path in a classically forbidden region. If a Euclidean spacetime is constructed by the analytic continuation ($\tau = it$), then the potential 'V' effectively behaves as a reversed one '$-V$' in a Euclidean spacetime as in Figure 1.2. We can find a classical path in a Euclidean spacetime by using the WKB approximation. This also gives the decay rate. This solution is called a 'bounce' and a bounce solution is a saddle point of the Euclidean action. When a vacuum bubble is nucleated in real spacetime, the bounce solution gives the initial value of the evolution of the bubble.

After finding the classical path, eigenmodes are obtained by investigating perturbative expansions around the path. The false vacuum state is unstable and it can tunnel to the true vacuum state through the channel governed by a negative mode. If we treat it as if it is a stationary point despite of the instability, the energy of the false vacuum becomes a complex number due to a negative mode. The energy is shifted by an imaginary number and the imaginary number gives us the decay rate per unit volume. A negative mode must exist not only to explain the instability of the state physically but also to give the factor of i that gives an imaginary part of the energy.[5]

On the other hand, by oscillating the path rapidly around the classical path with small amplitudes, the kinetic term can increase as much as possible. This means it is possible to find as many

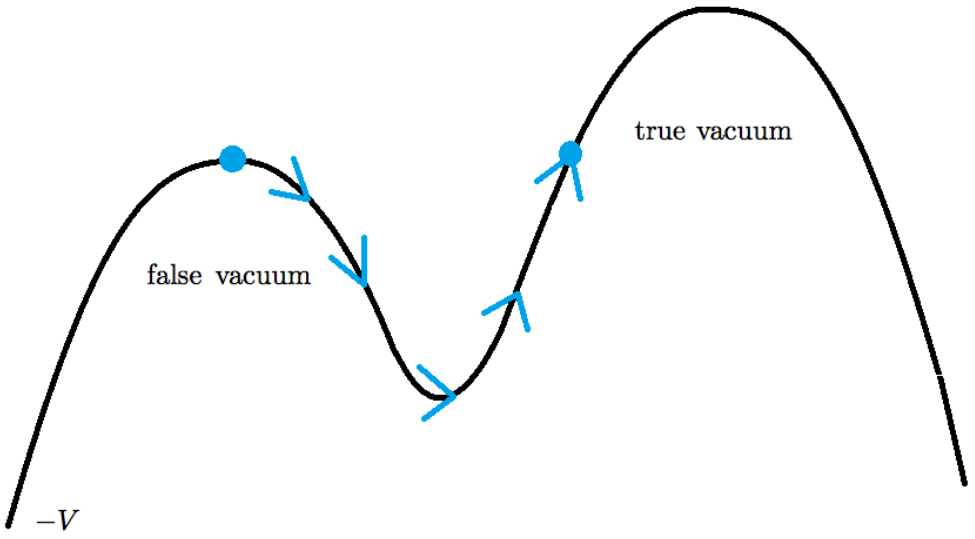

Figure 1.2: A reversed potential in a Euclidean spacetime. The potential 'V' effectively behaves as a reversed potential '$-V$' in a Euclidean spacetime. A classical path of vacuum decay is found in a Euclidean spacetime.

positive modes as we want in this way. There is no upper bound in the mode spectrum but the lower bound should exist among slowly varying modes. This implies the number of negative modes is restricted if they exist. It is known that there is only one negative mode in flat space[6].

In curved space, the way to find a bounce solution of a Euclidean action is similar to that in flat space[7]. However, the number of negative modes can be totally different from the number in flat space. In contrast with the previous example, a rapidly varying field with small amplitudes can generate a negative mode instead of a positive mode in curved space. This implies that there could be an infinite number of negative modes in curved space. This is an unusual effect of quantum gravity. Because the mode spectrum in curved space can be totally different from the number in flat space, we are led to ask about the physical interpretation of negative modes.

Vacuum decay is not only an interesting topic itself in field theory but also applicable to some models in cosmology. It is believed that there was an exponential expansion in the very early universe as known as 'inflation'. Theoretically, the inflationary picture can explain why the universe is so spatially homogeneous and isotropic, why the universe is so nearly flat and why magnetic monopoles are hardly observed. Direct evidence of inflation, the detection of gravitational waves

from inflation, was announced recently[8, 9].

Then, one can ask why there was an inflationary epoch at the very early universe. This is because the universe has undergone a phase transition. There are two types of phase transitions. The first one is a first-order phase transition, which creates a bubble of the new phase in the background of the old phase. This is a consequence of the vacuum decay process that I described earlier. The other one is a second-order phase transition, which is the case where the old phase continuously transforms itself into the new phase.

The first inflationary model suggested by Guth[1] was based on a first-order phase transition. However, it cannot explain how the universe reheats properly after being supercooled in the inflationary phase[10, 11]. To solve this problem, Linde and, Albrecht and Steinhardt developed the 'new inflation' model as known as slow-roll inflation[2, 3]. In this model, the field on the potential rolls down slowly during inflation, and then inflation stops and reheating begins where the potential becomes steeper. Some inflationary models imply that inflating bubbles can be created continuously while the volume of the background fields also undergoes inflation. If the volume of the background fields increases faster than the rate of bubble nucleations, the background space keeps expanding exponentially. This is called 'eternal inflation'. This also gives a multiverse picture, typically a fractal structure. In the endless production of bubbles, each bubble can be seen as an individual universe.

Vacuum decay is an essential concept to describe some inflationary models. It means that studying the vacuum decay helps us not only to understand inflation but also to find out the exact details of inflation, which has not been answered yet. To understand the vacuum decay process better, I will discuss various topics about negative modes in vacuum decay in this thesis. This thesis mainly consists of two parts. The first one is studying the nature of the vacuum decay process and the other part deals with the negative modes problem of the tunneling procedure.

In Chapter 2, I start by describing the tunneling problem based on the WKB approximation in both quantum mechanics and field theories. The decay rate turns out to depend on the Euclidean action of the classical solution. By summing all possible configurations of bounces, we can find the exact imaginary part of the energy shift. This gives the complete form of the decay rate.

In Chapter 3, I review vacuum decay in the presence of gravity. There are two different topologies of solutions. The first one implies a closed manifold which is approximated by a Euclidean

de Sitter space. The other one is an open manifold that is topologically equivalent to a Euclidean flat space or a Euclidean anti-de Sitter space. After constructing proper boundary conditions, I will determine the conditions for each case to exist. In a closed manifold, there are two unusual solutions because of the finiteness of the spacetime. The first one is the tunneling from the true vacuum to the false vacuum and the other one is a static solution known as the Hawking-Moss bounce.

In Chapter 4, I describe the thin-wall approximation. If the thickness of the wall is much less than the other length parameters, we can construct a valid approximation which leads us to find an analytic solution of the vacuum decay. Especially in curved space, we can see there are two different types of solutions. The first one is the type A bounce whose radius is smaller than the horizon. The other one is the type B bounce whose wall is located at the maximum of the metric factor.

In Chapter 5, I talk about thermal aspects of vacuum tunneling in both flat space and curved space. If and only if the volume of the curved spacetime is finite, the temperature of the system is also finite. Then, the tunneling occurs by not only quantum fluctuations but also by thermal excitation. By understanding the thermal picture in de Sitter background, we can find a Euclidean time coordinate in an analogy of the Lorentzian time and this allows us to interpret the horizon and the type B solutions properly.

In Chapter 6, I explain some negative mode issues in flat space based on Coleman's argument. I show there is one and only one negative mode in flat space and I introduce an approach to find eigenmodes analytically with the thin-wall approximation. For more details, I analyze cases with three vacua with one- or two-field potentials which have two negative modes. We will see how the action behaves around the bounce solutions and find out the dominant configuration in the decay process. If there are many vacua, there can be many small bubbles inside one large outer bubble. I investigate how small inner bubbles contribute to the system.

In Chapter 7, I discuss negative mode problems in vacuum decay with gravitational fields. Using a gauge independent approach, I show there are always an infinite number of negative modes for a de Sitter space. These negative modes are found by varying perturbative fields very rapidly in negative kinetic energy regions. There are two sorts of negative kinetic energy regions. The first one is found on the bubble wall if the height of the potential is sufficiently large and the second

one is located around the maximum of the metric factor. Because there is always a maximum if the manifold is closed, every bounce in a de Sitter background has this kind of negative kinetic energy region. These many negative modes could be removed if many bubbles are nucleated in de Sitter space, in an analogy with flat space. Furthermore, I describe how an ordinary negative mode behaves as the gravitational effects get stronger.

Finally I conclude in Chapter 8.

Chapter 2

Vacuum tunneling in flat spacetime

2.1 Vacuum tunneling in Quantum Mechanics

Let us briefly review one-dimensional quantum tunneling. By using the WKB approximation, a wave function on a barrier '$V(x)$' as in Figure 2.1 is given by

$$\Psi(x) = \frac{C}{\sqrt{p(x)}} e^{\pm i \int_0^x p(x)dx} \tag{2.1}$$

where

$$p(x) = \sqrt{2m[V(x) - E]}. \tag{2.2}$$

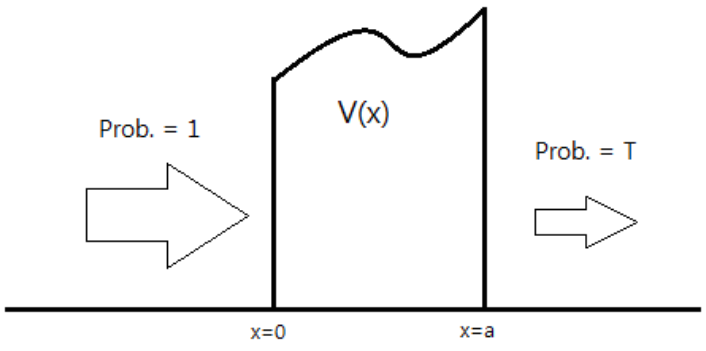

Figure 2.1: The tunneling in quantum mechanics.

We can find the tunneling coefficient (T) by matching boundary conditions,

$$T \sim e^{-2\int_0^a p(x)dx} = e^{-B}, \tag{2.3}$$

where a is the end point of the barrier. The exponent B is defined by

$$B = \int_0^a \sqrt{2m[V(x) - E]}dx + \int_a^0 \sqrt{2m[V(x) - E]}d(-x) = 2\int_0^a \sqrt{2m[V(x) - E]}dx. \tag{2.4}$$

In Euclidean coordinates, the potential '$V(x)$' behaves as '$-V(x)$' and the particle classically moves back and force within two classical turning points(x_i) such that '$V(x_i) = E$'. Note that the exponent B is the same as the Euclidean action of the particle for one period.

In this example, the tunneling amplitude informs us the probability to find the particle on the other side. In other words, it is interpreted as the probability to penetrate through to the other side when a particle hits the barrier.

If the potential has a classical equilibrium state, a so-called false vacuum as in Figure 2.2, the state entered on the false vacuum decays to the region outside the barrier because the false vacuum is not a true minimum[4]. The decay rate is determined by

$$\Gamma = -\frac{1}{|\Psi|^2}\frac{d}{dt}|\Psi|^2 \tag{2.5}$$

where Ψ is the wavefuction in the false vacuum side. By plugging the Schrodinger equation into (2.5), we can find that the imaginary part in the energy contributes to the decay rate,

$$\Gamma = 2 \cdot \mathrm{Im}(E). \tag{2.6}$$

Since we treat the false vacuum as if it were a stationary state, the energy E is allowed to be complex.

The eigenvalue of the Hamiltonian becomes a complex number and its imaginary part contributes to the decay rate. We can calculate the decay rate Γ by evaluating the path integral

$$\langle f|e^{-HT}|i\rangle = \int Dx e^{-S_E[x]}. \tag{2.7}$$

It is well-known that the decay rate is given by an expression of the form

$$\Gamma = Ae^{-B}(1 + O(\hbar)) \tag{2.8}$$

where

$$B = 2\int_0^a \sqrt{2m[V(x) - E]}dx. \tag{2.9}$$

I will show how to evaluate the path integral in field theory in Section 2.3. However, we can still see the decay rate has to be given by Equation (2.8) without calculating the path integral. Consider the classical motion of the particles in a well. The average time between collisions with the barrier is proportional to the inverse of the number of particles in the well. The number of decaying particles is determined by the product of the rate of collisions and the probability to penetrate on each collision, and the probability of penetration is the same as the tunneling coefficient.

$$\begin{aligned}(\#\text{ of decaying particles per unit time}) &\sim \Gamma \cdot |\Psi|^2 \\ \sim (\text{Prob. of penetration}) \times (\#\text{ of hitting the barrier per unit time}) &\sim T \cdot |\Psi|^2\end{aligned} \tag{2.10}$$

This means the decay rate (Γ) is proportional to the tunneling coefficient (T).

$$\begin{aligned}\Gamma \sim T \sim e^{-B}, \\ \Gamma = Ae^{-B}.\end{aligned} \tag{2.11}$$

We will check this again and find A exactly in Section 2.3.

Let us move to the tunneling process in many dimensions. In the case of one dimension, there is only one way to move classically so we do not have to worry about the path. There is only one possible point to penetrate while conserving the energy. In the case of d-dimensions, the possible penetration points form a (d-1)-dimensional surface. We can choose the initial point as the place of the false vacuum ($\vec{q}_f$). For given penetration point ($\vec{q}_p$), the path is determined by minimizing the Euclidean action.

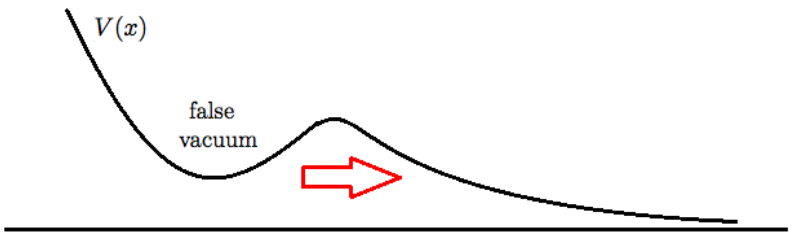

Figure 2.2: The potential for the false vacuum decay.

If we set the coordinates of the particle in the system ($\vec{q}$), the Euclidean action is given by

$$S_E = \int d\tau \left(\frac{1}{2} \frac{d\vec{q}}{d\tau} \cdot \frac{d\vec{q}}{d\tau} + V(\vec{q}) \right). \tag{2.12}$$

The initial point ($\vec{q}_f$) should be reached asymptotically since it is a maximum of the Euclidean potential ($-V$),

$$\lim_{\tau \to -\infty} \vec{q} = \vec{q}_f. \tag{2.13}$$

The penetration point ($\vec{q}_p$) has to be the turning point so $\dot{\vec{q}}$ vanishes there. Because the range of the time is infinite, we can set the time on the turning point to be $\tau = 0$,

$$\frac{d\vec{q}}{dt} = 0 \quad \text{at } \tau = 0. \tag{2.14}$$

In other words, the path is found by solving the Euler-Lagrange equation for the Euclidean Lagrangian

$$\frac{d^2\vec{q}}{d\tau^2} = \frac{\partial V}{\partial \vec{q}}. \tag{2.15}$$

with two boundary conditions. The solution has a time reversal symmetry, '$\vec{q}(\tau) = \vec{q}(-\tau)$', so it satisfies

$$\int_{-\infty}^{0} L_E[\vec{q}(\tau)] d\tau = \int_{0}^{\infty} L_E[\vec{q}(\tau)] d\tau. \tag{2.16}$$

The decay rate is given by

$$\Gamma \sim A e^{-B}. \tag{2.17}$$

As in the one-dimensional case, B stands for the action along the classical path

$$B = 2 \int_{-\infty}^{0} L_E[\vec{q}(\tau)] d\tau = \int_{-\infty}^{\infty} L_E[\vec{q}(\tau)] d\tau = S_E. \tag{2.18}$$

Any points on the (d-1)-dimensional surface that preserve the energy can be the penetration point, so there are many possible bounces. The preferred bounce is the one of minimum action, and it also has the highest decay rate. If the potential has some symmetries, some paths with the same symmetry are categorized and the decay rate (Γ) for the symmetry group is also given by the sum of them. For example, if the potential is totally symmetric, every penetration point is equivalent to each other and there is only one solution in the system.

2.2 Vacuum decay in field theory

We have studied the decay problem in quantum mechanics. Most of the properties in quantum mechanics are also applicable to quantum field theory, but one of the significant differences between them is the locality of vacua. In the setup of quantum mechanics, a potential is a function of coordinates so it is localized and the position of a local minimum is also fixed. On the contrary, in field theory, a potential is described in terms of fields so the tunneling can be located anywhere. It means the vacuum decay process can occur anywhere and the size of the false (or true) vacuum is also flexible.

In quantum mechanics, the penetration point on the potential is uniquely determined for the given path but it is not in the case of field theory because of the size of the false (or true) vacuum. Of course, if we seek the configuration which minimizes the action, it turns out to be unique and the penetration point is also always lower than the false vacuum. In the setup of quantum mechanics, they have to be the same to preserve the energy. Meanwhile, fields which manipulate the potential are dynamic variables in field theory, so they always have positive kinetic energy. Because the spatial gradient of fields also contributes to the energy, the penetration point is lower than the false vacuum to compensate for the energy due to the spatial gradient of fields as in Figure 2.3.

Let us assume the whole space was initially filled with the false vacuum. If the decay process takes place somewhere, then the true vacuum fills some finite regions. It has to be finite because of the energy issue. This true vacuum area is called by a vacuum bubble. Even in a d-dimensional Euclidean spacetime, the true vacuum still forms d-dimensional bubbles in the tunneling process for the same reason.

To describe the tunneling process in field theory, we can start with a scalar potential in flat spacetime[4]. Then, the Euclidean action is written by

$$S_E = \int d^4x \mathcal{L}_E = \int d\tau d^3x \left[\frac{1}{2}\partial_a\phi\partial_a\phi + U(\phi)\right], \tag{2.19}$$

and the Euclidean equation of motion is

$$\left(\frac{\partial^2}{\partial\tau^2} + \nabla^2\right)\phi = U'[\phi]. \tag{2.20}$$

We can find solutions of this equation after imposing proper boundary conditions to describe the vacuum decay process. By assuming there is one bubble in infinitely large spacetime, we can

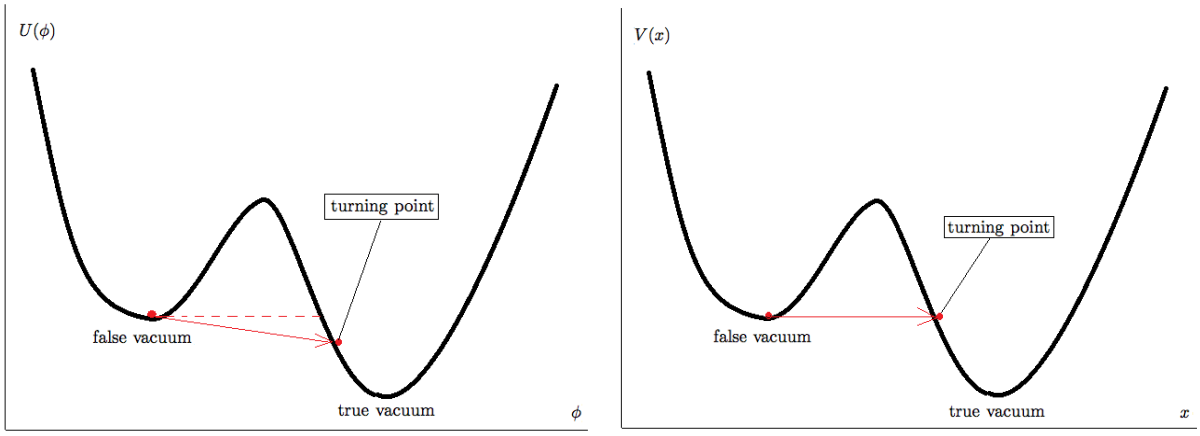

(a) Field theory ($U[\phi]$) (b) Quantum mechanics ($V(x)$)

Figure 2.3: The vacuum tunneling path in quantum mechanics and field theory. In field theory (a), the turning point is lower than the false vacuum but it is also higher than the exact true vacuum. On the contrary, the turning point (b) in quantum mechanics has the same energy as the false vacuum.

find the following boundary conditions.[1]

At first, the initial state has to be a pure false vacuum.

$$\lim_{\tau\to-\infty}\phi(\tau,\vec{x})=\phi_f. \tag{2.21}$$

We know there must be a classical turning point for the Euclidean potential '$-U$'. Since the initial condition is defined at $\tau=-\infty$, we can set the turning point as $\tau=0$ without loss of generality,

$$\frac{\partial\phi}{\partial\tau}(0,\vec{x})=0. \tag{2.22}$$

The action has to be finite because the decay rate, $\Gamma=Ae^{-B}$, vanishes if B diverges. In other words, the tunneling process does not take place if the action is not finite.

$$B=S_E[\text{bounce}]-S_E[\phi_f]=\int d\tau d^3x\left[\frac{1}{2}\left(\frac{\partial\phi}{\partial\tau}\right)^2+\frac{1}{2}\left(\vec{\nabla}\phi\right)^2+(U-U_f)\right]. \tag{2.23}$$

To make the action finite, the scalar field should be constant at $\tau=\infty$. Thus, the field has to come back to the pure false vacuum at $\tau=\infty$. This condition gives the last boundary condition,

$$\lim_{\tau\to\infty}\phi(\tau,\vec{x})=\phi_f. \tag{2.24}$$

[1]If there are many bubbles, this boundary condition is asymptotically valid provided they are widely separated.

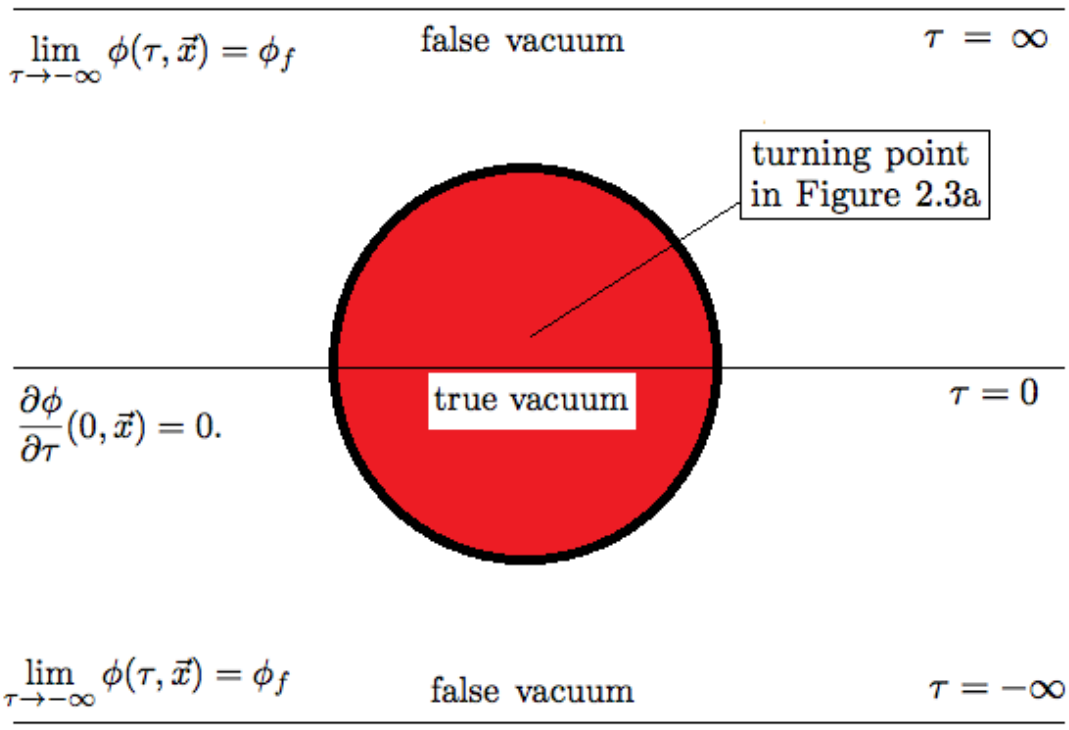

Figure 2.4: Creation of a vacuum bubble and boundary conditions. The field inside a bubble is not the exact true vacuum but the turning point as in Figure 2.3a, which is slightly higher than the exact true vacuum.

Let us describe how the scalar field behaves with these three boundary conditions. As in Figure 2.4, the field starts from the false vacuum, and at $\tau = 0$, the field is approximately at the true vacuum inside a vacuum bubble but it is near the false vacuum outside a vacuum bubble. With the boundary condition (2.22), the field starts to go back to the initial configuration at $\tau = 0$ all over the places. If there are only two vacua in the potential, the time reversal symmetry ($\phi(\vec{x},\tau) = \phi(\vec{x},-\tau)$) always exists but it is not necessarily true for generic potentials. Although fields would not follow the same path as the first time when the symmetry is not applicable, they eventually come back to the false vacuum. Since $\dot{\phi}$ vanishes everywhere at $\tau = 0$, the solution can be also a solution in a Lorentzian coordinate by taking $t = i\tau$. These Euclidean solutions are called **bounces**.

$$\phi_E(\vec{x},\tau=0)=\phi_L(\vec{x},t=0),\quad \left.\frac{d\phi_E}{d\tau}\right|_{\tau=0}=\left.\frac{d\phi_L}{dt}\right|_{t=0}=0. \tag{2.25}$$

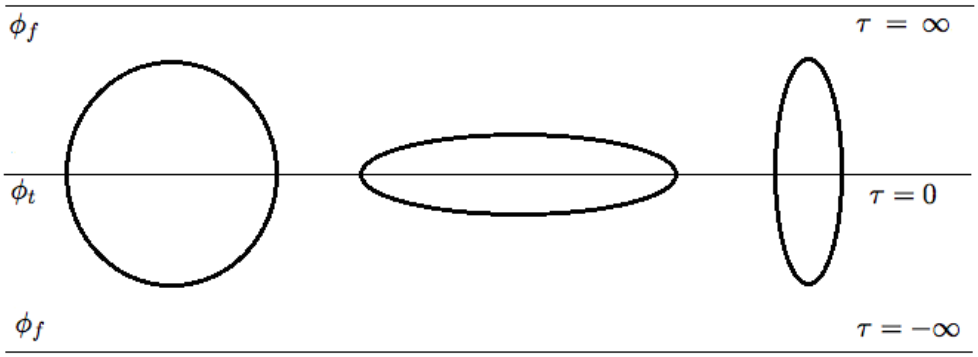

Figure 2.5: Many possible solutions with boundary conditions. The maximally symmetric one has the lowest action.

With these condition, $\phi_L(\vec{x}, t)$ also obeys the Lorentzian equation of motion.

$$-\frac{\partial^2 \phi_L}{\partial t^2} + \nabla^2 \phi_L = U'[\phi_L] \tag{2.26}$$

If we relax the second boundary condition (2.22), we can find more possible solutions. These solutions also obey the equation of motion, the initial and the final boundary conditions. However, they can not nucleate in a Lorentzian spacetime because there is no proper channel to continue to $\tau \to it$. These solution only exist in a Euclidean spacetime so they are not bounces and the interpretation of these solution is unclear. We will check an example of this case at the end of Section 6.3.3.

There are many possible classical solutions to satisfy these three boundary conditions as like Figure 2.5. Furthermore, every spatial translation of one solution is also a solution because the Lagrangian and the boundary conditions are invariant under spatial translations.

Among such many solutions, we are interested in finding the solution with the lowest action, which is the most preferred bounce. In most cases, the maximally symmetric solution with the same boundary conditions tends to have lower action than other less symmetric solutions. In the case of flat spacetime, it is proven by Coleman, Glaser and Martin that the $O(4)$-symmetric solution always exists and has the lowest action[12].

Let us investigate the maximally symmetric case. We can find a $O(4)$ symmetric field by defining $\rho = \sqrt{\tau^2 + |\vec{x}|^2}$. Then, the scalar field $\phi(\rho)$ is a function of ρ only. The equation of motion becomes

$$\frac{d^2\phi}{d\rho^2} + \frac{3}{\rho}\frac{d\phi}{d\rho} = U'[\phi(\rho)], \tag{2.27}$$

and the boundary conditions are

$$\phi'(0) = 0, \tag{2.28}$$

$$\phi(\infty) = \phi_f. \tag{2.29}$$

The action is given by

$$B = S_E[\text{bounce}] - S_E[\phi_f] = 2\pi^2 \int_0^\infty d\rho\rho^3 \left[\frac{1}{2}\phi'^2 + U[\phi(\rho)] - U_f\right]. \tag{2.30}$$

To find B, we need to evaluate S_E properly. It is always possible to find the solution which satisfies the boundary conditions numerically but there is no simple way to find an exact solution analytically for a generic potential. If the width of the wall between two vacua is much smaller than the radius of the bubble, we can assume the width is negligible and it is possible to calculate S_E analytically. This method is called the thin-wall approximation. We will discuss more details in Chapter 4.

2.3 Quantum approach of the tunneling rate

In this section, we study the quantum approach to the tunneling rate[5]. As we discussed in Section 2.1, the imaginary part of the energy determines the decay rate. Let us find out the complete form of the decay rate by evaluating the path integral properly.

Let us define T as the range of τ. In the limit of $T \to \infty$, only the lowest energy state contributes to the path integral so the imaginary part of the lowest energy contributes to the decay rate. To be precise, the path integral

$$\lim_{T\to\infty} I(T) = \lim_{T\to\infty} \langle \tau = T/2 | e^{-HT} | \tau = -T/2 \rangle = \int \mathcal{D}\phi e^{-S_E[\phi;T]} \tag{2.31}$$

is dominated by the lowest energy state as $T \to \infty$,

$$\lim_{T\to\infty} I(T) = \lim_{T\to\infty} \sum_i |a_i|^2 e^{-E_i T} = e^{-E_0 T}, \tag{2.32}$$

where $|\tau = -T/2\rangle = \sum_i a_i |E_i\rangle$ and set $|a_0|^2 = 1$ for a convention.

The functional integration becomes the product of ordinary integrations by the mode analysis because of the orthogonality of the eigenfuctions

$$\mathcal{D}\phi = \prod_n (2\pi\hbar)^{-1/2} dc_n. \tag{2.33}$$

Let us think about an arbitrary configuration of the scalar field ϕ. Then, ϕ is expressed by the sum of the classical solution ($\bar{\phi}$) and eigenfunctions (ϕ_n) of the second variational derivative of S at $\phi = \bar{\phi}$ as

$$\phi = \bar{\phi} + \sum_n c_n \phi_n. \tag{2.34}$$

Here, c_n's are coefficients of eigenfunctions. In our convention, the pre-factor $(2\pi\hbar)^{-1/2}$ is set to satisfy that

$$\int \prod_n (2\pi\hbar)^{-1/2} dc_n e^{-S_E/\hbar} = \int \prod_n (2\pi\hbar)^{-1/2} dc_n e^{-\lambda_m c_m^2/2\hbar} = \prod_n \frac{1}{\lambda_n^{1/2}}. \tag{2.35}$$

The lowest energy is given by

$$E_0 = \lim_{T\to\infty} -\frac{\ln I(T)}{T}. \tag{2.36}$$

Because bubbles can be nucleated all over the whole space with the same decay rate, the decay rate per unit volume is

$$\Gamma/V = \frac{2\,\mathrm{Im}\, E_0}{V} = \lim_{T,V\to\infty} \frac{2\,\mathrm{Im}\,(\ln I(T))}{VT}. \tag{2.37}$$

The path integral contains every possible configuration of fields and each configuration has a certain number of bounces. Define I_n as the path integral of n bounces. Then, the path integral is the sum of the path integrals of each number of bounces,

$$I = \sum I_n = I_0 + I_1 + I_2 + \cdots. \tag{2.38}$$

The first term (I_0) indicates a path integral of a homogenous field configuration. The field stays on the false vacuum all over the spacetime classically, $\phi(\vec{x}, \tau) = \phi_f$. In this case, there is no bounce and the path integral is

$$I_0 = \frac{1}{\left(\det S_E''[\phi_f]\right)^{1/2}} e^{-S_E[\phi_f]}. \tag{2.39}$$

Since each Gaussian integration gives $\lambda_i^{-1/2}$ in our convention (2.35), I_0 should contain the term of $\det S_E''[\phi_f] = \prod \lambda_i$ where λ_i's are eigenvalues of $S_E''[\phi_f]$. $S_E''[\phi]$ is the operator which generates the

eigenvalues and the eigenfunctions for given ϕ. In the case of no bounce, we can write as

$$S_E''[\phi_f] = -\Box + U''[\phi_f] = -\Box + \omega^2, \tag{2.40}$$

because $U''[\phi_f]$ is a positive constant, $\omega^2 \equiv U''[\phi_f]$.

The next step is evaluating I_1. As a first thought, we can naively write I_1 as like the I_0 case[2],

$$I_1 = \frac{1}{\left(\det S_E''[b]\right)^{1/2}} e^{-S_E[b]}. \tag{2.41}$$

Since the range of spacetime is infinite, a bubble can nucleate anywhere. A bubble is totally equivalent to other bubbles nucleated at different positions (or times) with the same boundary conditions. This implies the spatial (or time) translation symmetries of bubbles. These four translation symmetries allow four zero modes in four dimension. Because these four zero modes come out from the flat structure of the spacetime, they are universal in flat spacetime. If there are some internal symmetries in the system, those symmetries generate more zero modes[13]. Here, we only care about the case without internal symmetries.

Because a bubble can be nucleated at any points and any time, the path integral for one bounce (I_1) should be proportional to the volume of the whole spacetime which is infinite. This infinity does not cause any problems because we are interested in the decay rate per unit volume. Since '$\det S_E''[b]$' has four $\frac{1}{0^{1/2}}$'s, they have to be removed. Let us find explicit forms of these zero modes first. If the field is shifted as

$$\phi(x_\mu) = \phi(x_\mu + \alpha\hat{x}_1) = \phi(x_\mu) + \alpha\frac{\partial\phi(x_\mu)}{\partial x_1}\hat{x}_1 + O(\alpha^2), \tag{2.42}$$

zero modes correspond to $\Phi_\mu \sim \partial_\mu\phi$ for infinitesimal translations where $\mu = 0, 1, 2, 3$, respectively. Here, we denote four zero modes as Φ_μ. In order to find a normalization constant for a zero mode, we need to evaluate B,

$$B = \int d^4x \left(\frac{1}{2}\partial_\mu\bar{\phi}\partial^\mu\bar{\phi} + U[\phi]\right) = \frac{1}{4}\int d^4x \partial_\mu\bar{\phi}\partial^\mu\bar{\phi}. \tag{2.43}$$

This gives a complete form of Φ_μ,

$$\Phi_\mu = B^{-1/2}\partial_\mu\bar{\phi}. \tag{2.44}$$

[2] $S_E[b]$ stands for the action of one bounce.

The path integral from the zero modes is given by

$$\int \prod (2\pi\hbar)^{-1/2} dc_\mu e^{-\int d^4x \lambda_\mu \Phi_\mu \Phi_\mu} = \int \prod (2\pi\hbar)^{-1/2} dc_\mu \cdot 1 = \frac{1}{(2\pi\hbar)^2} \int \prod dc_\mu. \tag{2.45}$$

If there were only four zero modes in the system, the field is expanded by

$$\phi(x_\mu) = \bar{\phi}(x_\mu) + c_\mu \Phi_\mu(x_\mu) = \bar{\phi}(x_\mu) + c_\mu B^{-1/2} \partial_\mu \bar{\phi}(x_\mu) = \bar{\phi}(x_\mu + c_\mu B^{-1/2}), \tag{2.46}$$

so the field $\phi(x_\mu)$ is always described in terms of the classical solution $\bar{\phi}$ but it is moved by $c_\mu B^{-1/2}$. This implies that

$$\partial_\mu \phi(x_\nu) = \partial_\mu \bar{\phi}(x_\nu + c_\nu B^{-1/2}), \tag{2.47}$$

$$d\phi(x_\nu) = dx_\mu \cdot \partial_\mu \phi(x_\nu) = dx_\mu \cdot \partial_\mu \bar{\phi}(x_\nu + c_\nu B^{-1/2}). \tag{2.48}$$

In the expansion of (2.34), ϕ can be varied only by changing c_n's because $\bar{\phi}$ and ϕ_n's are fixed. To sum up, it turns out to be

$$d\phi(x_\nu) = dc_\mu \cdot \Phi_\mu(x_\nu) = dc_\mu \cdot B^{-1/2} \partial_\mu \bar{\phi}(x_\nu + c_\nu B^{-1/2}). \tag{2.49}$$

Now we can find the relationship between dx_μ and dc_μ for zero modes,

$$dc_\mu = B^{1/2} dx_\mu. \tag{2.50}$$

The path integral for zero modes (2.45) gives that

$$\int (2\pi\hbar)^{-1/2} dc_0 = \int \left(\frac{B}{2\pi\hbar}\right)^{1/2} dt = \left(\frac{B}{2\pi\hbar}\right)^{1/2} T, \tag{2.51}$$

$$\int \prod_\mu (2\pi\hbar)^{-1/2} dc_\mu = \left(\frac{B}{2\pi\hbar}\right)^2 VT. \tag{2.52}$$

Since the zero eigenvalues does not contribute to the determinant, 'det $S''_E[b]$', it should be modified to the determinant without zero modes, 'det$'$ $S''_E[b]$'.

There is one and only one negative mode[3]. For this negative mode, the gaussian integral over c_- diverges. In order to avoid this problem, we need an analytic continuation of the integration path. The existence of the negative mode implies that the bounce is on the saddle point, and the

[3]See Chapter 6 for details

path of contour integration can be distorted to the upper half plane from the saddle point. The imaginary part runs from 0 to either $\pm\infty$ ('$-$' when it goes to the lower half plane) not from $-\infty$ to ∞. The factor of 1/2 came out after Gaussian integration through the steepest-descent method because it only covers the half of the gaussian integration[5]. If the path is distorted to the upper half plane, the factor of i also appears.

The negative mode integration gives

$$\int (2\pi\hbar)^{-1/2} dc_- e^{-S_E[\phi_-]/\hbar} = \frac{i}{2}|\lambda_-|^{-1/2}. \tag{2.53}$$

where c_- is the coefficient in Equation (2.34), ϕ_- is the negative eigenmode and λ_- is the negative eigenvalue.

To sum up, I_1 is written by

$$I_1 = \frac{i}{2}\left(\frac{B}{2\pi\hbar}\right)^2 VT \left|\det' S_E''[b]\right|^{-1/2} e^{-S_E[b]} = iVTKe^{-B}I_0. \tag{2.54}$$

Define K as,

$$K = \frac{1}{2}\left(\frac{B}{2\pi\hbar}\right)^2 \left|\frac{\det' S_E''[b]}{\det S_E''[\phi_f]}\right|^{-1/2}. \tag{2.55}$$

For n bounces case, if bubbles are separated widely so that each bubble behaves as one bubble, then we can use the dilute gas approximation. Then, as like the I_1 case, I_n should be the form of

$$I_n \sim iVTKe^{-B}I_{n-1} \sim \left(iVTKe^{-B}\right)^n I_0. \tag{2.56}$$

More precisely, we need a factor of $\frac{1}{n!}$ because the path integral is invariant under exchanging any two bubbles.

$$I_n = \frac{1}{n!}\left(iVTKe^{-B}\right)^n I_0. \tag{2.57}$$

Rewrite Equation (2.38),

$$I = \sum_n I_n = I_0 + iVTKe^{-B}I_0 + \frac{1}{2!}\left(iVTKe^{-B}\right)^2 I_0 + \frac{1}{3!}\left(iVTKe^{-B}\right)^3 I_0 + \ldots = I_0 \exp\left(iVTKe^{-B}\right). \tag{2.58}$$

The decay rate per unit volume is

$$\begin{aligned} \Gamma/V &= \lim_{T,V\to\infty} \frac{2\,\mathrm{Im}\left(\ln I(T)\right)}{VT} \\ &= \left(\frac{B}{2\pi\hbar}\right)^2 \left|\frac{\det' S_E''[b]}{\det S_E''[\phi_f]}\right|^{-1/2} e^{-B}. \end{aligned} \tag{2.59}$$

Note K is a pure imaginary because the contour integration for the zero mode gives a pure imaginary number and the others should be real by the ordinary gaussian integration. I_0 does not contribute to the decay rate because it's a real number.

This result shows that

$$\Gamma/V = Ae^{-B} \tag{2.60}$$

and A is given by

$$A = \left(\frac{B}{2\pi\hbar}\right)^2 \left|\frac{\det' S_E''[b]}{\det S_E''[\phi_f]}\right|^{-1/2}. \tag{2.61}$$

This gives the complete form of the decay rate.

Chapter 3

Vacuum tunneling in curved spacetime

The vacuum tunneling process itself is an important topic in quantum field theory but it becomes more valuable in the context of quantum gravity because it helps us to understand the evolution of the early universe. To describe the very early universe, ordinary four dimensional quantum gravity would not be appropriate since the UV completeness problem arises beyond the Planck scale. However, it is still useful to see how the gravitational effects contribute to the tunneling process, and especially for the weak gravity limit, it gives well-suited results of the vacuum decay.

The first step to include gravity is constructing the metric to represent the spacetime manifold of the system. There are lots of choices of the metric. The most general case is the $O(4)$ symmetric metric which is as known as the Coleman-de Luccia metric[7]. In the case of flat space, it is proven that the maximally symmetric solution with the same boundary conditions has the lowest action, which is our main interest. Meanwhile, in curved space, the $O(4)$ symmetric solution seems to be the lowest action but this has not been proven exactly yet[14, 15]. We shall see an $O(5)$ symmetric solution known as the Hawking-Moss solution which is more symmetric than the CdL solution[16]. Although we can check the HM solution has always higher action than the CdL case, it cannot be a counterexample because it has different initial conditions. In this chapter, we focus on the $O(4)$ symmetric metric case.

3.1 The set-up

As in the flat space case, we need a Euclidean spacetime to understand the tunneling problems. Let us start with the Colemann-de Luccia metric, which is $O(4)$-symmetric,

$$ds^2 = B^2 d\xi^2 + \rho(\xi)^2 d\Omega_3^2. \tag{3.1}$$

The scalar field in the curved space satisfies

$$\nabla^\mu \nabla_\mu \phi = U'. \tag{3.2}$$

where ∇_μ is a covariant derivative in curved space. For the CdL metric, the field equation is given by

$$\ddot{\phi} + \frac{3\dot{\rho}}{\rho}\dot{\phi} = B^2 U'. \tag{3.3}$$

Since the metric only depends on ξ, the 00-component of the Einstein equation, '$G_{00} = \kappa T_{00}$', gives a constraint of the system, ($\kappa \equiv 8\pi G$)

$$\dot{\rho}^2 = B^2 + \frac{\kappa\rho^2}{3}\left(\frac{1}{2}\dot{\phi}^2 - B^2 U\right). \tag{3.4}$$

The other components of the Einstein equation are either identities or trivial consequences of the field equation and the constraint. If the metric is not $O(4)$ symmetric, the system is not invariant anymore under the rotational translation. Thus, the $0i$-components of the Einstein equation, '$G_{0i} = \kappa T_{0i}$', come out and there are more constraints in the system.

Since we derived the above equations by using the covariant derivatives and the Einstein equation, the total action should contain the Einsten-Hilbert term and the action of the covariant fields.

$$\begin{aligned} S_E &= \int d^4x\sqrt{|g|}\left(\frac{1}{2}\nabla_\mu\phi\nabla^\mu\phi + U[\phi] - \frac{1}{2\kappa}R\right) \\ &= 2\pi^2\int d\xi B\left[\rho^3\left(\frac{1}{2B^2}\dot{\phi}^2 + U[\phi]\right) + \frac{3}{\kappa B^2}\left(\rho^2\ddot{\rho} + \rho\dot{\rho}^2 - \rho B^2\right)\right]. \end{aligned} \tag{3.5}$$

Equations (3.3) and (3.4) are also obtained by the Euler-Lagrange equations of this Lagrangian. Since there is no $\dot{B}$ term in the Lagrangian, B is not a dynamical variable. It can be treated as a Lagrange multiplier and the existence of a Lagrange multiplier always implies a constraint in the system. As we checked earlier, this constraint is equivalent to the 00-component of the Einstein equation (3.4). It is not a surprising result because B is the coefficient of $d\xi$ in the metric. The constraint is also the same as $\delta\mathcal{L}/\delta B = 0$.

This fact also implies a gauge symmetry in the system. For a given manifold, it is always possible to choose any B without changing the manifold. Choosing different B means nothing but rescaling a ξ-coordinate. We can also check the action is invariant regardless of the value of B.

For a given B, define $d\tilde{\xi}$ as

$$d\tilde{\xi} = Bd\xi. \tag{3.6}$$

It is easy to check that the Lagrangian satisfies

$$\frac{1}{B}\mathcal{L}[\phi(B\xi), \rho(B\xi); B] = \tilde{\mathcal{L}}[\phi(\tilde{\xi}), \rho(\tilde{\xi}); B = 1], \tag{3.7}$$

where $\tilde{\mathcal{L}}$ is the Lagrangian in terms of $\tilde{\xi}$.

The action is written by

$$\begin{aligned} S_E &= 2\pi^2 \int_0^{B\xi_{\max}} d\xi B \left[\rho^3 \left(\frac{1}{2B^2}\dot{\phi}^2 + U[\phi]\right) + \frac{3}{\kappa B^2}\left(\rho^2\ddot{\rho} + \rho\dot{\rho}^2 - \rho B^2\right)\right] \\ &= \int_0^{\xi_{\max}} d\xi \mathcal{L}[\phi(\xi), \rho(\xi); B] \\ &= \int_0^{\xi_{\max}} d\xi \frac{1}{B}\tilde{\mathcal{L}}[\phi(\tilde{\xi}), \rho(\tilde{\xi}); B = 1], \quad (\tilde{\xi} = \xi) \\ &= \int_0^{B\xi_{\max}} d\tilde{\xi}\tilde{\mathcal{L}}[\phi(\tilde{\xi}), \rho(\tilde{\xi}); B = 1], \quad (\tilde{\xi}_{\max} = B\xi_{\max}). \end{aligned} \tag{3.8}$$

This is still true even if the range of ξ is infinite so the action is gauge-invariant.

For convenience, let us set the gauge $B = 1$. Then, the constraint and the field equation become

$$\dot{\rho}^2 = 1 + \frac{\kappa\rho^2}{3}\left(\frac{1}{2}\dot{\phi}^2 - U\right), \tag{3.9}$$

$$\ddot{\phi} + \frac{3\dot{\rho}}{\rho}\dot{\phi} = \frac{dU}{d\phi}. \tag{3.10}$$

By combining these two equations, we can find a useful but subordinate equation,

$$\ddot{\rho} = -\frac{\kappa\rho}{3}\left(\dot{\phi}^2 + U\right). \tag{3.11}$$

In a closed manifold, the action is written by the following after the integration by parts.

$$S_E = 2\pi^2 \int d\xi \left[\rho^3\left(\frac{1}{2}\dot{\phi}^2 + U\right) - \frac{3}{\kappa}\left(\rho\dot{\rho}^2 + \rho\right)\right]. \tag{3.12}$$

By plugging the constraint into (3.12), it can be rewritten as

$$S_E = 4\pi^2 \int d\xi \left[\rho^3 U - \frac{3\rho}{\kappa}\right]. \tag{3.13}$$

This is the simplest form of the action so we use this in most calculations.

If the manifold is open, the Gibbons-Hawking term[17] appears at the boundary,

$$S_E = 2\pi^2 \int_{\mathcal{M}} \left[\rho^3 \left(\frac{1}{2}\dot{\phi}^2 + U\right) - \frac{3}{\kappa}\left(\rho\dot{\rho}^2 + \rho\right)\right] d\xi + \left[\frac{6\pi^2}{\kappa}\rho^2\dot{\rho}\right]\Big|_{\rho=\partial\mathcal{M}}. \tag{3.14}$$

The GH term is canceled out in the calculation of B because the field is very close to the false vacuum for sufficiently large ρ. It is always possible to evaluate $S_E[b]$ numerically but there is no simple way to calculate it analytically, as in the flat space case. If the width of the wall is thin enough, we can use the thin-wall approximation to find an analytical solution. Similarly, the GH term in the action is treated as the region outside the wall in the context of the thin-wall approximation so it is canceled out by the same way.

3.2 Boundary conditions

Our main goal is calculating the decay exponent B. In the case of flat space, it is given by $B = S_E[\phi] - S_E[\phi_f]$ and it can be written by one integration $B = \int d^4x(\mathcal{L}[\phi] - \mathcal{L}[\phi_f])$. In curved space, B has to be obtained by separate calculations because the range of ξ of a bounce differs from that in the pure false vacuum case.

$$B = S_E[b] - S_E[\phi_f] = \int_{\mathcal{M}_b} d^4x\mathcal{L}[\phi] - \int_{\mathcal{M}_f} d^4x\mathcal{L}[\phi_f]. \tag{3.15}$$

We need to construct proper boundary conditions to find physical solutions of the actions, $S_E[b]$ and $S_E[\phi_f]$. Because zeros of ρ are good candidates for boundaries, it is important to check the existence of zeros of ρ in the system, and it is possible to show there must be at least one zero of ρ.

Suppose ρ is always positive so that there is no zero of ρ in the manifold. Then, ξ has to run from $-\infty$ to ∞ because ξ can stop only at $\rho = 0$. If ξ stops at some positive ρ other than $\rho = 0$, a discontinuity of the manifold arises at that point so it is not a physical solution. This shows that there must be a minimum of ρ, and $\dot{\rho}$ vanishes ($\dot{\rho} = 0$) at the minimum. By analyzing the constraint (3.9), U at the minimum ($\dot{\rho} = 0$) has to be positive ($U(\rho_{\min}) > 0$). At the minimum of ρ, $\ddot{\rho}$ is positive ($\ddot{\rho} > 0$) but Equation (3.11) implies $\ddot{\rho} < 0$ if $U(\rho_{\min}) > 0$. Thus, the assumption that ρ is always positive leads to a contradiction. Q.E.D.

There are at most two zeros of ρ. If there are more than two, $\ddot{\rho}$ is not continuous since $\dot{\rho} = \pm 1$ at $\rho = 0$ by the constraint. In other words, there can be only one or two zeros of ρ in the system,

corresponding to an open or closed manifold, respectively.

In the limit $\rho \to 0$, the metric behaves as

$$ds^2 = d\xi^2 + (\xi - \xi_0)^2 d\Omega_3^2 \tag{3.16}$$

to avoid a singular peak of the geometry. ξ_0 is the point where $\rho = 0$. This condition gives $\dot{\rho} = \pm 1$ at $\rho = 0$. We can doublecheck this by the fact that the constraint (3.9) also gives $\dot{\rho} = \pm 1$ at $\rho = 0$. Thus, we can construct the first boundary condition as

$$\dot{\rho} = \pm 1, \text{ at } \rho = 0. \tag{3.17}$$

The second term in the field equation (3.10) diverges as $\rho \to 0$ unless $\dot{\phi} \to 0$. This gives the second boundary condition,

$$\dot{\phi} = 0, \text{ at } \rho = 0. \tag{3.18}$$

If there are two zeros of ρ, the manifold is closed and there are two boundary conditions at each end. In the case of one zero of ρ, the metric represents an open manifold and there are two boundary conditions at $\rho = 0$, and the following condition is needed to make the action finite, as in the flat space case.

$$\phi = \phi_f, \text{ as } \rho \to \infty. \tag{3.19}$$

To summarize, there are four boundary conditions for a closed manifold: (3.17), (3.18) on both ends where $\rho = 0$, and there are three boundary conditions for an open manifold: two ((3.17), (3.18)) on zero of ρ and one (3.19) at the infinity of ρ. These conditions are written in terms of ρ which represents a physical quantity locally but it would be better to describe them by using a ξ-coordinate practically. Since ξ has a translational symmetry, it is possible to set a zero of ρ as $\rho(0) = 0$ without loss of the generality. The geometry can exist on the side of either positive or negative ξ. Conventionally, we choose ξ to run to the positive way. Then, the boundary condition has to be $\dot{\rho}(\xi = 0) = 1$. Once we choose $\rho(0) = 0$ due to the translational symmetry of ξ, the boundary conditions are written in terms of ξ,

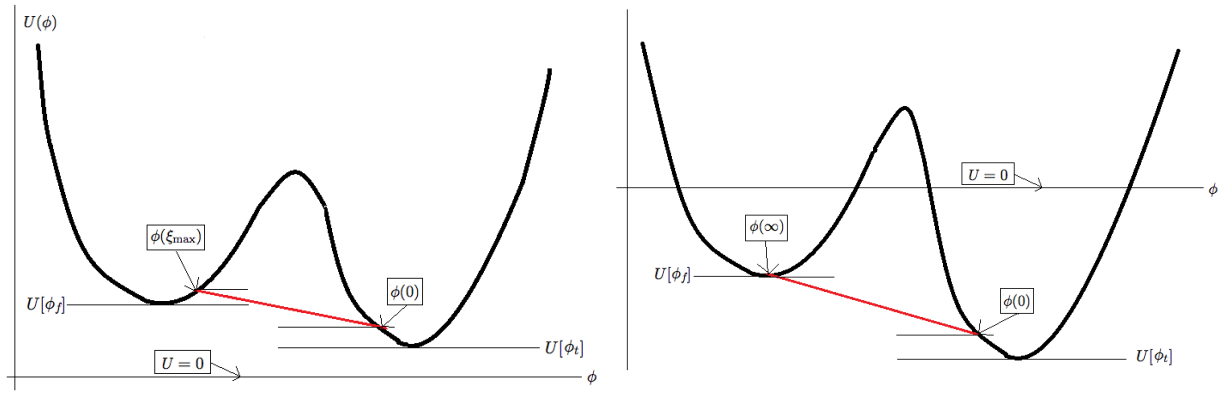

(a) In a closed manifold ($U[\phi(\xi_{\max})] > U[\phi_f]$)

(b) In an open manifold ($U[\phi(\infty)] = U[\phi_f]$)

Figure 3.1: The tunneling path in curved space. At $\xi = 0$, the field starts at $U[\phi(0)] > U[\phi_t]$ in a similar way to the flat space case but the end point is different from that if the manifold is closed.

$$\rho(0) = 0 \text{ (open \& closed)}, \quad \rho(\xi_{\max}) = 0 \text{ (closed)}, \tag{3.20}$$

$$\dot{\rho}(0) = 1 \text{ (open \& closed)}, \quad \dot{\rho}(\xi_{\max}) = -1 \text{ (closed)}, \tag{3.21}$$

$$\dot{\phi}(0) = 0 \text{ (open \& closed)}, \quad \dot{\phi}(\xi_{\max}) = 0 \text{ (closed)}, \tag{3.22}$$

$$\phi(\infty) = \phi_f \text{ (open)}. \tag{3.23}$$

For an open manifold, there is no $\xi_{\max}$ so the conditions at $\xi_{\max}$ cannot be determined. In a similar way, the last one (3.23) is omitted for a closed manifold. The number of boundary conditions in terms of ξ look different from the case in terms of ρ but the first condition (3.20) is not a real boundary condition but the definition of $\rho = 0$ points, so the condition (3.20) is a redundant condition. The condition $\phi(\infty) = \phi_t$ for an open manifold would be fine at a glance but it turns out to be wrong. We will discuss why this condition is not allowed later.

3.3 Solutions

If the field is stationary ($\dot{\phi} = 0$) everywhere, it is easy to find the solution which satisfies the boundary conditions. In this case, the field and the potential are

$$\dot{\phi} = \ddot{\phi} = 0, \quad U' = 0. \tag{3.24}$$

Namely, the field should be in the vacuum. This in a trivial solution and it does not imply a bounce. Let's say U_0 is the vacuum where the field is. If we define $\Lambda_0^2 \equiv \frac{3}{\kappa U_0}$, then the solution for ρ is written by

$$\rho(\xi) = \begin{cases} \Lambda_0 \sin\left(\frac{\xi}{\Lambda_0}\right) & \text{if } U_0 > 0 \\ \Lambda_0 \sinh\left(\frac{\xi}{\Lambda_0}\right) & \text{if } U_0 < 0 \\ \xi & \text{if } U_0 = 0\ . \end{cases} \tag{3.25}$$

Note that $\Lambda_0 \sinh\left(\frac{\xi}{\Lambda_0}\right) = |\Lambda_0| \sinh\left(\frac{\xi}{|\Lambda_0|}\right)$ even if $\Lambda_0 < 0$.

If U_0 is positive, ρ behaves as a sine function so there are two zeros, and the range of ξ is $[0, \pi\Lambda_0]$. The geometry of this case is the same as a Euclidean de Sitter space. In the other cases, there is only one zero so it represents an open manifold. The geometry for $U_0 < 0$ is a Euclidean anti-de Sitter space. The action for the stationary field for $U[\phi_0] = U_0 > 0$ is

$$\begin{aligned} S_E[\phi_0] &= 2\pi^2 \int_0^{\pi\Lambda_0} d\xi \left[\rho^3 U_0 - \frac{3}{\kappa}\left(\rho\dot{\rho}^2 + \rho\right)\right] \\ &= -4\pi^2 \int_0^{\pi\Lambda_0} \Lambda_0^3 U_0 \sin\left(\frac{\xi}{\Lambda_0}\right) \cos\left(\frac{\xi}{\Lambda_0}\right) d\xi \\ &= -\frac{8\pi^2}{\kappa}\Lambda_0^2 = -\frac{24\pi^2}{\kappa^2 U_0}. \end{aligned} \tag{3.26}$$

If U_0 is non-positive, the action diverges to $-\infty$. Even though the action diverges, B can be finite because the field configuration of the bounce for large enough ρ is almost the same as that of a pure vacuum, so the infinities of $S_E[b]$ and $S_E[\phi_f]$ cancel each other out. If there is a bounce with a finite action in this background, B diverges to ∞ so the tunneling rate goes to zero. The bubble cannot nucleate in this case.

We have studied that there are two possible cases of the manifold. Then, it is natural to ask what kinds of conditions determine the topology of a manifold. We can answer this by analyzing the constraint and the equation of the motion.

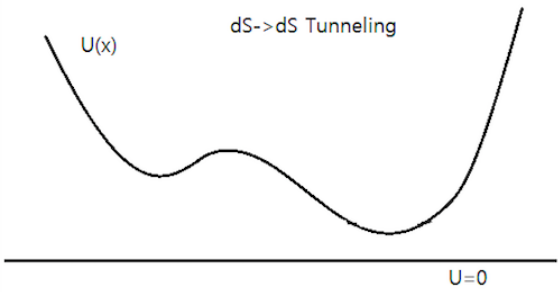

(a) $dS \to dS$ tunneling if $U_f > U_t > 0$,

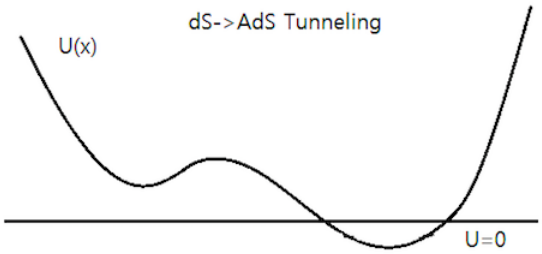

(b) $dS \to AdS$ tunneling if $U_f > 0 > U_t$,

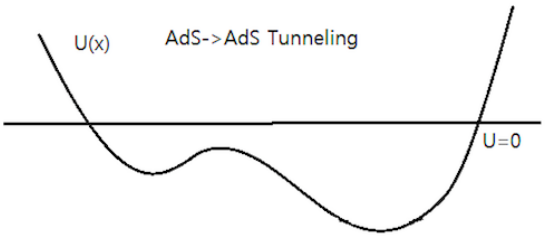

(c) $dS \to AdS$ tunneling if $0 > U_f > U_t$.

Figure 3.2: The conditions for three types of tunneling.

First of all, if the potential is non-negative everywhere, the manifold is always closed. This is the $dS \to dS$ tunneling case. Equation (3.11) gives $\ddot{\rho} < 0$ for all ξ,

$$\ddot{\rho} = -\frac{\kappa\rho}{3}\left(\dot{\phi}^2 + U\right) < -\frac{\kappa\rho}{3}U_t < 0. \tag{3.27}$$

This implies that $\dot{\rho}$ is always smaller than $\dot{\rho}$ on the pure true vacuum so ρ also moves slower than the case of the true vacuum. For any ξ^*, ρ and $\dot{\rho}$ obey

$$\dot{\rho}(\xi^*) = 1 + \int_0^{\xi^*} \ddot{\rho} d\xi < 1 + \int_0^{\xi^*} \frac{\kappa\rho}{3} U_t d\xi = \cos\left(\frac{\xi^*}{\Lambda_t}\right), \tag{3.28}$$

$$\rho(\xi^*) = \int_0^{\xi^*} \dot{\rho} d\xi < \Lambda_t \sin\left(\frac{\xi^*}{\Lambda_t}\right), \quad \left(\Lambda_t^2 \equiv \frac{3}{\kappa U_t}\right). \tag{3.29}$$

This means ρ becomes 0 before $\xi^* = \pi\Lambda_t$ ($\because \xi_{\max} < \pi\Lambda_t$) so there are two zeros of ρ if the potential is always non-negative.

On the contrary, if the potential is negative for all ξ, the manifold is always open. So as to construct a closed manifold, $\dot{\rho}$ has to be 0 at a certain point because $\dot{\rho}$ is continuous. The right-hand side of the constraint (3.9) is positive definite if the potential (U) is negative so the left-hand side

($\dot{\rho}^2$) cannot be zero ($\dot{\rho}^2 > 0$). This means there is no maximum of ρ. Since there is no turning point to make the second zero, the manifold is open. This fact cannot be observed in the thin-wall approximation approach but this is still true in more generic cases. Although the potential not in the classical path can be positive ($\exists\phi$ such that $U[\phi] > 0$ for $\phi < \phi(0)$ or $\phi > \phi(\infty)$ if $\dot{\phi} > 0$), this argument is still true since the outside of the path does not affect on the dynamics at all.

The next case we consider where both vacua are negative but the potential between them is positive in some area. We can also find the topology of this case by investigating the constraint. Before doing that, we need to check the following identity,

$$\frac{d}{d\xi}\left(U - \frac{1}{2}\dot{\phi}^2\right) = U'\dot{\phi} - \dot{\phi}\ddot{\phi} = \dot{\phi}\left(-\frac{3\dot{\rho}}{\rho}\dot{\phi}\right) = -\frac{3\dot{\rho}}{\rho}\dot{\phi}^2, \tag{3.30}$$

$$\left(U - \frac{1}{2}\dot{\phi}^2\right)\Big|_{\xi=\xi^*} = U_0 - \int_0^{\xi^*} \frac{3\dot{\rho}}{\rho}\dot{\phi}^2 d\xi. \quad (U_0 = U \text{ at } \xi = 0)\,. \tag{3.31}$$

At $\dot{\rho} = 0$ points, the constraint gives

$$\frac{3}{\kappa\rho^2} = U - \frac{1}{2}\dot{\phi}^2 < U_0 - \int_0^{\xi^*} \frac{3\dot{\rho}}{\rho}\dot{\phi}^2 d\xi. \tag{3.32}$$

The left-hand side is positive but the right-hand side is negative if U_0 is negative and $\dot{\rho}$ is positive. Before reaching $\dot{\rho} = 0$ points, $\dot{\rho}$ is always positive. This implies there is no $\dot{\rho} = 0$ point if the potential starts from a negative value even if the potential becomes positive somewhere. We can understand this in the other way. Before tunneling occurred, the spacetime was anti-de Sitter space because the potential at $\xi = 0$ is negative. If ρ had a maximum, $B = S_E[b] - S_E[\phi_0]$ goes to ∞ so the tunneling rate is zero. To sum up, in the case of the $AdS \to AdS$ tunneling, the manifold is open no matter how the potential looks.

The last case we examine is the $dS \to AdS$ tunneling. This is the case that the false vacuum is positive but the true vacuum is negative. If the field is in the true vacuum at $\xi = 0$ ($\phi(0) \cong \phi_t$), the manifold is closed as in the $dS \to dS$ case. At the end of the day, ρ moves slightly faster than $\Lambda_f \sin(\xi/\Lambda_f)$ so it has to go to zero. However, if the field starts from the false vacuum ($\phi(0) \cong \phi_f$), it would be possible to diverge since the field can eventually behave as $\Lambda_t \sinh(\xi/\Lambda_t)$, but we can show this is not allowed.

Suppose the field starts from the false vacuum and the manifold is open. The boundary condition shows us

$$\Delta U = U[\xi = \infty] - U[\xi = 0] = U_t - U_f < 0. \tag{3.33}$$

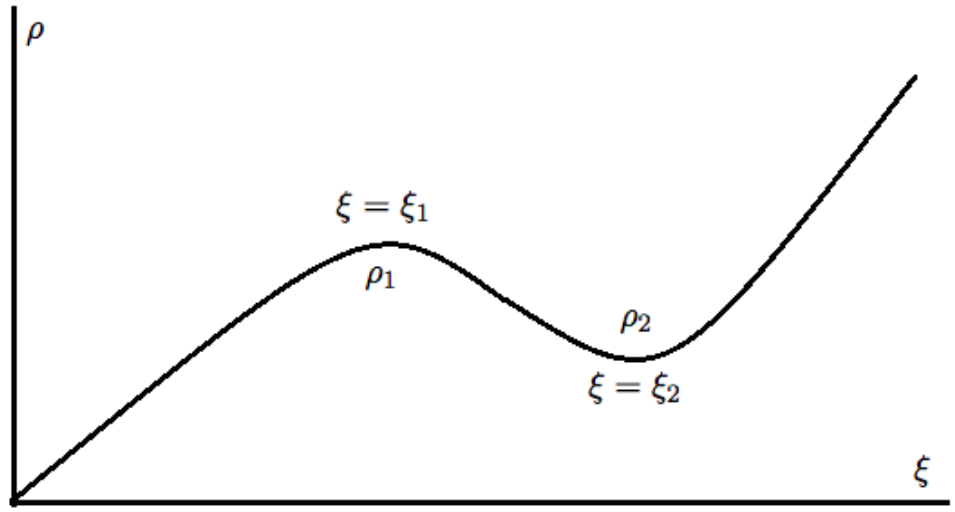

Figure 3.3: A hypothetical solution in $dS \to AdS$ tunneling. This cannot be a real solution.

Equation (3.30) gives

$$\Delta U = \int_0^\infty \frac{d}{d\xi}\left(U - \frac{1}{2}\dot{\phi}^2\right) = \int_0^\infty \frac{3\dot{\rho}}{\rho}\dot{\phi}^2 d\xi. \tag{3.34}$$

In order to satisfy this, $\dot{\rho}$ has to be negative in some region as like Figure 3.3. Let's say $\dot{\rho} = 0$ at $\xi = \xi_1$ and $\xi = \xi_2$ ($\xi_2 > \xi_1$). Then, $\rho_1 = \rho(\xi_1) > \rho_2 = \rho(\xi_2)$.

$$\int_{\xi_1}^{\xi_2} \frac{d}{d\xi}\left(\frac{1}{2}\dot{\phi}^2 - U\right) d\xi = \int_{\xi_2}^{\xi_1} \frac{d}{d\xi}\left(U - \frac{1}{2}\dot{\phi}^2\right) d\xi = \left(U - \frac{1}{2}\dot{\phi}^2\right)\Big|_{\xi=\xi_1} - \left(U - \frac{1}{2}\dot{\phi}^2\right)\Big|_{\xi=\xi_2}. \tag{3.35}$$

This can be evaluated by two different ways. The constraint at $\dot{\rho} = 0$ implies

$$\left(U - \frac{1}{2}\dot{\phi}^2\right)\Big|_{\xi=\xi_1} - \left(U - \frac{1}{2}\dot{\phi}^2\right)\Big|_{\xi=\xi_2} = \frac{3}{\kappa}\left(\frac{1}{\rho_1^2} - \frac{1}{\rho_2^2}\right) < 0 \quad (\because \rho_1 > \rho_2). \tag{3.36}$$

By integrating Equation (3.30), we found

$$\int_{\xi_1}^{\xi_2} \frac{d}{d\xi}\left(\frac{1}{2}\dot{\phi}^2 - U\right) d\xi = -\int_{\xi_1}^{\xi_2} \frac{3\dot{\rho}}{\rho}\dot{\phi}^2 d\xi > 0 \quad (\because \dot{\rho} < 0). \tag{3.37}$$

These results lead to a contradiction. This means the manifold is closed in the case of $dS \to AdS$ tunneling. This also verifies that the boundary condition (3.23) can be determined only for the false vacuum since the true vacuum cannot be the state at $\xi \to \infty$. Even though there is subtlety in defining the energy in curved space, if an open space is filled with the true vacuum after tunneling, there must be a serious problem. The energy issue also directly came out by taking the Newtonian

	$dS \to dS$	$dS \to AdS$	$AdS \to AdS$
Potential	$U_f > 0$, $U_t > 0$	$U_f > 0$, $U_t < 0$	$U_f < 0$, $U_t < 0$
Manifold	closed	closed	open
True→False	always possible	possible but cannot be thermally assisted from the pure true vacuum	impossible

Table 3.1: The three cases of CdL bounces.

limit. In the context of the thin-wall approximation, it is possible to change the topology of the manifold after the tunneling but it is only within the confines of the approximation. If there is such a solution, the tunneling rate B diverges so it becomes meaningless. However, we showed that it does not exist. If the vacuum is on $U_0 = 0$, it represents a flat spacetime. We can treat this case as the limit of $\Lambda_0 \to \infty$ in the AdS geometry.

We checked the field has to be near the true vacuum at $\xi = 0$ if the manifold is open. For a closed manifold, the field can be initially at either false or true vacuum because the geometries of both solutions are connected by the rotational symmetry. However, each case has a different interpretation. If the system is on the true vacuum initially, then it cannot tunnel to the false vacuum in flat space because of the conservation of the energy. However, the true vacuum is able to tunnel to the false vacuum if the manifold is closed in the presence of the gravity due to the finiteness of the spacetime[18]. The tunneling amplitude of the true to false decay is given by

$$B_{t\to f} = S_E[b] - S_E[\phi_t], \tag{3.38}$$

and the ratio of the decay rates is

$$\frac{e^{-B_{t\to f}}}{e^{-B_{f\to t}}} = e^{-S_E[\phi_f]+S_E[\phi_t]} \sim e^{1/U_f - 1/U_t} < 1. \tag{3.39}$$

The decay rate is smaller than the decay from false to true but it is finite. The true to false decay has a different picture from an ordinary tunneling case. Because a false vacuum bubble, if it exists, cannot be surrounded by the true vacuum, the true vacuum part remains inside the bubble and the outside of the bubble tunnels to the false vacuum. The solution where the field (ϕ) starts from the false vacuum at $\xi = 0$ can be interpreted as the decay from true vacuum to false

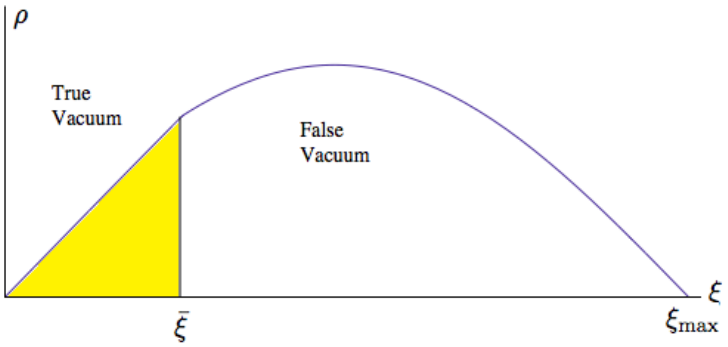

(a) False to True tunneling.

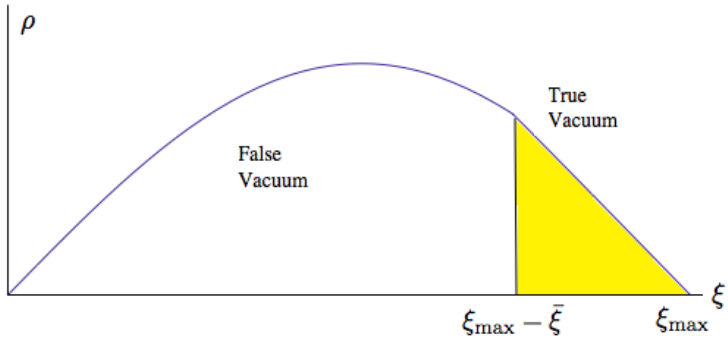

(b) True to False tunneling.

Figure 3.4: In a closed manifold, it is possible to find the solution (b) from the solution (a) because these two solutions are connected by the rotational symmetry of the manifold. If the spacetime is not finite, the symmetry does not exist so ϕ has to be at the true vacuum at $\xi = 0$. The picture (b) implies the true to false tunneling process.

vacuum. This decay process can be understood more precisely with the thermal interpretation of a CdL bounce. In the case of $U_t < 0$ and $U_f > 0$, the true to false tunneling would be possible if the initial state is thermally overexcited. However, the probability to be overexcited from the pure true vacuum is zero ($e^{-S_E[\text{initial}]+S_E[\phi_t]} = 0$) so it turns out to be impossible[1].

It is possible to obtain the tunneling exponent B in curved space since it is found by a semi-classical way. However, it is not easy to calculate the prefactor A exactly in the Coleman-de Luccia action because the mode spectrum has many(or infinite) negative modes if the gravitational effects get stronger. We will discuss more details about this in Chapter 7.

[1]See Chapter 5 for more details

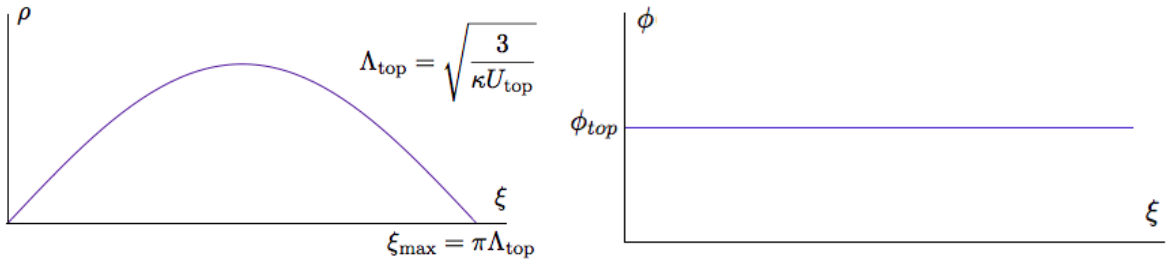

(a) ρ graph (b) ϕ graph

Figure 3.5: Hawking-Moss solution.

There is another type of solution as known as the Hawking-Moss solution[16]. It is the most trivial solution such that the field is a constant all over the spacetime and tunnels *homogeneously*,

$$\phi(\xi, \vec{x}) = \phi_{\text{top}}. \tag{3.40}$$

For a HM solution, ϕ is a constant all over the space-time.

In flat space, this kind of solution also satisfies the field equation (2.27) . However, it cannot be a real solution because it cannot cover the infinitely large spacetime with the same energy. In the same way, the HM solution exists only in a de Sitter space background. Furthermore, it is also possible to tunnel from the true vacuum to the HM case. The tunneling exponent is

$$B = S_E[\phi_{\text{top}}] - S_E[\phi_0] = \frac{24\pi^2}{\kappa^2}\left(\frac{1}{U_0} - \frac{1}{U_{\text{top}}}\right). \tag{3.41}$$

The HM solution can only exist in a de Sitter background since B should not diverge.

A HM solution always exists if $U_f > 0$ since it is a trivial solution. Especially, if

$$\Lambda_{\text{top}}^2 \cdot |U''(\phi_{\text{top}})| < 4, \tag{3.42}$$

the $O(4)$ symmetric CdL solution may not exist. If the top of the potential gets flatter, the field at $\xi = 0$ ($\phi(0)$) gets higher in order to compensate the time loss around the top since the field stays longer around the top.

Chapter 4

Thin-wall approximation

We have studied many properties of the vacuum tunneling process. Except for trivial solutions like the Hawking-Moss case, it is not possible to find an exact analytical solution. However, it would be helpful to understand the structure of the tunneling problems better if we can solve the field equation analytically with a proper approximation. The thin-wall approximation is the only way to find an approximate analytic solution. Let us investigate the thin-wall approximation more precisely.

4.1 Flat space

First of all, consider tunneling without gravity. Imagine a bounce solution which looks like Figure 4.1. If $\Delta\rho \gg \bar{\rho}$, we can approximately assume the field behaves like a step function,

$$\phi(\rho) = \begin{cases} \phi_t & \text{if } \rho < \bar{\rho} - \Delta\rho/2, \\ \phi_w(\rho) & \text{if } \bar{\rho} - \Delta\rho/2 < \rho < \bar{\rho} + \Delta\rho/2, \\ \phi_f & \text{if } \rho > \bar{\rho} + \Delta\rho/2, \end{cases} \tag{4.1}$$

$$\phi'(\rho) = \begin{cases} 0 & \text{if } \rho < \bar{\rho} - \Delta\rho/2, \\ \phi'_w(\rho) & \text{if } \bar{\rho} - \Delta\rho/2 < \rho < \bar{\rho} + \Delta\rho/2, \\ 0 & \text{if } \rho > \bar{\rho} + \Delta\rho/2. \end{cases} \tag{4.2}$$

The field satisfies the field equation (2.27) on the wall but the second term is negligible if

Figure 4.1: The thin-wall approximation is valid if $\Delta\rho \ll \bar{\rho}$ where $\bar{\rho}$ is the location of the wall and $\Delta\rho$ is the width of the wall.

$\bar{\rho} \gg \Delta\rho$,

$$U' = \phi_w''(\rho) + \frac{3}{\rho}\phi_w'(\rho) \approx \phi_w''(\rho). \tag{4.3}$$

This fact makes the action on the wall simpler. Define S_1 as the one-dimensional action of the wall,

$$S_1 \equiv \int_{\bar{\rho}-\Delta\rho/2}^{\bar{\rho}+\Delta\rho/2} d\rho \left(\frac{1}{2}\phi'^2 + U[\phi]\right). \tag{4.4}$$

The action on the wall is given by

$$S_{\text{wall}} = 2\pi^2 \int_{\bar{\rho}-\Delta\rho/2}^{\bar{\rho}+\Delta\rho/2} d\rho\rho^3 \left(\frac{1}{2}\phi'^2 + U[\phi]\right) \approx 2\pi^2\bar{\rho}^3 \int_{\bar{\rho}-\Delta\rho/2}^{\bar{\rho}+\Delta\rho/2} d\rho \left(\frac{1}{2}\phi'^2 + U[\phi]\right) = 2\pi^2\bar{\rho}^3 S_1. \tag{4.5}$$

The tunneling component B with the thin-wall approximation is written by

$$B = S_E[b] - S_E[\phi_f] = 2\pi^2\bar{\rho}^3 S_1 - \frac{1}{2}\pi^2\bar{\rho}^4\epsilon, \quad (\epsilon \equiv U[\phi_f] - U[\phi_t]). \tag{4.6}$$

For given S_1 and ϵ, the size of the wall ($\bar{\rho}$) is where the bounce action ($S_E[b]$) becomes the maximum[1]. Since $S_E[\phi_f]$ is a constant, this condition is the same as

$$\frac{dB[\bar{\rho}; S_1, \epsilon]}{d\bar{\rho}} = 6\pi^2\bar{\rho}^2 S_1 - 2\pi^2\bar{\rho}^3\epsilon = 0. \tag{4.7}$$

The radius of the wall in the thin-wall approximation turns out to be

$$\bar{\rho} = \frac{3S_1}{\epsilon}. \tag{4.8}$$

[1]The existence of a negative mode implies it has to be the maximum.

This is the solution which is on the saddle point of the action in the configuration space. However, the second derivative of the action,

$$\frac{d^2B}{d\bar{\rho}^2} = -\frac{18\pi^2 S_1^2}{\epsilon} < 0, \tag{4.9}$$

is negative. This means that the solution is on an unstable state and there is a negative mode in the system.

Let us check the validity of the approximation. Like the term *thin-wall*, this approximation is valid where the thickness of the wall is much smaller than any other length parameters. The size of the wall ($\bar{\rho}$) is the only length parameter and we checked the tunneling amplitude B with the thin-wall approximation (4.6) can be derived under the condition,

$$\bar{\rho} \gg \Delta\rho. \tag{4.10}$$

The width of the wall satisfies

$$\Delta\rho \sim \frac{\Delta\phi}{\sqrt{\Delta U}} \gg \bar{\rho} = \frac{3S_1}{\epsilon} \tag{4.11}$$

where $\phi'^2_w \sim U - U_f = \Delta U$. If the potential does not have an extreme peak, we can assume every parameter from the potential except ϵ has a similar mass scale,

$$\Delta\phi \sim (\Delta U)^{1/4} \sim (S_1)^{1/3} \sim m. \tag{4.12}$$

This showed the thin-wall approximation is valid if the difference between the two vacua is much smaller than the mass scale of the potential,

$$\epsilon \ll m^4 \sim \Delta U. \tag{4.13}$$

4.2 Curved space

The next step is investigating the thin-wall approximation in curved space. Because there are more parameters in this case, the validity condition is also more complicated, and the field and the metric are written in terms of the ξ-coordinate. The size of the wall ($\bar{\rho}$) is given by $\bar{\rho} = \rho(\bar{\xi})$. The physical width of the wall, if it is well-defined, is $\Delta\rho = \rho(\bar{\xi} + \Delta\xi/2) - \rho(\bar{\xi} - \Delta\xi/2) \approx \dot{\rho}\Delta\xi$. Here, $\bar{\xi}$ is the location of the wall and $\Delta\xi$ is the width of the wall in the ξ-coordinate.

As in flat space, the field in the thin-wall approximation is given by

$$\phi(\xi) = \begin{cases} \phi_t & \text{if } 0 < \xi < \bar{\xi} - \Delta\xi/2, \\ \phi_w(\xi) & \text{if } \bar{\xi} - \Delta\xi/2 < \xi < \bar{\xi} + \Delta\xi/2 \\ \phi_f & \text{if } \xi > \bar{\xi} + \Delta\xi/2, \end{cases} \tag{4.14}$$

$$\dot{\phi}(\xi) = \begin{cases} 0 & \text{if } 0 < \xi < \bar{\xi} - \Delta\xi/2, \\ \dot{\phi}_w(\xi) & \text{if } \bar{\xi} - \Delta\xi/2 < \xi < \bar{\xi} + \Delta\xi/2, \\ 0 & \text{if } \xi > \bar{\xi} + \Delta\xi/2. \end{cases} \tag{4.15}$$

Strictly speaking, $\phi(\xi)$ is not on the exact ϕ_t nor ϕ_f in curved space, so we can treat ϕ_t and ϕ_f as the beginning point and the end point of the field, respectively. Note that the end point is the exact ϕ_f if the manifold is open.

The field on the wall also satisfies the field equation but the second term is negligible if $\bar{\rho} \gg \Delta\rho \approx \dot{\rho}\Delta\xi$,

$$U' = \ddot{\phi}_w + \frac{3\dot{\rho}}{\rho}\dot{\phi}_w \approx \ddot{\phi}_w + \frac{3\dot{\rho}}{\bar{\rho}}\dot{\phi}_w \approx \ddot{\phi}_w. \tag{4.16}$$

With this condition, the field obeys that

$$\frac{1}{2}\dot{\phi}_w^2 + U[\phi_w] = U[\phi_0]. \tag{4.17}$$

Here, ϕ_0 is the initial value of ϕ. Define the one-dimensional action on the wall by

$$S_1 = \int_{\bar{\xi}-\Delta\xi/2}^{\bar{\xi}+\Delta\xi/2} \left(\frac{1}{2}\dot{\phi}^2 + U[\phi] - U[\phi_0] \right) d\xi = \int_{\bar{\xi}-\Delta\xi/2}^{\bar{\xi}+\Delta\xi/2} 2\left(U[\phi] - U[\phi_0]\right) d\xi. \tag{4.18}$$

Let us assume that the field is in the true vacuum at $\xi = 0$, the false to true vacuum tunneling[2]. Then, $\phi_0 = \phi_f$ in the previous formula. By using Equation (3.13), the tunneling exponent B on the wall ($B = S_E[b] - S_E[\phi_f]$) is given by

$$B_{\text{wall}} = 4\pi^2 \int_{\text{wall}} \rho^3 \left(U - U[\phi_f]\right) d\xi = 2\pi^2 \bar{\rho}^3 \int_{\text{wall}} 2\left(U - U[\phi_f]\right) d\xi = 2\pi^2 \bar{\rho}^3 S_1. \tag{4.19}$$

The part inside the wall contributes to B,

$$B_{\text{in}} \quad = \quad \int_0^{\bar{\rho}} d\rho \frac{1}{\dot{\rho}} \left(\rho^3 U[\phi_t] - \frac{3\rho}{\kappa} \right) - (\phi_t \to \phi_f)$$

[2]For a true to false vacuum case, the calculations of B are still valid because both cases have the same bounce configuration but different initial states.

$$\because \dot{\rho} = \cos\left(\frac{\xi}{\Lambda}\right) = \left(1 - \sin^2\left(\frac{\xi}{\Lambda}\right)\right)^{1/2} = \left(1 - \frac{\rho^2}{\Lambda^2}\right)^{1/2}$$
$$= -\frac{4\pi^2\Lambda_f^2}{\kappa}\left[\left(1 - \frac{\bar{\rho}^2}{\Lambda_f^2}\right)^{3/2} - 1\right] + \frac{4\pi^2\Lambda_t^2}{\kappa}\left[\left(1 - \frac{\bar{\rho}^2}{\Lambda_t^2}\right)^{3/2} - 1\right]. \quad (4.20)$$

Note that $\dot{\rho} = \cosh(\xi/\Lambda) = (1 - \rho^2/\Lambda^2)^{1/2}$ for an open manifold. The above result is still true if we define $\Lambda^2 = \frac{3}{\kappa U}$ in both open and closed cases.

When calculating the outside of the wall, there are two different cases. In Equation (4.20), $\dot{\rho}$ is always positive inside the wall but it can be negative in some regions outside the wall in the case of the de Sitter background or always negative if $\dot{\rho}$ is negative right after passing the wall. If ρ still increases after the wall ($\dot{\rho} > 0$), it is an intuitively acceptable case and the true vacuum bubble is surrounded by the false vacuum region. This solution is called by a type A bounce. On the contrary, if ρ starts to decrease after the wall ($\dot{\rho} < 0$), there is a subtlety in defining the outside of the wall physically so the geometry of this bounce needs to be specified carefully. We shall see the physical interpretation of this bounce in Chapter 5. This solution is known as a type B bounce. There are also types C and D bounces but they do not satisfy the equation of motion (3.11), so we do not have to count them in.[19–21]

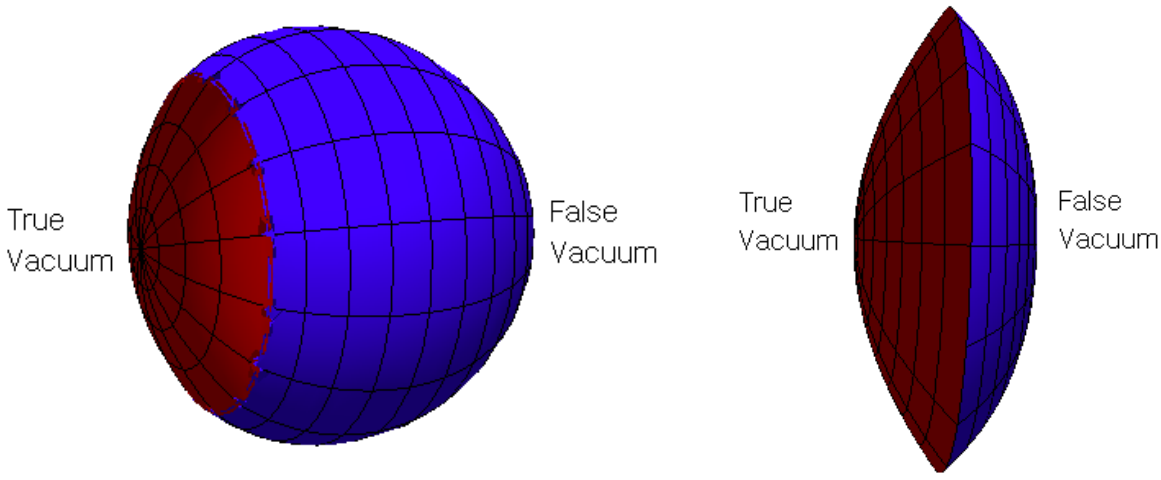

(a) Type A bounce (b) Type B bounce

Figure 4.2: Two different solutions in curved space.

The decay exponent B for the outside the wall is

$$B_{\text{out}} = \begin{cases} 0 & \text{for type A,} \\ \frac{8\pi^2\Lambda_f^2}{\kappa}\left(1-\frac{\bar{\rho}^2}{\Lambda_f^2}\right)^{3/2} & \text{for type B.} \end{cases} \tag{4.21}$$

In the case of type A, the outside of the wall is the same as the part in a pure false vacuum so it is canceled out. However, a type B bounce does not contain the region from the first $\rho = \bar{\rho}$ point to the second $\rho = \bar{\rho}$ point so it gives a non-trivial contribution.

Summing everything up, we can find that B in the thin-wall approximation is given by

$$B[\bar{\rho}] = S_E[b] - S_E[\phi_f] = 2\pi^2\bar{\rho}^3 S_1 + \frac{4\pi^2\Lambda_f^2}{\kappa}\left[\mp\left(1-\frac{\bar{\rho}^2}{\Lambda_f^2}\right)^{3/2}+1\right] + \frac{4\pi^2\Lambda_t^2}{\kappa}\left[\left(1-\frac{\bar{\rho}^2}{\Lambda_t^2}\right)^{3/2}-1\right], \quad (- : \text{type A}\ ,\ + : \text{type B}). \tag{4.22}$$

This formula is valid for both open and closed cases but there is no type B solution if the manifold is open because a type B solution has a maximum of ρ. It is possible to check that B becomes negative if type B solutions exist for an open manifold ($\Lambda_f^2 < 0$), so this fact also implies that type B bounces are allowed in only de Sitter backgrounds.

The tunneling from the true vacuum to the false vacuum is also possible if the true vacuum is positive ($U_t > 0$). In this case, the tunneling exponent B is also always positive for both cases,

$$B[\bar{\rho}] = S_E[b] - S_E[\phi_t] = 2\pi^2\bar{\rho}^3 S_1 + \frac{4\pi^2\Lambda_f^2}{\kappa}\left[\mp\left(1-\frac{\bar{\rho}^2}{\Lambda_f^2}\right)^{3/2}-1\right] + \frac{4\pi^2\Lambda_t^2}{\kappa}\left[\left(1-\frac{\bar{\rho}^2}{\Lambda_t^2}\right)^{3/2}+1\right] > 0, \quad (- : \text{type A}\ ,\ + : \text{type B}). \tag{4.23}$$

The size of the bubble is determined by where the action of the bounce is stationary.

$$\frac{dB}{d\bar{\rho}} = 6\pi^2\bar{\rho}^2 S_1 + \frac{12\pi^2\bar{\rho}}{\kappa}\left[\pm\left(1-\frac{\bar{\rho}^2}{\Lambda_f^2}\right)^{1/2} - \left(1-\frac{\bar{\rho}^2}{\Lambda_t^2}\right)^{1/2}\right] = 0, \quad \text{at the solution } \bar{\rho}. \tag{4.24}$$

The solution is found to be

$$\boxed{\frac{1}{\bar{\rho}^2} = \frac{1}{\Lambda_f^2} + \left(\frac{\epsilon}{3S_1} - \frac{\kappa S_1}{4}\right)^2 = \frac{1}{\Lambda_t^2} + \left(\frac{\epsilon}{3S_1} + \frac{\kappa S_1}{4}\right)^2,} \tag{4.25}$$

with the conditions

$$\frac{\epsilon}{3S_1} > \frac{\kappa S_1}{4}, \quad \text{for type A,}$$

$$\frac{\epsilon}{3S_1} < \frac{\kappa S_1}{4}, \quad \text{for type B.} \tag{4.26}$$

We can see that only type A bounces are allowed in the weak gravity limit. This is not surprising, because the geometry of a type A bounce around the bubble is similar to the flat space case. The term $\frac{\epsilon}{3S_1}$ is the inverse of the size of the bubble in flat space. If the size gets big enough to be comparable with the Planckian scale, then the type B bounce starts to appear.

The second derivative of the action is

$$\begin{aligned}
\frac{d^2B}{d\bar{\rho}^2} &= 12\pi^2\bar{\rho}S_1 + \frac{12\pi^2}{\kappa}\left[\pm\left(1-\frac{\bar{\rho}^2}{\Lambda_f^2}\right)^{1/2} - \left(1-\frac{\bar{\rho}^2}{\Lambda_t^2}\right)^{1/2}\right] \\
&\quad -\frac{12\pi^2}{\kappa}\left[\pm\frac{\bar{\rho}^2}{\Lambda_f^2}\left(1-\frac{\bar{\rho}^2}{\Lambda_f^2}\right)^{-1/2} - \frac{\bar{\rho}^2}{\Lambda_t^2}\left(1-\frac{\bar{\rho}^2}{\Lambda_t^2}\right)^{-1/2}\right] \\
&= \frac{12\pi^2}{\kappa}\left[\mp\left(1-\frac{\bar{\rho}^2}{\Lambda_f^2}\right)^{-1/2} + \left(1-\frac{\bar{\rho}^2}{\Lambda_t^2}\right)^{-1/2}\right] \\
&\quad \begin{cases} < 0 : \text{ type A}, \\ > 0 : \text{ type B}. \end{cases}
\end{aligned} \tag{4.27}$$

This is also true for either open or closed manifold. The action of a type A bounce is at a maximum in terms of $\bar{\rho}$ and it should be at a saddle point in the whole configuration space. This facts implies the existence of a negative mode in the system. However, a type B bounce is at the minimum as a function of $\bar{\rho}$ so it does not guarantee a negative mode, but this fact does not prove that there is no negative mode in the system because there could be another way to lower the action in the configuration space. We will study various topics about negative modes later on.

Let us check the validity of the thin-wall approximation in curved space. For either a type A or a type B bounce, the following conditions are always satisfied in a de Sitter background,

$$\Delta\rho = \dot{\rho}\Delta\xi < \Delta\xi, \quad \bar{\rho} < \bar{\xi} < \xi_{\max}. \tag{4.28}$$

This implies that the thin-wall approximation condition is $\Delta\xi \ll \bar{\rho}$. As in the flat space case, $\Delta\xi$ is approximately given by $\Delta\xi \sim \frac{\Delta\phi}{\sqrt{\Delta U}} \sim \frac{1}{m}$ if the potential obeys the condition (4.12). In the weak gravity limit, $\bar{\rho} \approx \frac{3S_1}{\epsilon}$. Thus, the validity condition is the same as in flat space (4.13),

$$\epsilon \ll m^4 \sim \Delta U. \tag{4.29}$$

	open	closed		flat
mass scale	any scale	$m \ll m_{\rm pl}$	$m \sim m_{\rm pl}$	N/A
validity condition	$\epsilon \ll m^4$	$\epsilon \ll m^4$	$U_f \ll m^4$	$\epsilon \ll m^4$

Table 4.1: The validity condition of the thin-wall approximation under the assumption $\Delta\phi \sim (\Delta U)^{1/4} \sim (S_1)^{1/3} \sim m$. $U_f \ll m^4$ also leads $\epsilon < U_f \ll m^4$ as like the other cases.

However, if the gravity is not weak enough, the size of the bubble ($\bar{\rho}$) depends on the gravitational factor κ. It should be always smaller than the horizon size (Λ_f) but it can be comparable with it ($\bar{\rho} \sim \Lambda_f$). In order to obey $\Delta\xi \ll \bar{\rho}$,

$$\Delta\xi \sim \frac{1}{m} \ll \sqrt{\frac{1}{\kappa U_f}} \sim \frac{1}{m_f^2\sqrt{\kappa}} \quad \rightarrow \quad \frac{m_f^2}{m} \ll m_{\rm pl}. \tag{4.30}$$

Since we assume that the gravitational effect is not weak, the mass scale of the potential can be comparable with the Planck scale ($m \sim m_{\rm pl}$). This means '$m_f \ll m$' and '$U_f \ll U_{\rm top}$'. If $U_f \ll U_{\rm top}$, then $\epsilon < U_f \ll U_{\rm top}$ so it leads to the same condition as Equation (4.29). Let us check the condition that the size of the bubble becomes comparable with the horizon regardless of the scale of the potential. According to Equation (4.25), the condition is given by

$$\epsilon \approx \frac{3\kappa S_1^2}{4} \sim \frac{m^6}{m_{\rm pl}^2} \sim \left(\frac{m}{m_{\rm pl}}\right)^2 \cdot m^4. \tag{4.31}$$

If $m \sim m_{\rm pl}$, then $\epsilon \sim m^4$. It seems that it does not need a very small ϵ but the width of the wall ($\Delta\xi$) is also comparable with the other length parameters so the thin-wall approximation breaks down and it becomes a thick-wall case. If $m \ll m_{\rm pl}$, then $\epsilon \ll m^4$ which is the same as the thin-wall condition (4.13).

In an open manifold, the size of the bubble ($\bar{\rho}$) is always larger than the size of the bubble in flat space because the gravitational effects pulls the bubble out if the vacuum has negative energy, so the same condition as in flat space is applied ($\Delta\xi \ll \frac{3S_1}{\epsilon} < \bar{\rho}$). It is also possible to check this by

$$\frac{1}{\bar{\rho}^2} < \frac{1}{\bar{\rho}^2} - \frac{1}{\Lambda_f^2} = \left(\frac{\epsilon}{3S_1} - \frac{\kappa S_1}{4}\right)^2 < \left(\frac{\epsilon}{3S_1}\right)^2 \quad \rightarrow \quad \bar{\rho} > \frac{3S_1}{\epsilon}. \tag{4.32}$$

Chapter 5

Thermal aspects in vacuum tunneling

At the end of Chapter 3, we studied the Hawking-Moss solution. One can ask how such a static solution can represent a tunneling process which is supposed to be dynamical. This motivates us to study thermal aspects of vacuum tunneling[22]. Since every de Sitter space has its own temperature, the thermal aspects are unavoidable in the de Sitter space. In addition, we shall see that the HM solution is the case of a pure thermal tunneling.

5.1 Flat space

Before analyzing thermal tunneling in curved space, let us start from the flat space case. All the properties we studied in Chapter 2 are based in the setup of zero temperature. In the absence of temperature, the initial state has to be on the exact vacuum because there is no chance to be excited thermally. At non-zero temperature, the energy of the initial state (E) is distributed by the Boltzmann factor, $P(E) \sim e^{-\beta(E-E_0)}$, where $\beta \equiv \frac{1}{T}$ and E_0 is the energy of the vacuum. It is better to use E_0 instead of E_f because the true vacuum to the false vacuum decay as in the case in a de Sitter background is possible at finite temperature.

Because a state with a higher energy has more chances to tunnel into the other side, the decay rate at higher temperature should become larger and the tunneling exponent B for a higher energy state also has to get smaller. If tunneling occurs by thermal excitation, the thermal tunneling rate has to be proportional to the Boltzmann factor at the top which is the probability to reach the top

thermally,

$$\Gamma_{\text{thermal}} \sim e^{-\beta(E_{\text{top}}-E_0)}. \tag{5.1}$$

The real tunneling at non-zero temperature includes all the energy levels with the probability given by the Boltzmann factor. Therefore, the decay rate becomes the sum of them. Without the normalization factor, we can write

$$\Gamma = \sum_E e^{-\beta(E-E_0)}\Gamma[E] \sim \int_{E_0}^{E_{\text{top}}} dE e^{-\beta(E-E_0)} \cdot e^{-B(E)}. \tag{5.2}$$

We assume the exponential factor '$e^{-B(E)}$' changes much faster than the pre-factor in the decay rate '$A(E)$' here, so $A(E)$'s are not counted in. Furthermore, the dominant term comes from the energy E^* which maximizes the integrand, so the decay rate is

$$\Gamma \sim e^{-\beta(E^*-E_0)-B(E^*)}. \tag{5.3}$$

As we studied earlier, $B(E)$ in flat space is given by

$$B = \int_{\vec{x}_1}^{\vec{x}_2} d\vec{x}\sqrt{2m(V(\vec{x})-E)}, \tag{5.4}$$

where $\vec{x}_1$ and $\vec{x}_2$ are the points at $V(\vec{x}) = E$.

To maximize the integrand of the decay rate, we got

$$\frac{d}{dE}\left(\beta(E-E_0) + 2\int_{\vec{x}_1}^{\vec{x}_2} d\vec{x}\sqrt{2m(V(\vec{x})-E)}\right)\Bigg|_{E=E^*} = 0. \tag{5.5}$$

The solution is found as

$$\beta = -2\frac{d}{dE}\left(\int_{\vec{x}_1}^{\vec{x}_2} d\vec{x}\sqrt{2m(V(\vec{x})-E)}\right)\Bigg|_{E=E^*} = 2\int_{\vec{x}_1}^{\vec{x}_2} d\vec{x}\sqrt{\frac{m}{2(V(\vec{x})-E^*)}}. \tag{5.6}$$

Since we know the Euclidean equation of motion gives

$$\sqrt{\frac{2(V(\vec{x})-E^*)}{m}} = \left|\frac{d\vec{x}}{d\tau}\right|, \tag{5.7}$$

we can evaluate β by

$$\beta = 2\int_{\vec{x}_1}^{\vec{x}_2} d\vec{x}\sqrt{\frac{m}{2(V(\vec{x})-E^*)}} = 2\int_{\vec{x}_1}^{\vec{x}_2} d\vec{x}\left|\frac{d\tau}{d\vec{x}}\right| = 2(\tau_1-\tau_2) = \Delta\tau, \tag{5.8}$$

where τ_1 and τ_2 represent the Euclidean time at $\vec{x}_1$ and $\vec{x}_2$, respectively. This means β is one period of a bounce since it also takes the same time to bounce back to the initial point $\vec{x}_1$. Recall the

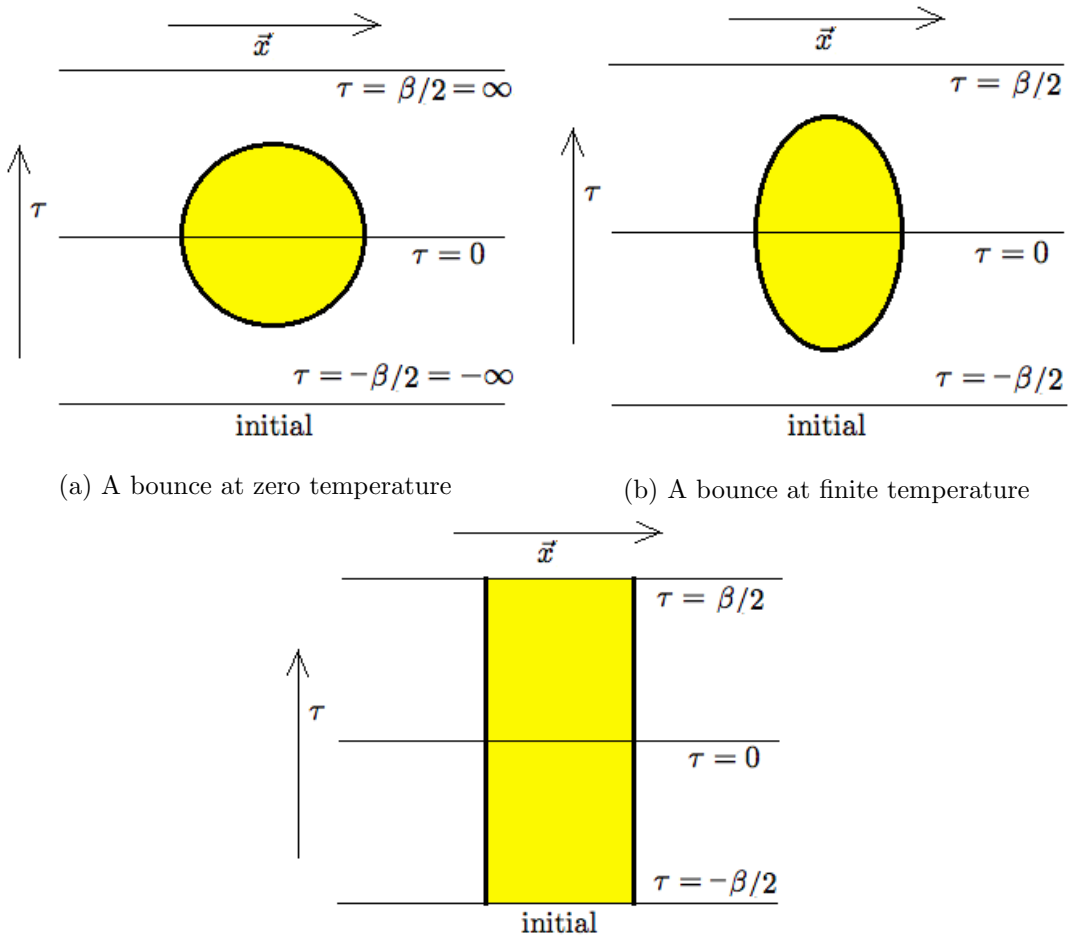

(a) A bounce at zero temperature

(b) A bounce at finite temperature

(c) A critical bubble

Figure 5.1: At zero temperature(a), the initial state is the pure false vacuum all over the region. The field configuration is $O(4)$ symmetric and the range of the Euclidean time is infinite ($\Delta\tau = \beta = 1/T$). At finite temperature(b), thermally excited states exist so it not the pure false vacuum everywhere. The range of the Euclidean time is finite and it is given by the temperature. If the temperature is sufficiently high, then it is thermally excited over the top of the potential and it forms a critical bubble(c).

boundary condition (2.29) in flat space. One period takes an infinite time at zero temperature but it is finite at non-zero temperature. We can also check the zero temperature limit ($\beta \to \infty$) also makes the period infinite ($\Delta\tau \to \infty$).

Now, we can evaluate the tunneling rate (5.3). By using Equation (5.8),

$$\beta(E^* - E_0) + 2\int_{\vec{x}_1}^{\vec{x}_2} d\vec{x}\sqrt{2m(V(\vec{x}) - E)} = \Delta\tau(E^* - E_0) + \int_0^{\Delta\tau} d\tau 2(V(\vec{x}) - E^*)$$
$$= \int_0^{\Delta\tau} d\tau\,(2V(\vec{x}) - E^*) - \int_0^{\Delta\tau} d\tau E_0 = S_E[b;T] - S_E[\phi_0;T] \tag{5.9}$$

Here, $S_E[b;T]$ is the bounce action of the energy E^* and $S_E[\phi_0;T]$ is the action for the initial pure vacuum ϕ_0 at finite temperature. Recall that $S_E = \int d\tau \left(\frac{1}{2}\dot{\vec{x}}^2 + V(\vec{x})\right) = \int d\tau(2V(\vec{x}) - E)$. The tunneling rate at finite temperature which has both thermal and quantum tunneling aspects is

$$\Gamma \sim e^{-S_E[b;T]-S_E[\phi_0;T]}. \tag{5.10}$$

This approach is also applicable to field theory. In field theory, the energy is given by

$$E = \int d^3x \left(\frac{1}{2}\dot{\phi}^2 + \frac{1}{2}(\nabla\phi)^2 + U[\phi]\right). \tag{5.11}$$

The optimal path E^* is also determined by minimizing the exponent as well. In order to make the energy finite, the thermally excited field configuration has to be localized. If it is excited all over the space, then the energy difference diverges.

$$E^* - E = \int d^3x\,(U^* - U_0) \to \infty. \tag{5.12}$$

Thus, the initial state cannot be a constant field configuration, and this is one reason there is no HM solution in flat space.

5.2 Curved space

The next step is investigating thermal aspects of the vacuum tunneling in curved space. There are two different topologies in curved space. A closed manifold is topologically equivalent to a Euclidean de Sitter space with the temperature,

$$T_{dS} = \frac{1}{\beta} = \frac{1}{2\pi\Lambda}. \tag{5.13}$$

It is not always possible to define the temperature of a generic closed manifold since it is not in thermal equilibrium. However, it cannot be also at the zero temperature so it naturally has unavoidable thermal aspects. On the contrary, the thermal properties are optional in an open

manifold, such as the case of flat space, so they do not show up at zero temperature. Let us consider only closed manifolds here.

We can start with a pure Euclidean de Sitter space. The field is in the vacuum all over the spacetime. The potential on the vacuum (ϕ_0) is positive ($U[\phi_0] > 0$) and the geometry is $O(5)$-symmetric. In the static patch coordinates, the range of the space is confined to the horizon and the metric is given by

$$ds^2 = d\xi^2 + \Lambda^2 \sin^2(\xi/\Lambda) d\Omega_3^2 = \left(1 - \frac{r^2}{\Lambda^2}\right) d\tau^2 + \left(1 - \frac{r^2}{\Lambda^2}\right)^{-1} dr^2 + r^2 d\Omega_2^2 = dx_i^2 \tag{5.14}$$

Tthis static patch space forms a 4-sphere with

$$\begin{aligned} x_1 &= r \sin\theta \cos\phi \\ x_2 &= r \sin\theta \sin\phi \\ x_3 &= r \cos\theta \\ x_4 &= -\sqrt{\Lambda^2 - r^2} \sin(\tau/\Lambda) \\ x_5 &= \sqrt{\Lambda^2 - r^2} \cos(\tau/\Lambda). \end{aligned} \tag{5.15}$$

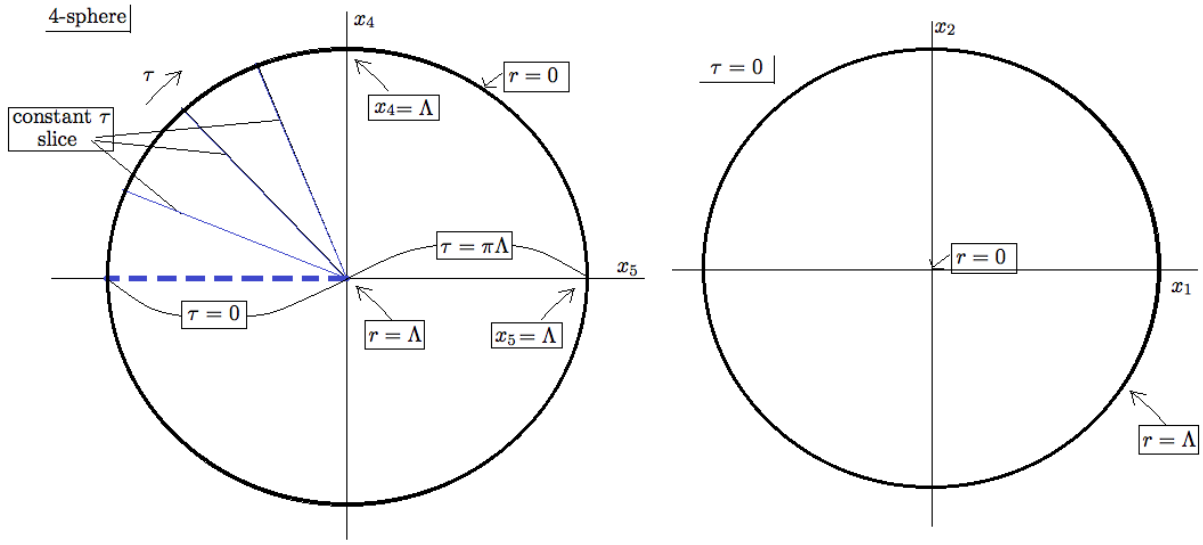

(a) Four-sphere given by (5.15)

(b) Three-ball by taking a constant τ slice

Figure 5.2: The figure (a) describes the metric (5.15). The figure (b) represents a three dimensional ball whose radius is the horizon. This is equivalent to the thick dashed blue line, a constant τ slice in (a).

The range of τ is $\tau = [0, 2\pi\Lambda)$ with the period $2\pi\Lambda$. The period is the same as $\beta = 1/T = \Delta\tau$ in flat space.

The horizon is located at $r = \Lambda$ and $x_4 = x_5 = 0$ and it is a 2-sphere ($x_1^2 + x_2^2 + x_3^2 = \Lambda^2$). This is τ-independent so every slice along a constant τ shares the same horizon. The center of the geometry is at $r = 0$, which is equivalent to $x_1 = x_2 = x_3 = 0$ and $x^4 + x^5 = \Lambda^2$. Each constant τ slice gives the configuration from the center ($r = 0$) to the horizon ($r = \Lambda$) in the static patch.

The Hawking-Moss solution has the same geometry as the pure vacuum case but the size of the horizon is $\Lambda_{\rm HM}$. The temperature $T = 1/(2\pi\Lambda_{\rm HM})$ is higher than the pure vacuum case. The initial state, the $\tau = 0$ slice, is acquired from the pure vacuum state by thermal excitation, and it has a homogenous configuration for a whole period, as in a critical bubble in flat space. This means this is the case of a pure thermal tunneling since it stays as it is after the thermal excitation. If the HM has a pure thermal nature, the tunneling amplitude is written by the form of

$$\Gamma_{\rm thermal} \sim e^{-\beta_{\rm HM} E_{\rm HM} + \beta_0 E_0}, \tag{5.16}$$

and it also has to be

$$\Gamma \sim e^{-S_E[\phi_{\rm top}] + S_E[\phi_0]}. \tag{5.17}$$

Let us check how these two different forms of the tunneling rate can coincide. The tunneling amplitude in thermal picture is somewhat complicated in curved space because the temperature is also affected by the geometry in de Sitter space. In other words, the only variable in flat space is the scalar field (ϕ), and the spacetime is fixed and independent from the temperature. However, the metric factor (ρ) is also a dynamical variable in curved space, and the structure of the spacetime also changes when the field varies. When the field is thermally excited, the temperature is also affected by the new field configuration. The energy is not well-defined in curved space so the Boltzmann factor is also hard to define. The probability to move to the energy E in flat space is given by the Boltzmann factor ($e^{-\beta(E-E_0)}$) but this has to be $e^{-\beta E + \beta_0 E_0}$ if the temperature of the excited state is well defined as β. If each state has a different temperature, the pre-factor has to be different but here we care about only the exponent term because it dominates the tunneling rate. In curved space, the Boltzmann factor is not of the form $e^{-\beta E}$ because the energy is ill-defined but it can be replaced by $e^{-S_E[E;\beta]}$. This is the result in quantum field theory at finite temperature which can be made without constructing the Hamiltonian's eigenstates. Thus, it is possible to use

this in the setup of quantum gravity.[1]

If β^* can be well-defined, the dominant term (E^*) in flat space would be given by

$$\Gamma \sim e^{-\beta^* E^* + \beta_0 E_0} e^{-B[E^*;\beta^*]} \sim (\text{Boltzmann factor}) \cdot e^{-B[E^*;\beta^*]}. \tag{5.18}$$

This is translated to the following in curved space,

$$\Gamma \sim e^{-S_E[\phi(\vec{x},0)]+S_E[\phi_0;\beta_0]} e^{S_E[b]-S_E[\phi(\vec{x},0)]} = e^{-(S_E[b]-S_E[\phi_0;\beta_0])} = e^{-B} \tag{5.19}$$

Since $S_E[\phi_0;\beta_0]$ is a constant, the dominant term comes from the saddle points of the bounce action ($S_E[b]$). This means the dominant term satisfies the Euler-Lagrange equation, so it is the same as the solution of the bounce and it is what we can expect.

The tunneling exponent B looks the same as in the result in Chapter 3 even though we include thermal effects here. Let us investigate more carefully. When $S_E[\phi_0]$ is subtracted from $S_E[b]$ in calculating B, $\phi = \phi_0$ point never appears in the configuration of the bounce because the initial point of the field $\phi(0)$ is slightly higher than the exact vacuum (ϕ_0) as in Figure 3.1, if the manifold is closed. The tunneling exponent B_{quantum} by quantum tunneling is

$$B_{\text{quantum}} = S_E[b] - S_E[\phi(\vec{x}, \tau = 0)], \tag{5.20}$$

but the initial configuration $S_E[\phi(\vec{x}, \tau = 0)]$ is obtained from the pure vacuum state by the probability of $e^{-B_{\text{thermal}}} = e^{-(S_E[\phi(\vec{x},\tau=0)]-S_E[\phi_0])}$ from the pure vacuum state. In Chapter 3, we just subtracted the initial pure vacuum state $S_E[\phi_0]$ from $S_E[b]$ without taking account of the initial state ($\tau = 0$) after the thermal excitation. As a consequence of the thermal process, we found the actual B as

$$B = B_{\text{quantum}} + B_{\text{thermal}} = S_E[b] - S_E[\phi_0]. \tag{5.21}$$

One can ask if the field starts from ϕ_1 ($U(\phi_1) > U(\phi_0)$), the part from ϕ_0 to ϕ_1 in the potential does not play any roles in tunneling process because the bounce is independent of the region. Although it does not affect the bounce action, it does contribute to the decay rate. The tunneling in a de Sitter background can be completely understood when we take account of the thermal aspects since it has its own temperature. This thermal point of views also explain why the field

[1]There is still the UV completeness problem in this setup of quantum gravity but that is the problem when we construct the Einstein-Hilbert action at the beginning. Let's assume the Hilbert space is well-defined here.

configuration cannot be on the exact vacuum in de Sitter background. Since a de Sitter space is at non-zero temperature, the optimal path to decay is always thermally excited. In the case of the HM bounce, B_{quantum} vanishes since there is no dynamics. It means the tunneling component B is given by $B = B_{\text{thermal}}$ for the HM case, and this fact does doublecheck that the HM bounce has a pure thermal nature.

We checked that CdL bounces in closed manifolds always have both quantum and thermal properties. The geometry of bounces is not $O(5)$-symmetric so the metric should be modified from Equation (5.15). Since it has an $O(4)$ symmetry, it is possible to choose the coordinates to form a 3-sphere with the radius $\rho(\xi)$ in the ξ-coordinate,

$$\begin{aligned} y_1^2 + y_2^2 + y_3^2 + y_5^2 &= \rho(\xi)^2, \\ dy_1^2 + dy_2^2 + dy_3^2 + dy_5^2 &= \rho(\xi)^2 d\Omega_3^2, \\ y_4 &= \xi. \end{aligned} \tag{5.22}$$

This choice of the coordinates is based on the $O(4)$ symmetry in terms of ξ so it is not adjusted to see the thermal picture the evolution through a τ-coordinate.

If the thin-wall approximation holds, then the true vacuum side is filled with the field slightly higher than the false vacuum so it has an approximately $O(5)$ symmetry locally. In this case, we can write the metric in the part of the false vacuum as

$$\begin{aligned} x_1 &= r\sin\theta\cos\phi \\ x_2 &= r\sin\theta\sin\phi \\ x_3 &= r\cos\theta \\ x_4 &= -\sqrt{\Lambda_f^2 - r^2}\sin(\tau/\Lambda_f) \\ x_5 &= \sqrt{\Lambda_f^2 - r^2}\cos(\tau/\Lambda_f). \end{aligned} \tag{5.23}$$

This is valid if $x_4 \subset (x_4$ of the false vacuum side). The size of the horizon in this case is almost the same as Λ_f for the type A case. There is also a true vacuum region inside the wall. The metric in the side of the true vacuum($x_4 \subset (x_4$ of the true vacuum side)) is modified as

$$\begin{aligned} \tilde{x}_4 &= -\sqrt{\Lambda_t^2 - r^2}\sin(\tilde{\tau}/\Lambda_t) \\ \tilde{x}_5 &= \sqrt{\Lambda_t - r^2}\cos(\tilde{\tau}/\Lambda_t). \end{aligned} \tag{5.24}$$

If the wall gets thicker, these coordinates cannot be applicable. However, the $O(4)$ symmetry still defines a 2-sphere as the horizon which is still shared for each τ slice, but the size of the horizon

(ρ_M) is always smaller than the horizon of the false vacuum ($\rho_M < \Lambda_f$) because the field is always higher than the false vacuum ($\phi(\vec{x}, \tau_0) > \phi_f$ for $\forall \vec{x}$) in at least one configuration of a constant τ and the gradient of the field also makes it more massive. In the case of type B, the horizon is located on the wall and it can be much smaller than Λ_f. We used $\tilde{\tau}$ in the true vacuum side since it is different from τ in the false vacuum. When a constant τ slice is taken from $r = 0$ to $r = \rho_M$, $\tilde{\tau}$ runs faster than τ. This happens because a CdL bounce is not in thermal equilibrium and it is also ambiguous how to choose a constant τ slice properly. We shall check these shortly.

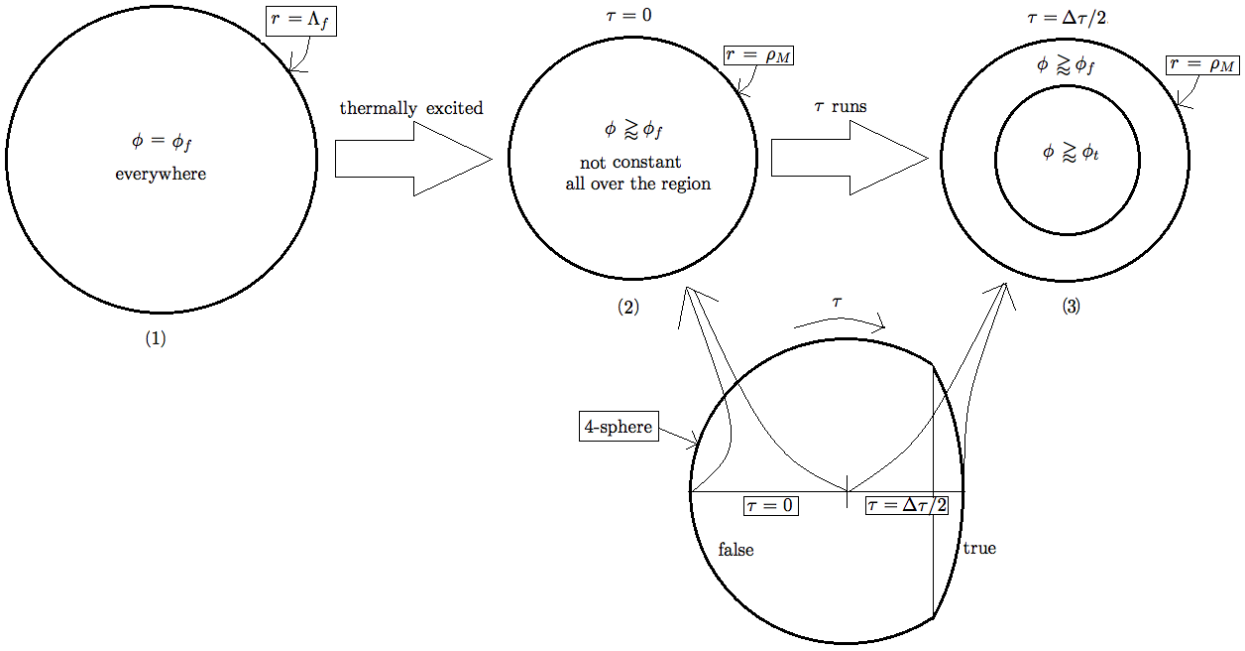

Figure 5.3: Interpretation of type A bounce. CdL bounces are interpreted in a thermal picture. Before the thermalization, the field is on the exact false vacuum (1). The initial state (2) is given by thermal fluctuations so the configuration of the field is not constant. This state tunnels into the state at $\tau = \Delta\tau/2$ (3).

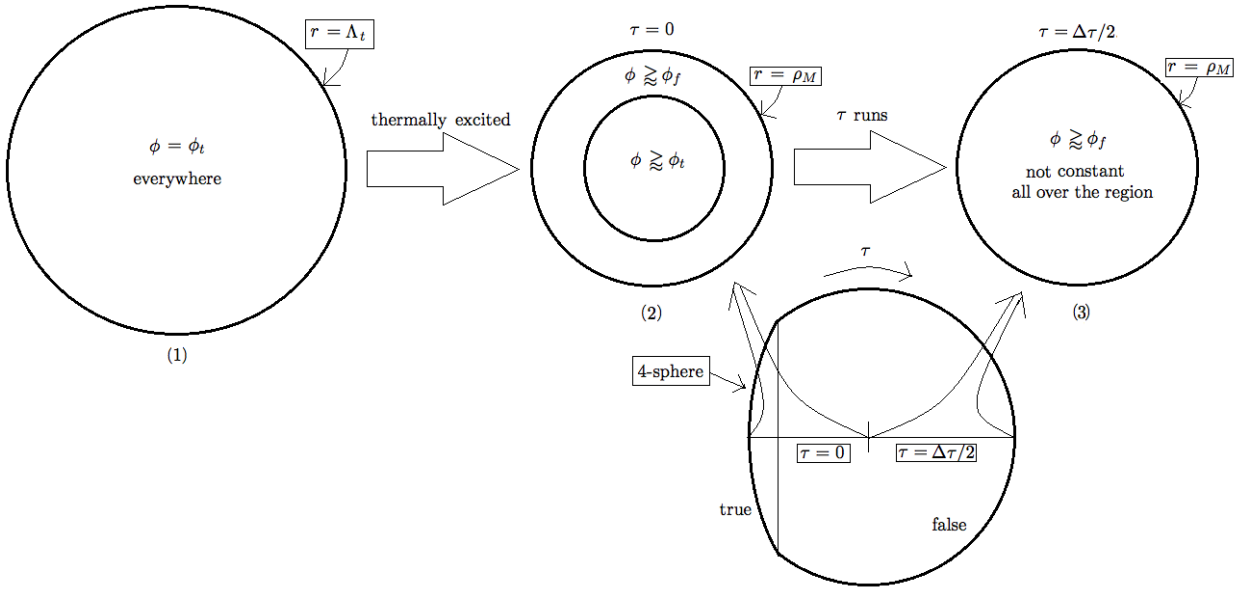

(a) Interpretation of True to False tunneling. The initial state is the case (3) in Figure 5.3. Then, it tunnels to the initial state of Figure 5.3.

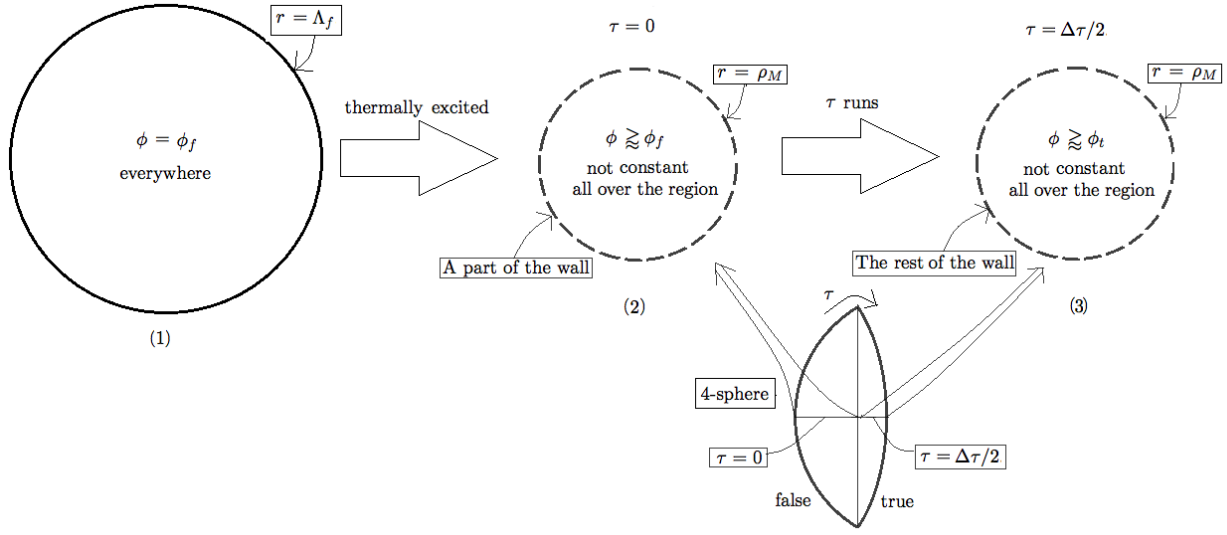

(b) Interpretation of type B bounce. The radius of a constant τ slice is given by ρ_M which is somewhat smaller than the horizon size of the false vacuum ($\rho_M < \Lambda_f$) and only a part of the wall is embedded around $r \lessapprox \rho_M$. We will study more details of interpretation of a type B bounce in Section 5.3.

Figure 5.4: Interpretation of True to False tunneling and type B bounce

5.3 Interpretation of the horizon

It is easy to check the existence of the horizon for the configuration of a constant ϕ such as a pure false vacuum and the HM case. For an ordinary bounce, the metric is not static so it is not a very straightforward result. Let us find a Schwarzchild-like metric when a bubble nucleates. At $\tau = 0$ and $\Delta\tau/2$, the field is static everywhere, $\frac{d\phi}{d\tau} = \frac{d\phi}{dt} = 0$. It is known that if the mass density is static and spherically symmetric the metric is given by the form of the following metric[23],

$$ds^2 = -e^{2\phi}dt^2 + \frac{1}{1 - \frac{2GM(r)}{r}}dr^2 + r^2 d\Omega_2^2. \tag{5.25}$$

If the mass density is constant everywhere, this metric describes a de Sitter space and $e^{2\phi} = 1 - \frac{2GM(r)}{r} = 1 - \frac{r^2}{\Lambda^2}$. The mass density of an ordinary CdL bounce is not constant so it cannot be an exact de Sitter space, but the horizon still exists where $1 - \frac{2GM(r)}{r} = 0$.

First of all, let us check the horizon in the setup of the thin-wall approximation. The integrated mass at the radius r is defined by

$$M(r) = 4\pi \int_0^r r^2 U(r) dr + 4\pi \int_{\text{wall}} r^2 \left(\frac{1}{2}\phi'^2 + U(r)\right) dr \quad \text{at } t = 0, \tag{5.26}$$

$$M(r) = \begin{cases} \frac{4\pi}{3} r^3 U_t & \text{if } 0 < r < \bar{\rho} \\ \frac{4\pi}{3}\bar{\rho}^3 U_t + \frac{4\pi}{3}\left(r^3 - \bar{\rho}^3\right) U_f + 4\pi\bar{\rho}^2 \mathcal{M}_{\text{wall}} & \text{if } \bar{\rho} < r. \end{cases} \tag{5.27}$$

For a type A solution, the horizon has to be located at $r = \Lambda_f$,

$$1 - \frac{2GM(r)}{r} = 1 - \frac{\kappa M(r)}{4\pi r} = 0 \quad \text{at } r = \Lambda_f. \tag{5.28}$$

Since $\frac{\partial\phi}{\partial t} = \frac{\partial\phi}{\partial\tau} = 0$ at $t = 0$, the $\mathcal{M}_{\text{wall}}$ in the ξ-coordinate is

$$\mathcal{M}_{\text{wall}} = \int_{\text{wall}} dr \left(\frac{1}{2}\phi'^2 + U(r)\right) = \int_{\text{wall}} \left|\frac{dr}{d\xi}\right| d\xi \left(\frac{1}{2}\dot{\phi}^2 + U(\phi(\xi))\right) \quad \text{at } t = 0. \tag{5.29}$$

Even though the wall is infinitely thin, the Jacobian factor is not constant on the wall. At the beginning of the wall, it is given by the curvature of the true vacuum but the curvature of the false vacuum determines it at the end of the wall,

$$\left|\frac{dr}{d\xi}\right|_{\text{begin}} = \sqrt{1 - \frac{\bar{\rho}^2}{\Lambda_t^2}}, \quad \left|\frac{dr}{d\xi}\right|_{\text{end}} = \sqrt{1 - \frac{\bar{\rho}^2}{\Lambda_f^2}}. \tag{5.30}$$

Since we don't know the exact Jacobian factor on the wall in the thin-wall approximation, we can take the leading order of the Jacobian as the average of each ends in order to complete the integration of $\mathcal{M}_{wall}$. Up to the leading order, we find

$$\begin{aligned}\mathcal{M}_{\rm wall} &= \int_{\rm wall}\left|\frac{dr}{d\xi}\right| d\xi\left(\frac{1}{2}\dot{\phi}^2+U(r)\right)\\ &= \frac{1}{2}\left(\sqrt{1-\frac{\bar{\rho}^2}{\Lambda_t^2}}+\sqrt{1-\frac{\bar{\rho}^2}{\Lambda_f^2}}\right)\cdot\int_{\rm wall}d\xi\left(\frac{1}{2}\dot{\phi}^2+U(\phi(\xi))\right)\\ &= \frac{1}{2}\left(\sqrt{1-\frac{\bar{\rho}^2}{\Lambda_t^2}}+\sqrt{1-\frac{\bar{\rho}^2}{\Lambda_f^2}}\right)S_1. \end{aligned} \tag{5.31}$$

Plugging $\mathcal{M}_{\rm wall}$ into Equation (5.28), we can find

$$\frac{\epsilon\bar{\rho}}{3}=\frac{1}{2}\left(\sqrt{1-\frac{\bar{\rho}^2}{\Lambda_t^2}}+\sqrt{1-\frac{\bar{\rho}^2}{\Lambda_f^2}}\right)S_1. \tag{5.32}$$

The solution of this equation for type A case $\left(\frac{\epsilon}{3S_1}>\frac{\kappa S_1}{4}\right)$ is the same as the $\bar{\rho}$ equation (4.25),

$$\frac{1}{\bar{\rho}^2}=\frac{1}{\Lambda_f}+\left(\frac{\epsilon}{3S_1}-\frac{\kappa S_1}{4}\right)^2=\frac{1}{\Lambda_t}+\left(\frac{\epsilon}{3S_1}+\frac{\kappa S_1}{4}\right)^2. \tag{5.33}$$

We can see here that taking the leading order in $\mathcal{M}_{\rm wall}$ is a valid approximation while the thin-wall approximation holds.

By using the analysis for type A, it is possible to investigate the type B case. Consider the $\epsilon=0$ case at first. Define the maximum of ρ as ρ_M ($\dot{\rho}=0$ at $\rho=\rho_M$). If $\rho=\rho_M$ represents the horizon, then the horizon is located at the center of the wall. By assuming this, we can evaluate the followings

$$\left|\frac{dr}{d\xi}\right|_{\rm begin}=\sqrt{1-\frac{\bar{\rho}^2}{\Lambda_t^2}},\quad \left|\frac{dr}{d\xi}\right|_{\rm top}=0,\quad \left|\frac{dr}{d\xi}\right|_{\rm end}=-\sqrt{1-\frac{\bar{\rho}^2}{\Lambda_f^2}}. \tag{5.34}$$

We want to check whether the horizon of type B is located on the wall. If it is so, the half of the wall mass$(S_1/2)$ contributes to $\mathcal{M}_{\rm wall<}$ inside the horizon in the case of $\epsilon=0$. The mass of the wall inside the horizon is

$$\begin{aligned}\mathcal{M}_{\rm wall<} &= \int_{\rm wall<}\left|\frac{dr}{d\xi}\right| d\xi\left(\frac{1}{2}\dot{\phi}^2+U(r)\right)\\ &= \frac{1}{2}\left(\sqrt{1-\frac{\bar{\rho}^2}{\Lambda_t^2}}+0\right)\cdot\int_{\rm wall<}d\xi\left(\frac{1}{2}\dot{\phi}^2+U(\phi(\xi))\right)\end{aligned}$$

$$= \frac{1}{2}\left(\sqrt{1-\frac{\bar{\rho}^2}{\Lambda_t^2}}\right)\frac{S_1}{2} = \frac{S_1}{4}\sqrt{1-\frac{\bar{\rho}^2}{\Lambda_t^2}}. \tag{5.35}$$

Note that only half of the wall contributes to the mass if the horizon is located at the middle of the wall,

$$\frac{S_1}{2} = \int_{\text{wall}<} d\xi \left(\frac{1}{2}\dot{\phi}^2 + U(\phi(\xi))\right) = \frac{1}{2}\int_{\text{wall}} d\xi \left(\frac{1}{2}\dot{\phi}^2 + U(\phi(\xi))\right). \tag{5.36}$$

The horizon (ρ_M) should satisfy that

$$1 - \frac{2GM(r)}{r} = 1 - \frac{\kappa\left(\frac{4\pi}{3}r^3 U_t + 4\pi^2\bar{\rho}^2\frac{S_1}{4}\sqrt{1-\frac{\bar{\rho}^2}{\Lambda_t^2}}\right)}{4\pi r} = 0 \quad \text{at } r = \rho_M. \tag{5.37}$$

It is possible to check this holds by using Equation (4.25) with $\rho_M = \bar{\rho}$. Furthermore, integrating the mass over the other part(false vacuum) gives the same result by symmetry. Thus, even though it is hard to see the horizon of the type B bounce directly, it exists on the wall in the setup of the thin-wall approximation upto the leading order of the Jocabian factor.

Let us consider a generic case of type B ($\epsilon \geq 0$). The true vacuum part has a larger portion of the wall than the false vacuum in order to compensate the smaller mass density in(out)side of the wall. Let us say α is the portion of the wall in the false vacuum part within the horizon.

$$\mathcal{M}_{\text{wall}<} = \frac{1}{2}\left(\sqrt{1-\frac{\bar{\rho}^2}{\Lambda_t^2}}\right)\alpha S_1 = \frac{\alpha S_1}{2}\sqrt{1-\frac{\bar{\rho}^2}{\Lambda_t^2}}. \tag{5.38}$$

The condition for the horizon is

$$1 - \frac{2GM(r)}{r} = 1 - \frac{\kappa\left(\frac{4\pi}{3}r^3 U_t + 4\pi^2\bar{\rho}^2\frac{\alpha S_1}{2}\sqrt{1-\frac{\bar{\rho}^2}{\Lambda_t^2}}\right)}{4\pi r} = 0 \quad \text{at } r = \rho_M. \tag{5.39}$$

We can check this conditions holds by using Equation (4.25) provided α is

$$\alpha = \frac{1}{2} + \frac{2\epsilon}{3\kappa S_1^2}. \tag{5.40}$$

The minimum of α is $\frac{1}{2}$, corresponding to the case that two vacua are degenerated ($\epsilon = 0$). The portion of the wall in the false vacuum side becomes unity ($\alpha = 1$) at the criteria of type A/B solution $\left(\frac{4\epsilon}{3\kappa S_1^2} = 1\right)$. The range of α is $\alpha = [1/2, 1]$, which verifies the true vacuum side contains more parts of the wall.

Also, we can confirm this by assuming the false vacuum part contains the mass of the wall as $(1-\alpha)S_1$

$$\mathcal{M}_{\text{wall}>} = \frac{1}{2}\left(\sqrt{1-\frac{\bar{\rho}^2}{\Lambda_f^2}}\right)(1-\alpha)S_1 = \frac{(1-\alpha)S_1}{2}\sqrt{1-\frac{\bar{\rho}^2}{\Lambda_f^2}}. \tag{5.41}$$

The condition for the horizon is also satisfied with Equations (4.25) and (5.40),

$$1-\frac{2GM(r)}{r}=1-\frac{\kappa\left(\frac{4\pi}{3}r^3U_f+4\pi^2\bar{\rho}^2\frac{(1-\alpha)S_1}{2}\sqrt{1-\frac{\bar{\rho}^2}{\Lambda_f^2}}\right)}{4\pi r}=0 \quad \text{at } r=\rho_M. \tag{5.42}$$

We checked that the horizon of the type B bounce is located on the wall and the portion (α) of the wall in the true vacuum side is given by Equation (5.40). More generally, the maximum of ρ ($\dot{\rho}=0$) indicates the horizon in any cases of field configurations. We can show this by using the field equations.

For an arbitrary $O(3)$-symmetric field configuration, $M(r)$ is given by the integration

$$M(r^*)=4\pi\int_0^{r^*}drr^2\left(\frac{1}{2}\phi'^2+U(r)\right)=4\pi\int_0^{r^*}drr^2\left(\frac{1}{2}\dot{\phi}^2+U(r)\right) \quad \text{at } t=0. \tag{5.43}$$

If the maximum of ρ becomes the horizon of the Schwarzchild-like metric, it should satisfy that

$$1-\frac{\kappa M(\rho_M)}{4\pi\rho_M}=1-\frac{\kappa\int_0^{\rho_M}d\rho\rho^2\left(\frac{1}{2}\dot{\phi}^2+U\right)}{\rho_M}=0, \quad \dot{\rho}=0 \text{ at } \rho=\rho_M. \tag{5.44}$$

The field equation (3.10) gives us

$$d\left(\frac{1}{2}\dot{\phi}^2-U\right)=-\frac{3\dot{\rho}\dot{\phi}^2}{\rho}d\xi=-\frac{3\dot{\phi}^2}{\rho}d\rho. \tag{5.45}$$

By using this identity, we can find that

$$d\left[\rho^3\left(\frac{1}{2}\dot{\phi}^2-U\right)\right]=-3\rho^2\left(\frac{1}{2}\dot{\phi}^2+U\right)d\rho. \tag{5.46}$$

The constraint equation at $\dot{\rho}=0$ is the following

$$\left(\frac{1}{2}\dot{\phi}^2-U\right)\Big|_{\rho=\rho_M}=\frac{3(\dot{\rho}^2-1)}{\kappa\rho_M^2}=-\frac{3}{\kappa\rho_M^2}. \tag{5.47}$$

By combining (5.46) and (5.47), we can show that the horizon condition (5.44) holds at $\rho=\rho_M$,

$$1-\frac{\kappa M(\rho_M)}{4\pi\rho_M}=1+\frac{\kappa\rho_M^3\left(\frac{1}{2}\dot{\phi}^2-U\right)\Big|_{\rho=\rho_M}}{3\rho_M}=0. \tag{5.48}$$

This horizon condition is valid if the field is static, so either the $\tau=0$ slice or the $\tau=\Delta\tau/2$ slice has the 2-sphere horizon at $r=\rho_M$. This result shows that the horizon exists for any kind of the field configuration in a closed manifold, such as type A, type B and thick wall solutions. However,

after a nucleation, the horizon and the inner field configuration can vary as time (t) goes by because the field is static only at a moment ($\tau = t = 0$).

If the geometry of the solution is totally symmetric ($O(5)$), τ is defined as Equation (5.15) so there is no subtlety how to slice the equal τ line. For a generic CdL bounce, slicing constant τ lines is ambiguous except $\tau = 0$ and $\Delta\tau/2$. The next easy example is the vertical line through the horizon as like Figure 5.5. Because ϕ is constant through the path, $\phi' = 0$ everywhere but $\frac{\partial\phi}{\partial\tau} \neq 0$. Since this is not static, Equation (5.25) is not the right form of the metric so the horizon is also not well-defined. The integrated mass is

$$M(r^*) = 4\pi \int_0^r dr r^2 \left(\frac{1}{2}\phi'^2 + U(r)\right) = 4\pi \int_0^{r^*} dr r^2 U(r^*) = \frac{4\pi (r^*)^3 U(r^*)}{3}. \tag{5.49}$$

We can also check the 2-sphere at $r^* = \rho_M$ cannot be a horizon in this case,

$$1 - \frac{2GM(\rho_M)}{\rho_M} = 1 - \frac{\kappa\rho_M^2}{3} U(\rho_M) = \frac{1}{2}\dot{\phi}_M^2 + \dot{\rho}_M^2 = \frac{1}{2}\dot{\phi}_M^2 > 0 \tag{5.50}$$

where $\dot{\phi}_M = \dot{\phi}$ at $\rho = \rho_M$.

This implies that each constant τ slice ends at the 2-sphere at $r = \rho_M$ but it can be the horizon only if the field is static. A bubble can nucleate only with the condition $\frac{\partial\phi}{\partial\tau} = \frac{\partial\phi}{\partial t} = 0$ to satisfy

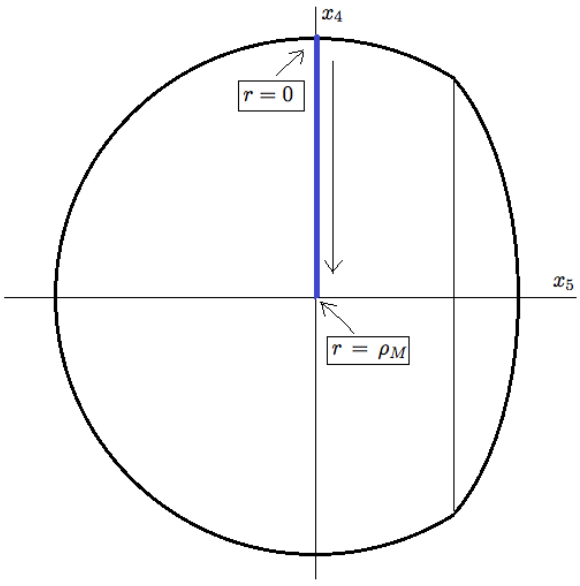

(a) The vertical line through the horizon

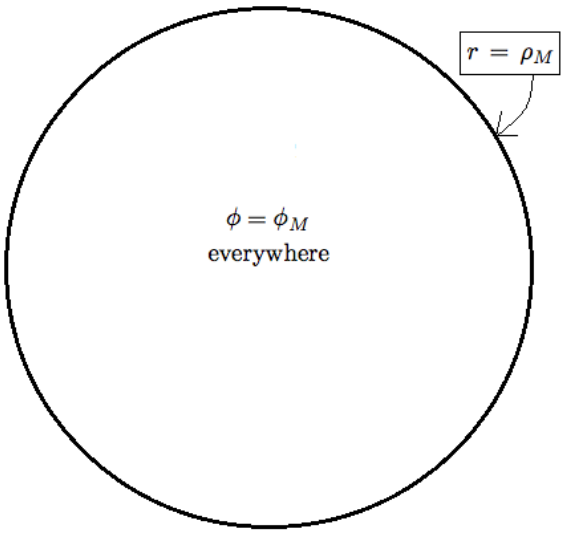

(b) Three ball along the thick blue line in (a)

Figure 5.5: The vertical integration path.

Equation (2.25). Thus, the other non-static field configurations are not the channels to nucleate and they only exist in a Euclidean spacetime. The coordinate of τ on the slice at $\tau = 0$ and $\Delta\tau/2$ is uniquely determined because τ is analytically continued to t in a Lorentzian coordinate when it nucleates. However, choosing a constant τ line not on the channels ($\tau \neq 0, \Delta\tau/2$) is just a choice of a coordinate which does not change physical properties. The tunneling exponent B is also independent of the choice of the coordinate τ.

In an anti-de Sitter geometry, thermal excitation has to be localized as in the flat space case because the space is infinitely large. We need further investigations to study this problem.

Chapter 6

Negative mode problem in flat spacetime

We have investigated the bounce solution of the vacuum decay in various cases. The bounce solution is the primary key to understand the tunneling process since it represents the dynamics in a Euclidean spacetime and also contributes to the decay rate. Another essential fact in the vacuum transition is the mode spectrum of the second order variation of the action at the bounce since it gives the insight to understand how the bounce solution behaves and also determines the pre-factor A in the decay rate. In particular, the negative mode in the spectrum implies the state is unstable as the energy shift is imaginary. Let us discuss the negative modes in flat space in more details in this chapter.

6.1 Coleman's argument

There are several simple ways to find out the existence of a negative mode in flat space. The first one is seen by the fact that the second order variation of the action in thin-wall approximation is negative, as in Equation (4.9). The other approach is investigating zero modes. There are the four translational zero modes and each mode has a node because all of them are $l = 1$ modes. This implies that there must be at least one negative mode since the eigenvalue of the mode without nodes is less than zero. We also found that the factor of i in the path integral comes out as the consequence of the existence of a negative mode. Then, one can ask whether any number of negative

modes in the system is allowed. It is possible to show there is one and only one negative mode if the bounce action has a minimal tunneling path of the action among the configurations whose Euclidean energy E is the same as in the solution at the turning point of the path[6].

Among the paths of the field through the configuration space, the Euclidean energy at the turning point is not necessarily the same as the energy of bounce solutions so there could be under- and overshooting cases. A path whose energy differs from the energy of the system E can bounce back since it does not have to obey the equation of motion in the configuration space. However, if the path obeys the equation of motion, it keeps going ahead after passing a $V = E$ point or it turns back before reaching a $V = E$ point and then keeps going to the opposite direction after passing the original point. The former case is an overshooting case and the latter one is an undershooting case.

Let us assume a functional of the paths that begins at the false vacuum and bounce back somewhere on the $V = E$ hypersurface to avoid under- or overshooting mode. Among these paths, the path which minimizes the action gives the bounce solution and satisfies the equation of motion. There would be many possible bounce solutions but the path with the lowest action has the largest decay rate ($\Gamma \sim e^{-B}$). This means the minimal tunneling path of the action becomes the dominant channel in the tunneling process.

We can choose the minimal penetration path ($q_0(t)$) which gives the lowest action (2.18).

$$B = S_B[q_0(t)]. \tag{6.1}$$

Because it is at the minimum, any second order variations with fixed energy should be positive,

$$\delta^2 S_B\big|_{q_0(t)} \geq 0. \tag{6.2}$$

The minimal path ($q_0(t)$) has a time reversal symmetry such that

$$q_0(-t) = q_0(t). \tag{6.3}$$

Since $q_0(t)$ is even, the eigenfuctions of the second variation of the action should be either even or odd. This implies the lowest eigenfuction has to be even because an odd function cannot be the lowest mode. Let us say the lowest negative mode ψ_1. In order to verify that there is only one negative mode, let assume that there is another negative mode ψ_2. Neither negative mode, it can

bounce back from a $V = E$ point because we checked every configuration which ends at a $V = E$ point cannot be a negative mode by the condition (6.2). This implies that a negative mode should be an under- or overshooting case. Namely, a negative mode (ψ) always satisfies that

$$\psi(0) \cdot \nabla V(q_0(0)) \neq 0. \tag{6.4}$$

If ψ_2 is even, it is possible to find coefficients a and b such that

$$(a\psi_1(0) + b\psi_2(0)) \cdot \nabla V(q_0(0)) = 0. \tag{6.5}$$

If we define a path with these negative modes,

$$q_\lambda(t) = q_0(t) + \lambda \left(a\psi_1(t) + b\psi_2(t)\right), \tag{6.6}$$

then this path ($q_\lambda(t)$) stops on a $V = E$ point at $t = 0$ so it should obey the condition (6.2). However, the second order variation by the sum of two negative mode must be negative. This leads to a contradiction.

If ψ_2 is odd, $\psi_2(0) = 0$ and it does not satisfy the condition (6.4) so there is a contradiction. To sum up, if there is another negative mode ψ_2, we have a true contradiction so there must be only one negative mode.

Let us briefly explain what happened here. A negative mode cannot bounce back from a $V = E$ point by the condition (6.4). However, it is possible to make the sum of two different negative modes turn back on a $V = E$ point so this proves there must be only one negative mode. This argument is true if the action has the minimum among the configurations with fixed energy E at the turning point ($t = 0$). If it is not a minimum of the action, there can be more negative modes. We shall discuss these cases in Section 6.3.

6.2 Thin-wall analysis

We have shown there is one and only one negative mode in the vacuum decay process. However, it is hard to find an analytic form of the negative mode in general but it is possible to find it in the format of the thin-wall approximation.

The field equation (2.27) and its derivative in flat space are

$$\Box\phi = \phi'' + \frac{3\phi'}{\rho} = U'[\phi] \tag{6.7}$$

$$\phi''' + \frac{3\phi''}{\rho} - \frac{3\phi'}{\rho^2} = U''[\phi] \cdot \phi'. \tag{6.8}$$

Let us consider the perturbative expansion of the scalar field,

$$\phi(\rho, \Omega) \to \phi(\rho) + \Phi(\rho) Y_l(\Omega) \tag{6.9}$$

where $Y_l(\Omega)$'s are the $O(4)$ harmonics. Then, the mode equation for the perturbative field becomes

$$-\Box\Phi + U''[\phi] \cdot \Phi = -\Phi'' - \frac{3\Phi'}{\rho} + \frac{l(l+2)\Phi}{\rho^2} + U''[\phi] \cdot \Phi = \lambda \cdot \Phi. \tag{6.10}$$

We can check a translational zero mode($\phi'(\rho)Y_1$) given by (2.44) gives zero eigenvalue by (6.8),

$$-\Phi'' - \frac{3\Phi'}{\rho} + \frac{3\Phi}{\rho^2} + U''[\phi] \cdot \Phi = -\phi''' - \frac{3\phi''}{\rho} + \frac{3\phi'}{\rho^2} + U''[\phi] \cdot \phi' = 0. \tag{6.11}$$

For a zero mode, $\phi'(\rho)Y_1$ becomes an eigenfunction all the time. If the wall is infinitely thin, ϕ' vanishes in-/outside the wall and ρ is a constant ($\bar{\rho}$) on the wall. Thus, we can write the mode equation by assuming $\Phi = \phi'$,

$$-\phi''' - \frac{3\phi''}{\rho} + \frac{l(l+2)\phi'}{\rho^2} + U''[\phi] \cdot \phi' = \lambda\phi', \tag{6.12}$$

$$\frac{l(l+2) - 3}{\bar{\rho}^2}\phi'(\xi) = \lambda\phi'(\xi), \tag{6.13}$$

$$\lambda = \frac{l(l+2) - 3}{\bar{\rho}^2}. \tag{6.14}$$

The eigenfunction of the perturbative field is $\phi'(\rho)Y_l(\Omega)$ and the corresponding eigenvalue is $(l(l+2) - 3)/\bar{\rho}^2$. This means the perturbative terms ($\delta\phi = \phi'(\rho)Y_{lm}(\Omega)$) are always eigenvalues for given l. This mode spectrum gives a negative mode for $l = 0$, four zero modes for $l = 1$ and many positive modes for $l \geq 2$. Although this gives the whole negative mode and zero modes we discussed in Section 2.3, this spectrum cannot cover the whole eigenfunctions.

In the case of $l = 0$, the eigenfunction is ϕ' and the eigenvalue is negative ($-3/\bar{\rho}^2$). This is the only negative eigenmode in flat space-time. This is a $O(4)$ symmetric mode and it means that the mode is one where the wall moves back and forth in a spherically symmetric way.

$$\phi(\rho) \to \phi(\rho) + \alpha\phi'(\rho) = \phi(\rho + \alpha). \tag{6.15}$$

Zero modes are related with the translational invariance of the system. These are $O(3)$ symmetric modes and mean the modes which move the wall in the same direction.

$$\phi(\vec{\rho}) \to \phi(\vec{\rho}) + \alpha\phi'(\rho)\hat{\rho}\cos\theta = \phi(\vec{\rho} + \alpha\hat{z}). \tag{6.16}$$

If the wall has a finite width, Equation (6.14) does not give an eigenvalue anymore but it still approximately an eigenmode because $(l(l+2)-3)/\rho^2$ is almost constant on the wall. However, if the width of the wall gets thicker, then the thin-wall approximation fails and this approach does not give the mode spectrum anymore.

6.3 Three vacua cases

If there are only two vacua in the potential, it is straightforward to determine the starting point and the ending point in the tunneling process so there is only one wall which gives the only negative mode. In the case of many vacua, there can be several choices of field configuration at a turning point. There are many different walls and each wall implies a different negative mode. This means there can be more than one negative mode. It seems to be contrary to Coleman's argument but we can point out how they are equivalent to each other. In this section, we assume that all the tunneling process can be described in the thin-wall approximation. After that, we will cover the tunneling problems with three vacua. The basic approach is finding all possible configurations by fixing the energy in the system.

6.3.1 One bubble case

Before starting to study three vacua cases, let us consider one bubble case. The coordinates are described in Figure 6.1. The euclidean time τ is defined as

$$\tau = R\cos\alpha, \quad d\tau = R\sin\alpha d\alpha. \tag{6.17}$$

The euclidean action in quantum mechanics is written by

$$B = \int d\tau \left[\frac{1}{2}\dot{q}^2 + (V - V_0)\right] = \int dq\sqrt{2\Delta V}. \tag{6.18}$$

In field theory, it is possible to find the form

$$B = \int d\tau d^3x \left[\frac{1}{2}\dot{\phi}^2 + \frac{1}{2}(\nabla\phi)^2 + (U - U_0)\right] = \int ds\sqrt{2\Delta U}, \tag{6.19}$$

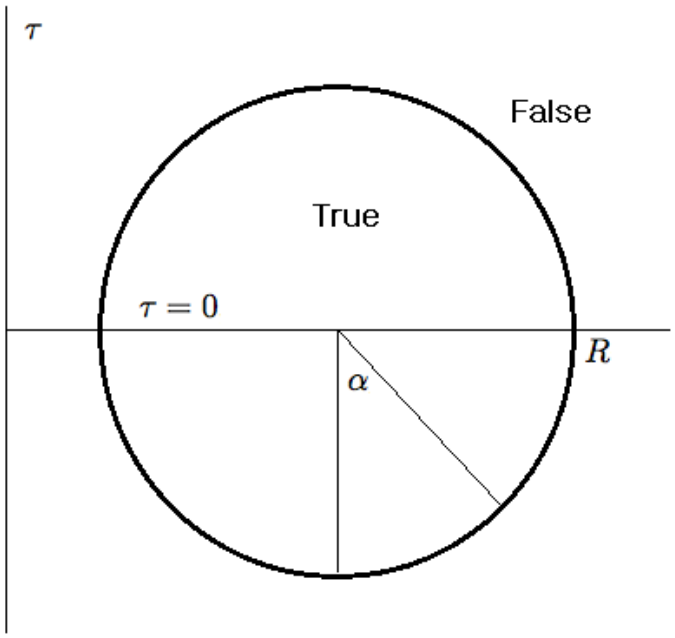

Figure 6.1: One bubble case.

provided

$$ds^2 = \int d^3x (d\phi)^2, \quad \Delta U \equiv \int d^3x \left(\frac{1}{2} (\nabla \phi)^2 + U - U_0 \right) \tag{6.20}$$

because Equation (6.19) is equivalent with Equation (6.18) if

$$\frac{1}{2} \left(\frac{dq}{d\tau} \right)^2 = \int \frac{1}{2} \left(\frac{d\phi}{d\tau} \right)^2 d^3x. \tag{6.21}$$

We can evaluate (ds) and ΔU separately.

$$\begin{aligned} (ds)^2 &= \int d^3x (d\phi)^2 = 4\pi R^2 \sin^2 \alpha \int dx \left(\frac{d\phi}{d\tau} \right)^2 (d\tau)^2 \\ ds &= \sqrt{4\pi} R^2 \sin^2 \alpha \sqrt{\frac{\cos^2 \alpha}{\sin \alpha} \cdot \sigma} d\alpha \end{aligned} \tag{6.22}$$

Note that $d^3x = 4\pi (R \sin^2 \alpha)^2 dx$. Derivatives of the field on the wall are given by

$$\left(\frac{d\phi}{d\tau} \right)^2 = \left(\frac{d\phi}{dr} \right)^2 \cos^2 \alpha, \quad \left(\frac{d\phi}{dx} \right)^2 = \left(\frac{d\phi}{dr} \right)^2 \cos^2 \alpha. \tag{6.23}$$

Because the thickness of the wall (dx) is enlarged by $1/\sin \alpha$, this expression gives

$$\sigma = \int dr \left(\frac{d\phi}{dr} \right)^2 = \frac{\sin \alpha}{\cos^2 \alpha} \int dx \left(\frac{d\phi}{d\tau} \right)^2 \tag{6.24}$$

which confirms Equation (6.22).

We are considering a configuration such that the energy at the nucleation is the same as in the initial state. This fact implies R has to satisfy at $\tau = 0$,

$$4\pi R^2\sigma - \frac{4}{3}\pi R^3\epsilon = 0. \tag{6.25}$$

This condition gives the same result as Equation (4.8)

$$R = \frac{3\sigma}{\epsilon}, \tag{6.26}$$

which is the radius of the wall in the thin-wall approximation. This is not surprising because the solution is the only possible $O(4)$ symmetric configuration of fields for given energy.

The potential part in the integration is

$$\begin{aligned} 2\Delta U &= 2\cdot 4\pi R^2\sin^2\alpha\int dx\left(\frac{1}{2}\left(\frac{\partial\phi}{\partial x}\right)^2 + U\right) - 2\cdot\frac{4\pi}{3}\epsilon R^3\sin^3\alpha \\ &= 4\pi R^2\sin^2\alpha\cdot\sigma\left(\frac{1}{\sin\alpha} + \sin\alpha\right) - 2\cdot 4\pi R^2\sigma\sin^3\alpha \\ &= 4\pi R^2\sigma\sin\alpha\cos^2\alpha. \end{aligned} \tag{6.27}$$

Now we can evaluate Equation (6.19),

$$B = S_B = 4\pi R^3\sigma\int_0^{\pi/2}\sin^2\alpha\cos^2\alpha d\alpha = \frac{\pi^2}{4}\sigma R^3. \tag{6.28}$$

It is integrated over the lower semicircle as ($\tau = [-\infty, 0]$). The full action is twice of Equation (6.28) and it equals Equation (4.6).

If there are only two vacua, there is one $O(4)$ symmetric configuration for given energy. Since the maximally symmetric case has the lowest action in field space[12], it satisfies the condition (6.2). According to the result of Section 6.1, there is only one negative mode. However, it does not always guarantee the condition (6.2) for many vacua cases. Let us investigate a three vacua case as a simple example.

6.3.2 Three vacua problem in a one-field potential

Consider a potential with three vacua, as in Figure 6.2a. This type of potential has been studied to explain resonant tunneling[24] but we focus on the negative modes of the potential. Here, we

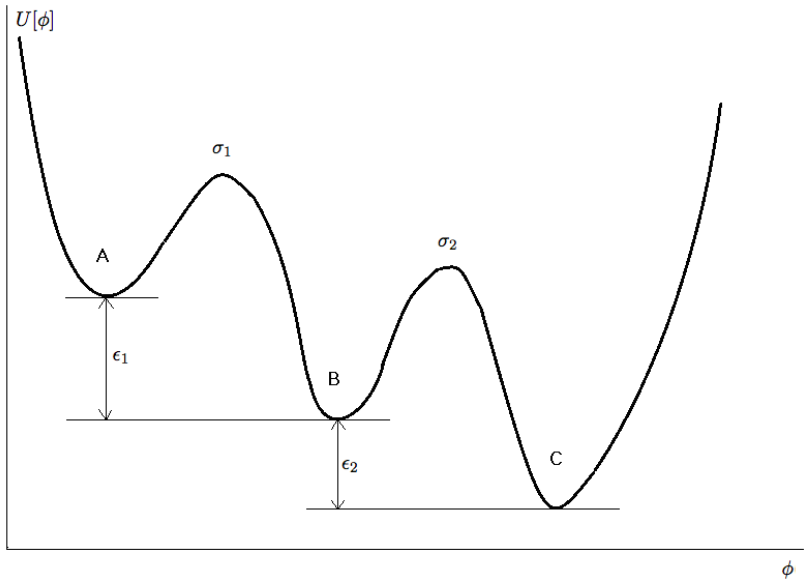

(a) A potential with three vacua.

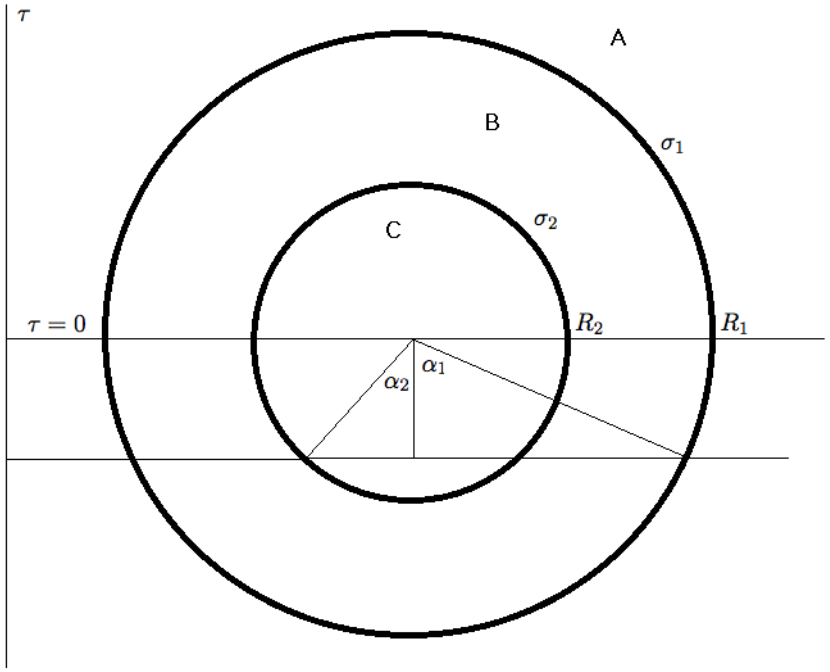

(b) The configuration of two bubbles.

Figure 6.2: Three vacua problem. σ_1: The wall tension between A and B, σ_2: The wall tension between B and C, $\epsilon_1 = U_A - U_B$ and $\epsilon_2 = U_B - U_C$.

still keep the $O(4)$ symmetric condition of the field configuration. Then, it is possible to nucleate two bubbles as described in Figure 6.2b. The coordinates obey

$$R_1 \cos\alpha_1 = R_2 \cos\alpha_2, \tag{6.29}$$

$$d\tau = R_1 \sin\alpha_1 d\alpha_1 = R_2 \sin\alpha_2 d\alpha_2 \tag{6.30}$$

where the range of the α's are $\alpha_1 = [0, \pi/2]$ and $\alpha_2 = [0, \pi/2]$ and α_2 is only defined if $\alpha_1 = [\alpha_0, \pi/2]$ if $\alpha_0 = \cos^{-1}(R_2/R_1)$.

In order to satisfy the energy condition at $\tau = 0$, the radii of the bubbles must obey

$$\begin{aligned} -\tfrac{4\pi}{3} R_1^3 \epsilon_1 + 4\pi R_1^2 \sigma_1 - \tfrac{4\pi}{3} R_2^3 \epsilon_1 + 4\pi R_2^2 \sigma_1 = 0, \\ -R_1^3 \epsilon_1 + 3R_1^2 \sigma_1 - R_2^3 \epsilon_2 + 3R_2^2 \sigma_2 = 0. \end{aligned} \tag{6.31}$$

Define stationary points of each bubble as

$$\bar{R}_1 = \frac{3\sigma_1}{\epsilon_1}, \quad \bar{R}_2 = \frac{3\sigma_2}{\epsilon_2}. \tag{6.32}$$

We can evaluate the action by following the approach of the two vacua case. First of all, the (ds) term is written by

$$(ds)^2 = \int d^3x (d\phi)^2 = 4\pi R_1^2 \sin^2\alpha_1 \cdot \int_{R_1} dx \left(\frac{d\phi}{d\tau}\right)^2 (d\tau)^2 + 4\pi R_2^2 \sin^2\alpha_2 \cdot \int_{R_2} dx \left(\frac{d\phi}{d\tau}\right)^2 (d\tau)^2, \tag{6.33}$$

$$(ds) = \begin{cases} \left(4\pi\sigma_1 R_1^2 \sin\alpha_1 \cos^2\alpha_1\right)^{1/2} d\tau & \text{if } 0 \le \alpha_1 \le \alpha_0, \\ \left(4\pi\sigma_1 R_1^2 \sin\alpha_1 \cos^2\alpha_1 + 4\pi\sigma_2 R_2^2 \sin\alpha_2 \cos^2\alpha_1\right)^{1/2} d\tau & \text{if } \alpha_0 \le \alpha_1 \le \pi/2. \end{cases} \tag{6.34}$$

The potential part is given by

$$2\Delta U = \begin{cases} \sigma_1 R_1^2 \sin\alpha_1 \left(1 + \left(1 - \frac{2R_1}{\bar{R}_1}\right) \sin^2\alpha_1\right) & \text{if } 0 \le \alpha_1 \le \pi/2, \\ \sigma_1 R_1^2 \sin\alpha_1 \left(1 + \left(1 - \frac{2R_1}{\bar{R}_1}\right) \sin^2\alpha_1\right) + \sigma_2 R_2^2 \sin\alpha_2 \left(1 + \left(1 - \frac{2R_2}{\bar{R}_2}\right) \sin^2\alpha_1\right) & \text{if } \alpha_0 \le \alpha_1 \le \pi/2. \end{cases} \tag{6.35}$$

The action becomes

$$\begin{aligned} S_B[R_1, R_2] = 4\pi \int_0^{\pi/2} d\alpha_1 \cdot R_1 \sin\alpha_1 \cdot \left(R_1^2 \sigma_1 \sin\alpha_1 \cos^2\alpha_1 + \Theta(\alpha - \alpha_0) R_2^2 \sigma_2 \sin\alpha_2 \cos^2\alpha_2\right)^{1/2} \\ \cdot \left[\sigma_1 R_1^2 \sin\alpha_1 \left(1 + \left(1 - \frac{2R_1}{\bar{R}_1}\right) \sin^2\alpha_1\right) + \Theta(\alpha - \alpha_0)\sigma_2 R_2^2 \sin\alpha_2 \left(1 + \left(1 - \frac{2R_2}{\bar{R}_2}\right) \sin^2\alpha_2\right)\right]^{1/2} \end{aligned} \tag{6.36}$$

with the energy condition (6.31) and $R_1 \cos\alpha_1 = R_2 \cos\alpha_2$.

If the radii are on the stationary points ($R_1 = \bar{R}_1, R_2 = \bar{R}_2$), it is possible to evaluate the action. With this condition, the action (6.36) is written by

$$\begin{aligned} S_B[\bar{R}_1, \bar{R}_2] &= 4\pi \int_0^{\pi/2} d\alpha_1 \cdot R_1 \sin\alpha_1 \cdot \left(R_1^2 \sigma_1 \sin\alpha_1 \cos^2\alpha_1 + \Theta(\alpha - \alpha_0) R_2^2 \sigma_2 \sin\alpha_2 \cos^2\alpha_2 \right)^{1/2} \\ &\quad \cdot \left(\sigma_1 R_1^2 \sin\alpha_1 \cos^2\alpha_1 + \Theta(\alpha - \alpha_0) \sigma_2 R_2^2 \sin\alpha_2 \cos^2\alpha_2 \right)^{1/2} \\ &= 4\pi \int_0^{\alpha_0} \sigma_1 R_1^3 \sin^2\alpha_1 \cos^2\alpha_1 d\alpha_1 \\ &\quad + 4\pi \int_0^{\pi/2} \left(\sigma_1 R_1^2 \sin^2\alpha_1 \cos^2\alpha_1 + \sigma_2 R_2^2 \sin^2\alpha_2 \cos^2\alpha_2 \right) R_2 \sin\alpha_2 d\alpha_2 \\ &= \frac{\pi^2}{4} \left(\sigma_1 R_1^3 + \sigma_2 R_2^3 \right). \end{aligned} \tag{6.37}$$

As we expected, this is the sum of each bubble's action. We need to check if this action is at the minimum under the variation of R_1 and R_2.

Let us introduce small perturbations around the stationary point as

$$R_1 = \bar{R}_1 + \delta_1, \quad R_2 = \bar{R}_2 + \delta_2. \tag{6.38}$$

According to the energy condition (6.31), δ's satisfy that

$$\begin{aligned} \sigma_1 \bar{R}_1 \delta_1 + \sigma_2 \bar{R}_2 \delta_2 = 0, \\ \delta_2 = -\tfrac{\sigma_1 \bar{R}_1}{\sigma_2 \bar{R}_2} \delta_1. \end{aligned} \tag{6.39}$$

Basically, we can write $S_B[R_1, R_2]$ in terms of one variable as $S_B[\delta_1]$. Then, it is possible to check where it is on the minimum by taking $\frac{d^2 S_B[\delta_1]}{d\delta_1^2}$. By expanding the action (6.36) up to the second order in perturbations, it is given by

$$\begin{aligned} S_B[\delta_1] &= S_B[\bar{R}_1, \bar{R}_2] - 3\pi^2 \sigma_1 \bar{R}_1 \delta_1^2 - 3\pi^2 \sigma_2 \bar{R}_2 \delta_2^2 \\ &= S_B[\bar{R}_1, \bar{R}_2] - 3\pi^2 \left(\frac{\sigma_1 \bar{R}_1}{\sigma_2 \bar{R}_2} \right) \cdot \left(\sigma_1 \bar{R}_1 + \sigma_2 \bar{R}_2 \right) \delta_1^2. \end{aligned} \tag{6.40}$$

This means that the action on $R_1 = \bar{R}_1$ and $R_2 = \bar{R}_2$ is not at the minimum. This is at the maximum in the $O(4)$ symmetric configurations for fixed energy but it is not at the maximum in the whole configuration space because less symmetric cases imply higher actions. Then, one can ask that there is a global minimum of the action in the three vacua case. If it exists it should be on the stationary point in the whole configuration space including the cases which do not conserve the energy. The only possible candidate is the one bubble limit as like $R_1 = \bar{R}_1$ and $R_2 = 0$.

We can also check whether the one bubble limit is a minimum of the action by introducing small perturbations,

$$R_1 = \bar{R}_1 + \delta_1, \quad R_2 = \delta_2 > 0. \tag{6.41}$$

The energy condition (6.31) becomes

$$-3\sigma_1 \bar{R}_1 \delta_1 + 3\sigma_2 \delta_2^2 = 0. \tag{6.42}$$

With this relationship, we can evaluate the action (6.36),

$$S_B[R_1, R_2] = S_B[\bar{R}_1, 0] + \pi^2 \sigma_1 \cdot \delta_2^3 - 3\pi^2 \sigma_1 \bar{R}_1 \left(1 + \frac{\sigma_1 \bar{R}_1}{2\sigma_2 \bar{R}_2}\right) \cdot \delta_1^2. \tag{6.43}$$

The lowest order in δ_1 is $O(\delta_1^{3/2})$ from the δ_2^3 term, which is positive. Thus, the action monotonically increases at the limit of $R_1 \to \bar{R}_1$ and $R_2 \to 0$. This means the action of this one bubble limit is the global minimum in the whole configuration space for fixed energy.

Let us see what happens here. As we studied in Section 6.2, the negative mode is the mode which moves the wall in and out. The small variation of the wall $R_1 = \bar{R}_1 + \delta_1$ decreases the action. If there is only one bubble, it cannot conserve energy so this mode does not show up in the configuration with fixed energy. If there are two bubbles, it is possible to preserve the energy by combining these modes. If each bubble moves in a different direction as in Equation (6.39), it can keep the energy constant. Since each mode makes the action lower, it cannot be the minimum of the action. This is the same process as choosing a and b in Equation (6.5). If there are indeed two negative modes, it is possible to find the mode which maintains the energy of the system as in Equation (6.5), so the action of the solution is not the lowest action for given energy. On the contrary, the action becomes a minimum in the limit of $R_1 = \bar{R}_1$ and $R_2 = 0$. As like the previous example, the δ_1^2 term decreases the action. If there is only the term from the outer bubble (R_1), it cannot preserve the energy so it would not be allowed. However, the small inner bubble (δ_2) makes up the energy loss and the action increases because of the inner bubble. In this case, there is only one wall moving mode since moving the inner bubble does not take place near the solution ($R_2 = \bar{R}_2$). Namely, there is only one negative mode and the action is at the minimum.

We discussed the local properties around the maximum and the minimum of the action. We need to see how the action behaves along the path which obeys the energy condition (6.31). The path looks like Figure 6.4.

If ΔU is always positive, the action (6.36) is well-defined. We can check that the action has a peak at the stationary point with two bubbles and gets the minimum in the one bubble limit ($R_2 = 0$). If ΔU is negative somewhere, the integration is ill-defined there so the $R_1 - R_2$ curve is disconnected. We call the region where ΔU is negative a classically allowed region and the region that ΔU is positive is a classically forbidden region. We can easily check there is no classically allowed region around the stationary point with two bubbles ($R_1 \approx \bar{R}_1$ and $R_2 \approx \bar{R}_2$). ΔU from the outer bubble becomes negative for large R_1 but the positive contribution from the inner bubble can make it up. This means ΔU can be negative if the inner bubble does not contribute when ΔU by an outer bubble becomes negative. Thus, a classically allowed region would start to appear as R_2 gets smaller. Let us find out the condition for a classically allowed region more precisely.

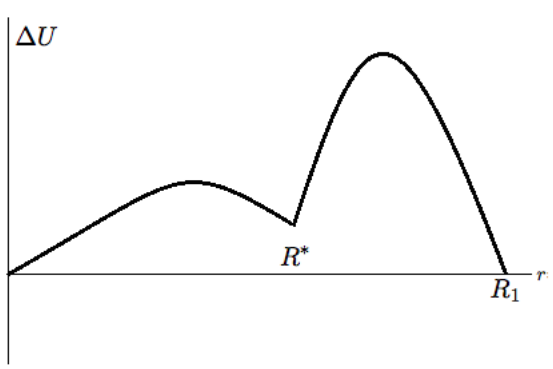

(a) The case 1: no classically allowed region

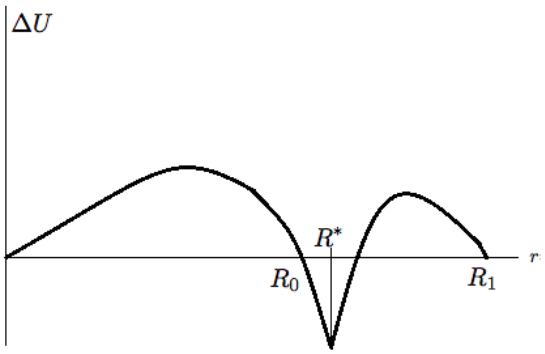

(b) The case 2: classically allowed region

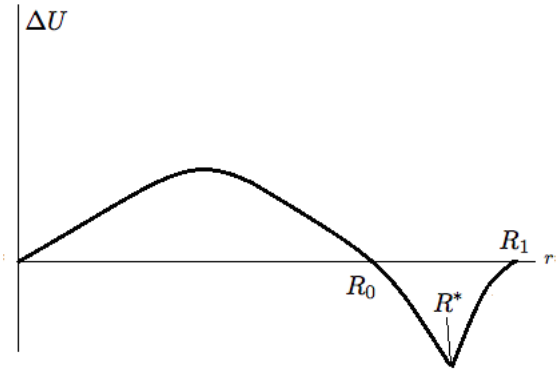

(c) The case 3: one classically forbidden region

Figure 6.3: Three cases of ΔU. r is defined as $r = R_1 \sin\alpha_1$. Because of the energy condition, $\Delta U = 0$ at $r = 0$ and $r = R_1$.

There are three cases of ΔU as shown in Figure 6.3. If there is classically allowed region, the configuration of ΔU varies from case 3 through case 2 to case 1 as R_2 increases. If there is no classically allowed region, the configuration of ΔU stays as case 1 along the $R_1 - R_2$ curve.

First of all, let's find out the condition for case 3. As $\Delta U(R_1) = 0$ by the energy condition, it becomes the case 3 if the derivative of ΔU at R_1 is positive. At the boundary between case 2 and case 3, the potential obeys $\frac{d\Delta U}{dr}\big|_{r=R_1} = 0$. The condition $\frac{dU}{dr}\big|_{r=R_1} = 0$ is found as

$$\left.\frac{dU}{dr}\right|_{r=R_1} = \sigma_1\left(\frac{3r^2}{R_1} + R_1\right) - 2\epsilon_1 r^2 + \left[\sigma_2\left(\frac{3r'^2}{R_2} + R_2\right) - 2\epsilon_2 r'^2\right]\frac{r}{r'} = 0 \quad \text{at } r = R_1, r' = R_2. \tag{6.44}$$

This gives that

$$2\sigma_1 - \epsilon_1 R_1 + 2\sigma_2 - \epsilon_2 R_2 = 0. \tag{6.45}$$

The condition for the case 3, $\left(\frac{d\Delta U}{dr}\big|_{r=R_1} < 0\right)$, becomes that

$$2\sigma_1 - \epsilon_1 R_1 + 2\sigma_2 - \epsilon_2 R_2 > 0. \tag{6.46}$$

This is a straight line on the graph. If this line crosses the $R_1 - R_2$ curve, there is the case 3 below the point they meet. Thus, the case 3 exists if

$$2\sigma_2 > \sigma_1. \tag{6.47}$$

The next step is investigating the condition for case 2. Define R_0 such that $U_1(R_0) = 0$ where U_1 is ΔU in terms of only the outer bubble (R_1),

$$U_1(R_0) = \sigma_1 R_1^2 \sin\alpha_1\left(1 + \left(1 - \frac{2R_1}{\bar{R}_1}\right)\sin^2\alpha_1\right) = 0, \quad \sin\alpha_1 = \frac{R_0}{R_1} \quad \text{at } R = R_0. \tag{6.48}$$

R_0 turns out to be

$$R_0^2 = \frac{R_1^2\bar{R}_1}{2R_1 - \bar{R}_1}. \tag{6.49}$$

Define R^* where the contribution from the inner bubble begins, then $R^* = \left(R_1^2 - R_2^2\right)^{1/2}$. $\Delta U(R^*)$ is local minimum and it becomes the case 2 if its value is negative there. Namely, the boundary between 1 and 2 is at $R_0 = R^*$. If $R_2 = 0$ and $R_1 = \bar{R}_1$,

$$R^* = R_0 = R_1. \tag{6.50}$$

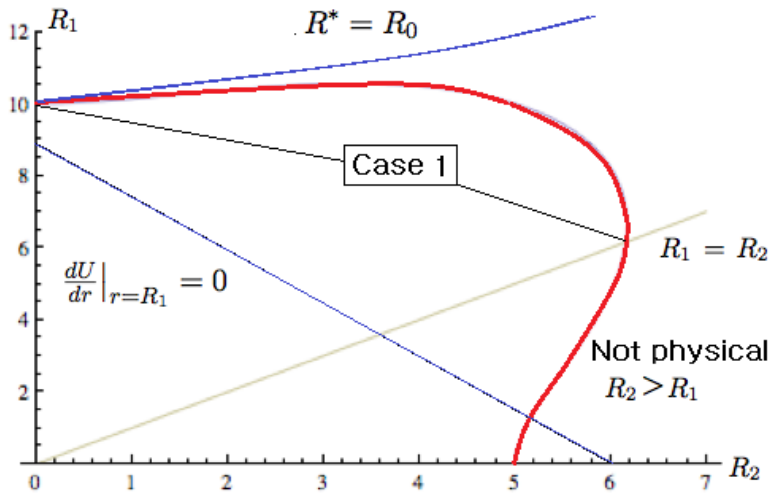

(a) $\sigma_1 > 2\sigma_2$

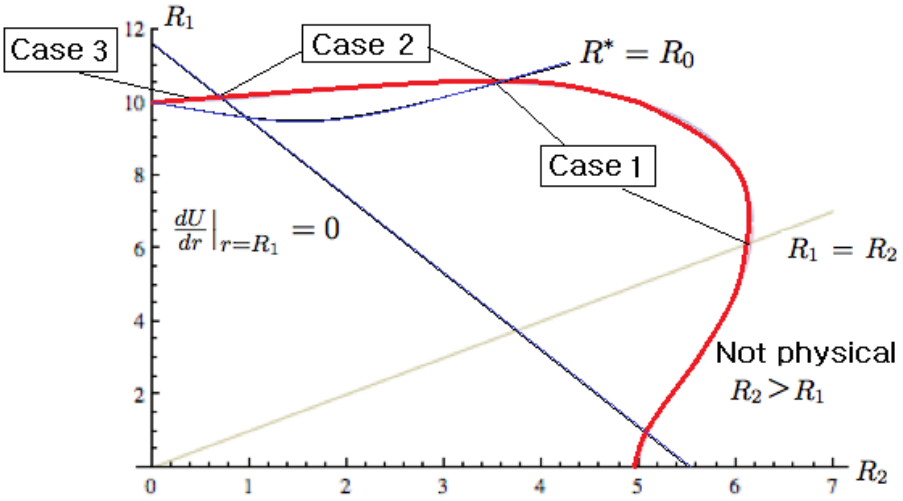

(b) $\sigma_1 < 2\sigma_2$

Figure 6.4: 'The $R_1 - R_2$ curve' is given by Equation (6.31). If $R_2 > R_1$, the inner bubble is greater than the outer bubble so it cannot be a physical solution. The cases 1, 2 and 3 are described in Figure 6.3. The curve $R^* = R_0$ always meet the $R_2 = 0$ point but the slope of the curve there is determined by σ_1 and σ_2. If $\sigma_1 > 2\sigma_2$, there is no classically allowed region. However, if $\sigma_1 < 2\sigma_2$, classically allowed region exist in the cases 2 and 3, so the curve is disconnected from $R_2 = 0$ point to $R^* = R_0$ point.

In the one bubble case, it is hard to determine whether it is the case 2 or not. In order to see how R^* and R_0 evolves as R_2 increases, let's find their derivatives.

$$\frac{d(R^*)^2}{dR_2} = 2R_1\frac{dR_1}{dR_2} - 2R_2 = -2R_2\left(1 + \frac{\epsilon_2 R_2 - 2\sigma_2}{\epsilon_1 R_1 - 2\sigma_1}\right). \tag{6.51}$$

$$\frac{dR_0^2}{dR_2} = -2\left(\frac{R_1\bar{R}_1}{2R_1 - \bar{R}_1} - \frac{\bar{R}_1 R_1^2}{\left(2R_1 - \bar{R}_1\right)^2}\right)\cdot\frac{dR_1}{dR_2} = \frac{2R_2\bar{R}_1^2}{\left(2R_1 - \bar{R}_1\right)^2}\cdot\frac{\epsilon_2 R_2 - 2\sigma_2}{\epsilon_1 R_1 - 2\sigma_1}. \tag{6.52}$$

The difference of these derivatives is

$$\frac{d}{dR_2}\left[(R^*)^2 - R_0^2\right] = -2R_2\left(1 + \frac{\bar{R}_1^2}{(2R_1 - \bar{R}_1)^2}\cdot\frac{\epsilon_2 R_2 - 2\sigma_2}{\epsilon_1 R_1 - 2\sigma_1}\right). \tag{6.53}$$

. This becomes positive in the limit $R_2 \to 0$ if $\sigma_2 > \sigma_1$,

$$\frac{d}{dR_2}\left[(R^*)^2 - R_0^2\right] > 0 \quad \text{as } R_2 \to 0. \tag{6.54}$$

. This means that the case 2 exists and there is a classically allowed region if $\sigma_2 > \sigma_1$. On the contrary, Equation (6.53) is always negative if $\sigma_2 < \sigma_1$,

$$\frac{d}{dR_2}\left[(R^*)^2 - R_0^2\right] = -\frac{2R_2}{\epsilon_1 R_1 - 2\sigma_1}\left((\epsilon_1 R_1 - 2\sigma_1) + \frac{\bar{R}_1^2}{(2R_1 - \bar{R}_1)^2}\cdot(\epsilon_2 R_2 - 2\sigma_2)\right) < 0. \tag{6.55}$$

$$\because \epsilon_1 R_1 - 2\sigma_1 - 2\alpha\cdot\sigma_2 = \epsilon_1\delta_1 + \sigma_1 - 2\alpha\cdot\sigma_2 > 0 \tag{6.56}$$

where $\delta_1 = R_1 - \bar{R}_1 > 0$ and $\alpha = \frac{\bar{R}_1^2}{(2R_1 - \bar{R}_1)^2} < 1$. This implies $(R^*)^2 - R_0^2$ is monotonically decreasing function if $\sigma_2 < 2\sigma_1$. The case 2 does not exist because $(R^*)^2 - R_0^2 = 0$ at $R_2 = 0$ gives that

$$R^* < R_0. \tag{6.57}$$

To sum up, there is no classically allowed region and only the case 1 appears if $\sigma_1 > 2\sigma_2$. Meanwhile, there is a always classically allowed region in the limit $R_2 \to 0$ and the potential (ΔU) varied from case 3 through case 2 to case 1 as R_2 increases if $\sigma_1 < 2\sigma_1$.

Let us interpret this result. The volume of the outer bubble when the inner bubble starts to show up ($\alpha_2 = 0$) gets larger as the size of the inner bubble (R_2) gets smaller. The size of the wall also increases but it grows up slower than the size of the bubble does. This means that if a classically allowed region exists, it always appears at $R_2 \to 0$. This also implies the condition for the existence of a classically allowed region is determined at $R_2 \to 0$. In this limit, the energy

in the volume of the inner bubble is negligible compared to the energy in the inner wall, and the energy in the outer wall increases twice as fast as than the energy in the volume of the outer bubble decreases because of the volume/surface ratio. This explains why the condition only depends on the mass densities of the wall (σ_1, σ_2). If there is a classically allowed region, the $R_1 - R_2$ curve is disconnected. This would mean is the one bubble solution ($R_1 = \bar{R}_1$ and $R_2 = 0$) which gives the global minimum of the action is disconnected from the stationary point with $R_1 = \bar{R}_1$ and $R_2 = \bar{R}_2$. However, it is only disconnected in the $O(4)$ symmetric configuration space so they can be connected through less symmetric configurations. We can conclude that the one bubble case limit has the lowest action for a given energy regardless of the existence of a classically allowed region.

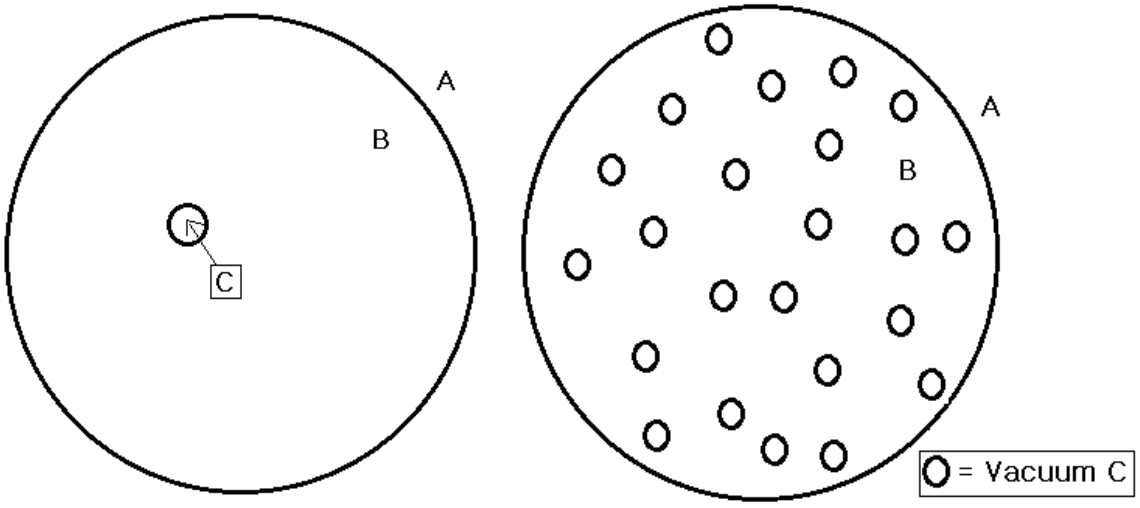

(a) One inner bubble if $\mathcal{V}_4\Gamma_2 \ll 1$ (b) Many inner bubbles if $\mathcal{V}_4\Gamma_2 \gg 1$

Figure 6.5: Two regimes when the radius of an inner bubble is much smaller than that of an outer one.

There are two stationary points on the action. Since the one with lower action has a much greater tunneling rate, we would expect that the tunneling with one bubble occurs much more often. Suppose the radius of inner bubbles (R_2) is much less than R_1. Then, there can be many small inner bubbles inside one outer bubble. In this case, the path integral is evaluated by

$$I = I_0 \sum_{n=0}^{\infty} \frac{1}{n!} \left[iV_1 T_1 K_1 e^{-B_1} \sum_{k=0} \frac{1}{k!} \left(i\mathcal{V}_4 K_2 e^{-B_2} \right)^k \right]^n$$

$$
\begin{aligned}
&= I_0 \sum_{n=0}^{\infty} \frac{1}{n!} \left[iV_1 T_1 K_1 e^{-B_1} \sum_{k=0} \frac{1}{k!} \left(\frac{i}{2} \mathcal{V}_4 \Gamma_2 \right)^k \right]^n \\
&= I_0 \exp \left[iV_1 T_1 K_1 e^{-B_1} \sum_{k=0} \frac{1}{k!} \left(\frac{i}{2} \mathcal{V}_4 \Gamma_2 \right)^k \right] \qquad (6.58)
\end{aligned}
$$

where

$$\mathcal{V}_4 = \frac{81\pi^2}{2} \left(\frac{\sigma_1}{\epsilon_1} \right)^4 \qquad (6.59)$$

is the four-volume of the outer bounce and Γ_2 is the bubble nucleation rate for inner bubbles. Because the outer bubbles fills in infinitely large spacetime, the sum of n runs to the infinity so it becomes an exponential. On the contrary, the volume of the outer bubble ($\mathcal{V}_4$) is finite so the sum does not have to be necessarily an exponential. In the expansion of an exponential, $e^{\alpha} = \sum \frac{1}{n!} \alpha^n = 1 + \alpha + \frac{1}{2}\alpha^2 + ...$, the dominant term comes from $n \approx \alpha$. This fact implies the two following situations. If $\mathcal{V}_4 \Gamma_2 \ll 1$, the sum over k is dominated by the $k = 0$. This corresponds to just the one bubble case so there is no significant correction to Γ_1. If $\mathcal{V}_4 \Gamma_2 \gg 1$, the sum over k is approximately an exponential so Equation (6.58) becomes

$$I \approx I_0 \exp \left[iV_1 T_1 K_1 e^{-B_1 - i\mathcal{V}_4 \Gamma_2 / 2} \right]. \qquad (6.60)$$

This means many small inner bubbles effectively shift B_1 by

$$\tilde{B}_1 = B_1 - \frac{i}{2} \mathcal{V}_4 \Gamma_2 = \frac{27\pi^2}{2} \frac{\sigma_1^4}{\epsilon_1^3} \left(1 - \frac{3i}{2} \frac{\Gamma_2}{\epsilon_1} \right). \qquad (6.61)$$

The leading order gives

$$\epsilon_1 \to \epsilon_1 + i\Gamma_2/2. \qquad (6.62)$$

This is the same as shifting the energy density of vacuum B by the imaginary number, $i\Gamma_2/2$. This effectively imaginary energy means the vacuum B is sufficiently unstable so the small inner bubbles already exist when one outer bubble nucleates.

6.3.3 Three vacua problem in a multi-field potential

Let us move to another three vacua case. Consider a two-field potential with three vacua as in Figure 6.6. The bounce solution and negative modes of this case have been studied in [25, 26]. There are three kinds of walls (σ_{AB}, σ_{BC} and σ_{AC}). For the maximally symmetric configuration, the field is $O(3)$ symmetric because scalar fields in two dimension can create a junction of three

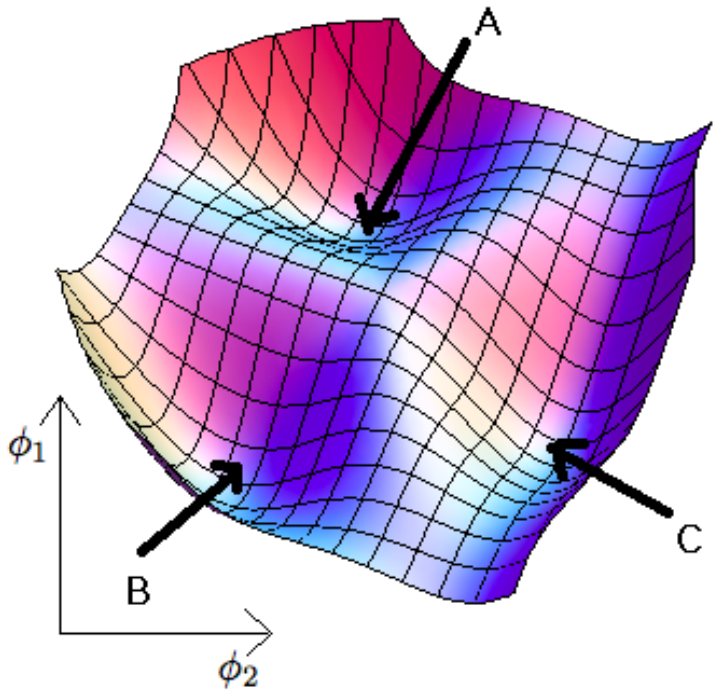

Figure 6.6: Two-fields potential with three vacua.

walls that breaks the $O(4)$ symmetry. For the saddle point of the action, the wall between two different vacua forms a partial three-sphere with radius $3\sigma/\epsilon$, the same as in the one bubble case.

The tensions of wall are determined by

$$\begin{aligned}
\sigma_{AB} &= \min \int_A^B dl \sqrt{2(U[\vec{(}\phi_l)] - V_0)}, \\
\sigma_{AC} &= \min \int_A^C dl \sqrt{2(U[\vec{(}\phi_l)] - V_0)}, \\
\sigma_{BC} &= \min \int_B^C dl \sqrt{2(U[\vec{(}\phi_l)] - V_0)}.
\end{aligned} \tag{6.63}$$

These definitions of $\sigma's$ imply triangle inequalities for the wall tensions,

$$\begin{aligned}
\sigma_{AC} &< \sigma_{AB} + \sigma_{BC}, \\
\sigma_{AB} &< \sigma_{AC} + \sigma_{BC}, \\
\sigma_{BC} &< \sigma_{AB} + \sigma_{AC}.
\end{aligned} \tag{6.64}$$

Of course, the bounce solution we described in Section 6.3.2 exist. In this section we focus on the bounce solutions with junctions of three walls as shown in Figure 6.7. Among the many

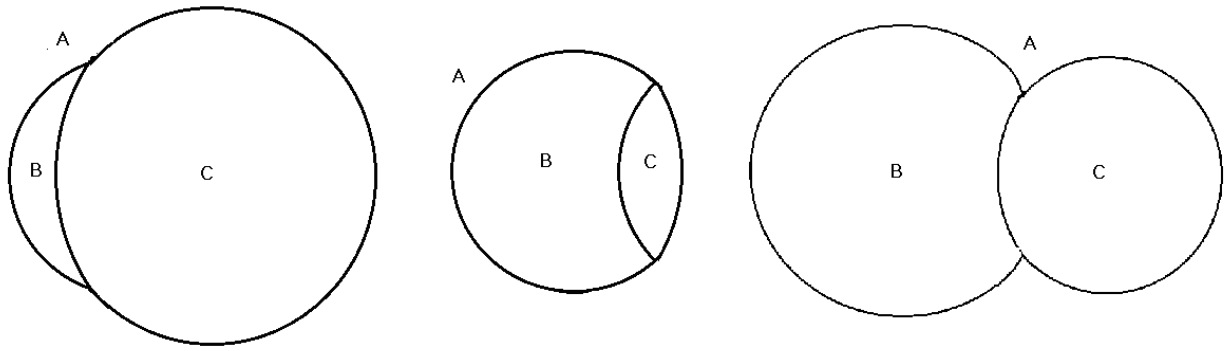

Figure 6.7: Many types of bounce solutions.

possible types of bounce solutions, let us deal with the simplest case to approach negative modes problems, as shown in Figure 6.8. Suppose $\sigma = \sigma_{AB} = \sigma_{AC}$, $\sigma' = \sigma_{BC}$ and $\epsilon = \epsilon_{AB} = \epsilon_{AC}$. We are going to evaluate the action for a given energy by using the approach in Section 6.3.1. Because $\epsilon_{BC} = 0$, the wall between B and C has no curvature for the bounce solution. Among all possible variations from the bounce solution, we consider only the case that the wall between B and C has no curvature, to reduce the number of degrees of freedom since we are mainly interested in local behavior near saddle points.

To describe bounce solutions, we need to introduce the parameters ($z's$, $r's$, $\theta's$ and $\alpha's$) which are defined in Figure 6.8. They obey the following relationships for a given τ slice,

$$\begin{aligned} z_B &= R_B \cos\theta_B, \\ r &= R_B \sin\theta_C, \\ r_B &= R_B \sin\alpha_B, \\ R_B \cos\alpha_B &= R_C \cos\alpha_C. \end{aligned} \tag{6.65}$$

In terms of these parameters, it is possible to write the area between A and B, the volume of B and the area between B and C as

$$\begin{aligned} \text{Area}(\sigma) &: 2\pi r_B^2 \cdot \left(1 + \frac{z_B}{r_B}\right) = 2\pi R_B^2 \sin^2\alpha_B \cdot \left(1 + \frac{\cos_*\theta_B}{\sin\alpha_B}\right), \\ \text{Vol}(\epsilon) &: \pi\left[\frac{2}{3}r_B^3 + z_B\left(r_B^2 - \frac{z_B^2}{3}\right)\right] = \frac{2}{3}\pi R_B^3 \sin^3\alpha_B + \pi R_B^3 \cos_*\theta_B \left(\sin^2\alpha_B - \frac{\cos_*^2\theta_B}{3}\right), \\ \text{Area}(\sigma') &: \pi\left(r_B^2 - z_B^2\right) = \pi R_B^2 \cdot \left(\sin^2\alpha_B - \cos_*^2\theta_B\right), \end{aligned} \tag{6.66}$$

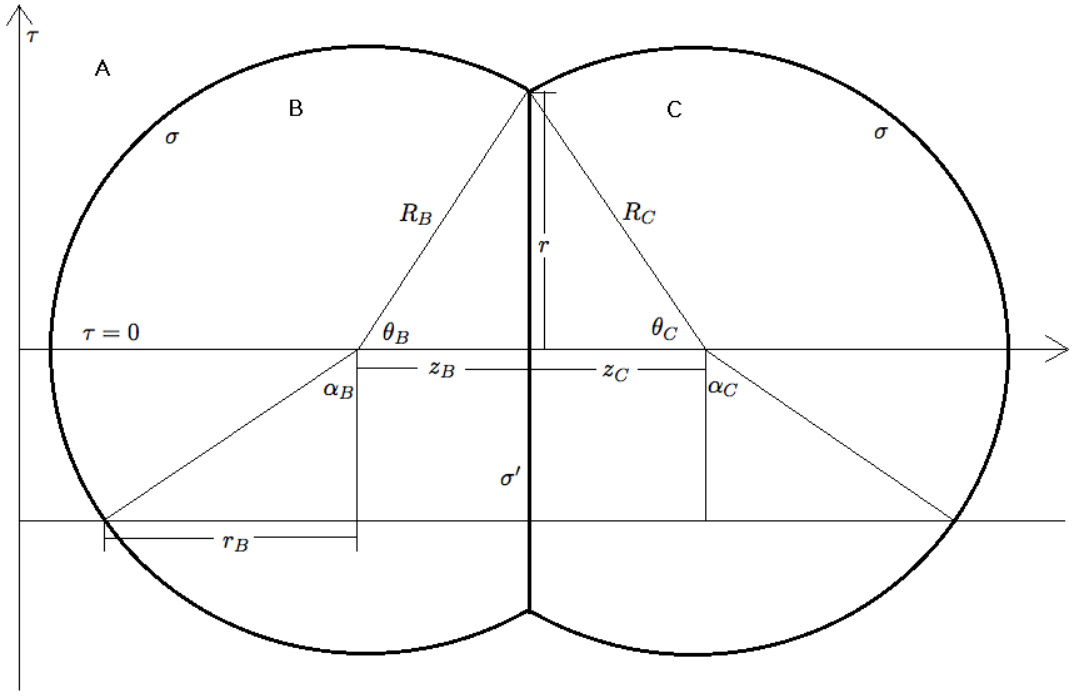

Figure 6.8: The parameters of the barnacle of our example. ($\sigma = \sigma_{AB} = \sigma_{AC}$, $\sigma' = \sigma_{BC}$ and $\epsilon = \epsilon_{AB} = \epsilon_{AC}$).

where $\cos_* \theta_B$ is defined by

$$\cos_* \theta_B = \begin{cases} \cos\theta_B & \text{if } \cos\theta_B < \sin\alpha_B, \\ \sin\alpha_B & \text{if } \cos\theta_B \geq \sin\alpha_B. \end{cases} \tag{6.67}$$

Equation (6.20) gives that

$$\begin{aligned} (ds) &= \left[2\pi R_B^2 \sigma \cos^2\alpha_B \left(\sin\alpha_B + \cos_*\theta_B\right) + 2\pi R_C^2 \sigma \cos^2\alpha_C \left(\sin\alpha_C + \cos_*\theta_C\right)\right]^{1/2} d\tau \\ &= \sqrt{2\pi\sigma} R_B^2 \sin\alpha_B \left[\sin\alpha_B + \cos_*\theta_B + \sin\alpha_C + \cos_*\theta_C\right]^{1/2} d(\sin\alpha_B) \end{aligned} \tag{6.68}$$

and

$$\begin{aligned} 2\Delta U = 2\pi \Big\{ & \sigma R_B^2 \left(\sin\alpha_B + \cos_*\theta_B\right)\left(1+\sin^2\alpha_B\right) + \sigma R_C^2 \left(\sin\alpha_C + \cos_*\theta_C\right)\left(1+\sin^2\alpha_C\right) \\ & + \sigma' R_B^2 \left(\sin^2\alpha_B - \cos_*^2\theta_B\right) - 2\sigma \frac{1}{\bar{R}} \left[R_B^3 \sin^3\alpha_B + R_C^3 \sin^3\alpha_C\right] \\ & - \frac{\sigma}{\bar{R}} \left[R_B^3 \cos_*\theta_B \left(3\sin^2\alpha_B - \cos_*^2\theta_B\right) + R_C^3 \cos_*\theta_C \left(3\sin^2\alpha_C - \cos_*^2\theta_C\right)\right] \Big\}. \end{aligned} \tag{6.69}$$

Recall that $\Delta U = 0$ at $\tau = 0$ due to the energy condition. The radii of the bubbles have to be $R = R_B = R_C = \bar{R} \equiv \frac{3\sigma}{\epsilon}$ at the stationary point. The angle $\theta = \theta_B = \theta_C$ at the stationary point

can be found by rewriting Equation (6.69),

$$\frac{2\Delta U}{4\pi R^2\sigma} = 2(1+\cos\theta) + \frac{\sigma'}{2\sigma}\sin^2\theta - 2 - \cos\theta\left(3-\cos^2\theta\right) = \left(\frac{\sigma'}{2\sigma} - \cos\theta\right)\cdot\sin^2\theta = 0. \tag{6.70}$$

This gives that $\Delta U = 0$ if $\theta = 0$ or $\cos\theta = \frac{\sigma'}{2\sigma}$. These two cases are shown in Figure 6.9.

Define $\theta_0 \equiv \cos^{-1}\left(\frac{\sigma'}{2\sigma}\right)$ which represents Figure 6.9a. If $\frac{\sigma'}{2\sigma} > 1$, there is no solution for $\cos\theta = \frac{\sigma'}{2\sigma}$. However, this case cannot arise because of the triangle inequalities (6.64) of the $\sigma' s$.

Let us see how the action behaves by varying the radii from the solution. In the case of three vacua in a one dimensional potential, there is a constraint (6.31) for R_1 and R_2 so there is only one direction to vary them. However, there are many degrees of freedom for barnacles.

Consider infinitesimal variations which do not change r, the radius of the wall between B and C,

$$R_B = \bar{R} + \delta_B, \quad R_C = \bar{R} + \delta_C, \quad \theta_B = \theta_0 + \Delta\theta_B, \quad \theta_C = \theta_0 + \Delta\theta_C, \tag{6.71}$$

where

$$r = R_B\sin\theta_B = R_C\sin\theta_C = (\text{const.}). \tag{6.72}$$

The energy condition $\Delta U = 0$ at $\tau = 0$ and the fact that r is fixed give that

$$\Delta\theta_B = -\tan\theta_0\cdot\frac{\delta_B}{\bar{R}} = -\Delta\theta_C = \tan\theta_0\cdot\frac{\delta_C}{\bar{R}}. \tag{6.73}$$

We can evaluate the action with these small perturbation by using Equations (6.68) and (6.69),

$$S[R_B, R_C] = S[\bar{R},\bar{R}] - \frac{1}{2}\pi\sigma\bar{R}\left[12\pi - 12\theta_0 + 4\sin(2\theta_0) + \sin(4\theta_0)\right]\cdot\delta_B^2. \tag{6.74}$$

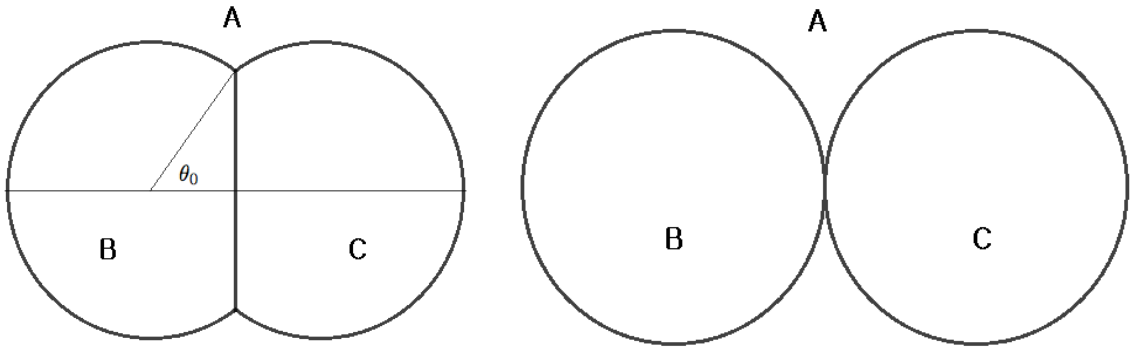

(a) The case $\theta = \theta_0 = \cos^{-1}\left(\frac{\sigma'}{2\sigma}\right)$

(b) The case $\theta = 0$

Figure 6.9: Two bounce solutions. The case $\theta = 0$ is the situation two bubbles meet at one point(b).

The second derivative of the action is given by

$$\left.\frac{d^2R[R_B,R_C]}{d\delta_B^2}\right|_{R_B=R_C=\bar{R}} = -\pi\sigma\bar{R}\left[12\pi - 12\theta_0 + 4\sin(2\theta_0) + \sin(4\theta_0)\right] < 0, \quad (0 \le \theta < \pi/2). \tag{6.75}$$

Note that the range of θ is $[0, \pi/2)$ in our example. This means the variations (6.73) always lower the action so it is the local maximum along a path which does not change r.

Consider another type of variations, $R = R_B = R_C = \bar{R} + \delta$. The radius of each bubble equals to each other in the variations. Then, the condition $\Delta U = 0$ at $\alpha = \pi/2$ gives that

$$2\left(1 - \frac{R}{\bar{R}}\right)(1 + \cos\theta) + \left(\frac{\sigma'}{2\sigma} - \frac{R}{\bar{R}}\cos\theta\right)\sin^2\theta = 0. \tag{6.76}$$

It is possible to see local properties of the action by considering the infinitesimal variation,

$$R = \bar{R} + \delta, \quad \theta = \theta_0 + \Delta\theta. \tag{6.77}$$

The condition (6.76) gives that

$$\Delta\theta = \frac{-2 - 3\cos\theta_0 + \cos^3\theta_0}{\sin^3\theta_0} \cdot \frac{\delta}{\bar{R}}. \tag{6.78}$$

We can expand the action around the solution,

$$S[R,\theta] = S[\bar{R},\theta_0] - \pi\sigma\bar{R}\left[6\pi - 6\theta_0 - 4\left(-8 + \csc^4\left(\frac{\theta_0}{2}\right)\right)\sin\theta_0 + 21\sin(2\theta_0) - 2\sin(4\theta_0)\right]\delta^2 \tag{6.79}$$

The second derivative of the action becomes

$$\begin{aligned}\left.\frac{d^2S}{d\delta^2}\right|_{R=\bar{R}} &= -2\pi\sigma\bar{R}\left[6\pi - 6\theta_0 - 4\left(-8 + \csc^4\left(\frac{\theta_0}{2}\right)\right)\sin\theta_0 + 21\sin(2\theta_0) - 2\sin(4\theta_0)\right] \\ &= \begin{cases} > 0 & \text{if } 0 \le \theta_0 < \tilde{\theta}_0 \\ < 0 & \text{if } \tilde{\theta}_0 < \theta_0 < \pi/2. \end{cases}\end{aligned} \tag{6.80}$$

Here, $\tilde{\theta}_0 = 1.0181...$ is found numerically. Remind $\theta_0 = \cos^{-1}(1/2) = 1.0472...$ if $\sigma' = \sigma$. In this case θ_0 is slightly larger than $\tilde{\theta}_0$. In other words, the action is the local minimum for sufficiently large σ'. However, as σ' gets smaller, the action on the solution turns into the local minimum where σ' is slightly bigger than σ, (at $\theta_0 = \tilde{\theta}_0$).

Let us see what happens here. According to [25], a barnacle has two negative modes. If a wall between two vacua is bigger than a hemisphere, the mode moving the wall back and forth

has a negative eigenvalue. On the contrary, moving the wall which is smaller than a hemisphere cannot lower the action. In our example, moving σ_{AB} and σ_{AC} give negative modes, since θ_B and θ_C cannot be greater than $\pi/2$. The mode that varies r is a positive mode. In the first case we studied, the radius between B and C, r, is fixed so the mode moving r is not included. This means this variation is basically the sum of two negative modes which move the walls with σ_{AB} and σ_{AC}, respectively. The sum of two negative modes decreases the action so we found a local maximum there. For the variation with $R_A = R_B$, the inner radius r also changes as R_A and R_B vary. Since the contribution from A and B is the same as each other, we can deal with them as one mode. Thus, the variation is the sum of the mode which moves $R = R_A = R_B$ and the mode by varying r which has a positive eigenvalue. Because the variation is a mixed mode with different signs, the action gets a local minimum where the positive mode becomes dominant. This explains why large σ' makes the action to be a local minimum. On the other hand, the action becomes a local maximum as σ' gets smaller.

Consider the case that the size of a bubble C is much smaller than that of a bubble B. This can happen if the radius of C (R_C) is smaller than R_B or the angle θ_B is very close to π ($\theta_B \lesssim \pi$). Then, as in the case of Figure 6.5, a lot of small bubbles C can be attached to a bubble B. This is a so-called 'barnacle'[26]. In this case, the wall tension σ_{AB} is shifted as

$$\sigma_{AB} \to \tilde{\sigma}_{AB} = \sigma_{AB} - iK_b e^{-B_b} = \sigma_{AB} - i\Gamma_b, \tag{6.81}$$

where B_b is the increase in the action with one small bubble C and Γ_b is the decay rate from the wall to a bubble C per wall three-volume.

Coleman's argument implies that S_B is not the minimum of the action for given Euclidean energy if there are more than one negative modes. Because every barnacle solution has two negative modes, it should not be the global minimum within the field configuration which preserves the Euclidean energy according to Coleman's argument. We have checked that the action on the bounce solution is not the global minimum in either case. We can also see it is possible to construct the mode which satisfies the energy condition by summing two negative modes since S_B is not at the minimum among the states with fixed energy. The global minimum of the action is the one bubble case as like the example in Section 6.3.2. In this case, there is only one negative mode.

If there are more than three vacua in a multi-field potential, there can be more types of the

bounce solutions. For the case of four vacua, the center of bubbles can form a triangle[1]. Because a triangle is a two dimensional object, the plane which contains the triangle can be the $\tau = t = 0$ slice. For the case of five vacua, the center of bubbles form a tetrahedron. Since a tetrahedron is a three dimensional object, we can still find a $\tau = 0$ three dimensional slice such that $\dot{\phi} = 0$. If there are six vacua, the center of bubbles form a 5-cell which is a four-dimensional object bounded by five tetrahedral cells. In this case, it is impossible to find a three dimensional slice which gives $\dot{\phi} = 0$. Because this solution does not obey the boundary condition (2.22), this is not a bounce solution and the interpretation is unclear.

[1] A straight line is also an extreme case of a triangle.

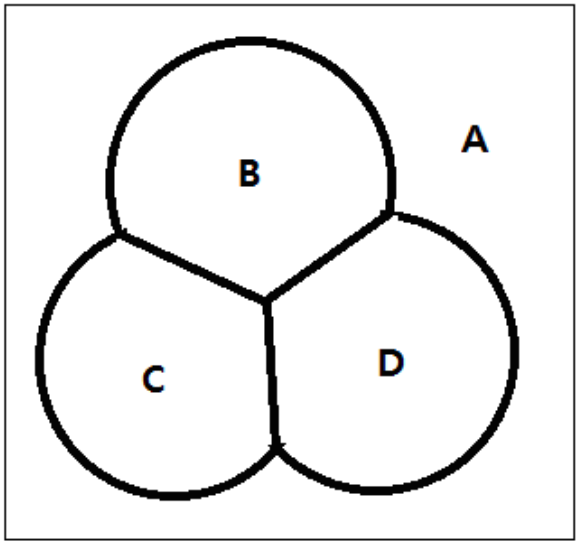

(a) Four vacua

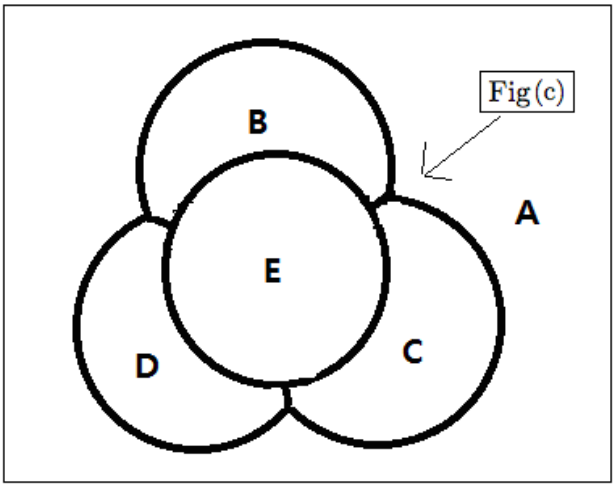

(b) Five vacua

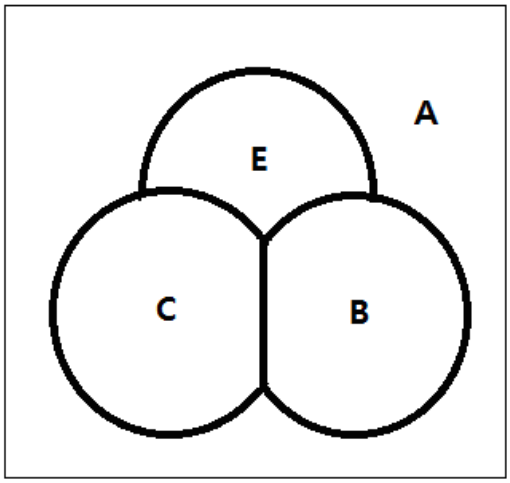

(c) Five vacua

Figure 6.10: Bounce solutions for multiple vacua. Figure (c) is the five vacua case as seen in the direction of the arrow in (b). If there are six vacua, the center of bubbles form a 5-cell, which is hard to be drawn here.

Chapter 7

Negative mode problem in curved spacetime

This chapter mainly deals with the mode spectrum of Coleman-de Luccia bounces. We studied the semi-classical approach of CdL in Chapter 3 and the quantum approach to the vacuum decay in flat space is covered in Section 2.3. One can ask how to develop a quantum approach in curved space to fill the question marks in Figure 7.1.

This is the area of quantum gravity so there are many open questions. In this chapter, we

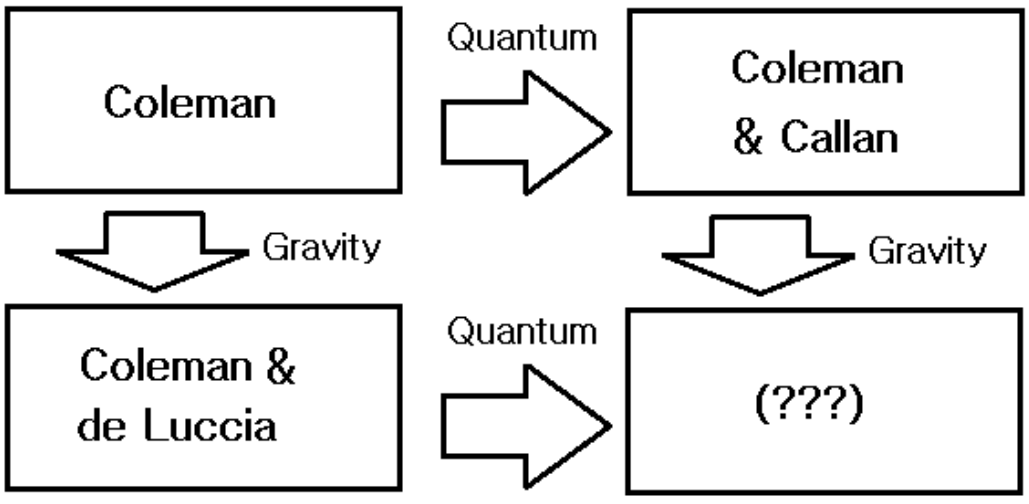

Figure 7.1: A simple diagram about the vacuum decay.

suggest the answer in the low energy limit, the weak gravity limit. Additionally, we can show many interesting properties in the strong gravity case.

The first relevant work has been done by Lavrelashvili, Rubakov and Tinyakov[27]. They found that the kinetic energy term in the second order Lagrangian in the $O(4)$-invariant perturbative expansion with the $\Psi = 0$ gauge is given by

$$S_{\rm LRT}(\text{quadratic in } \dot{\Phi}) = \int \frac{\pi^2 \rho^2 \dot{\rho}^2}{Q_{LRT}} \dot{\Phi}^2 d\xi, \tag{7.1}$$

where Φ is the perturbative field of ϕ and $Q_{\rm LRT} = 1 - \frac{1}{3}\kappa\rho^2 U$. They showed that $Q_{\rm LRT}$ can be negative somewhere so there can exist a large number of negative modes with rapidly varying perturbations concentrated in the region where $Q_{\rm LRT} < 0$. They claimed these negative modes are the consequences of the breakdown of the quasi-classical approximation.

After LRT's work, Tanaka and Sasaki[28] argued that the negative kinetic energy region exists in neither the $O(4)$ symmetric case nor the case of a higher angular momentum by choosing the gauge conditions $A + \Psi = 0$ and $C = 0$.[1]. However, we will see that this result cannot be applicable to the $O(4)$ symmetric case in Section 7.1.

We developed a gauge independent approach to the second order Lagrangian[29]. It shows us that there is a negative kinetic region in the $O(4)$ symmetric case, as LRT found before, and that a negative kinetic region does not exist for a higher angular momentum case, as Tanaka and Sasaki argued.

We will see that the second order Lagrangian in the $O(4)$ symmetric perturbation expansions can be written as Equation (7.24),

$$\mathcal{L}_E^{(2)} = \frac{\rho^3}{2Q}\dot{\chi}^2 + \frac{\rho^3}{2Q} f \chi^2. \tag{7.2}$$

If Q becomes negative in some region, it implies a negative kinetic term. Then, it is possible to lower the action arbitrary by varying fields very rapidly so there are an infinite number of negative modes.[2] If Q is positive everywhere on the bubble wall, there is a negative mode in analogy of the negative mode in flat space. As gravitational effects get stronger, the eigenvalue of this mode

[1] These fields are defined in Section 7.1.2.

[2] See Section 7.2.

approaches zero and then it turns into a positive mode.[3] We will discuss this approach and its interpretation throughout this chapter.

Let us warm up first before studying the details of the perturbative expansions. In Section 6.2, we developed an approach to find negative eigenvalues analytically with the thin-wall approximation. However, the thin-wall approximation no longer gives the eigenvalue in curved space because gravitational effects on the wall cannot be described suitably in the format of the thin-wall approximation. Nevertheless, it is still helpful to get an insight about the mode structure. Recall that the field equation and its derivatives of the Coleman-de Luccia metric are given by

$$\Box\phi(\xi) = \ddot{\phi}(\xi) + \frac{3\dot{\rho}}{\rho}\dot{\phi}(\xi) = U'[\phi], \tag{7.3}$$

$$\dddot{\phi} + \frac{3\dot{\rho}}{\rho}\ddot{\phi} + \left(\frac{3\ddot{\rho}}{\rho} - \frac{3\dot{\rho}^2}{\rho^2}\right)\dot{\phi} = U''[\phi]\cdot\dot{\phi}. \tag{7.4}$$

By combining the constraint (3.9) and the equation (3.11), we can rewrite (7.4) as

$$\dddot{\phi} + \frac{3\dot{\rho}}{\rho}\ddot{\phi} + \frac{3}{\rho^2}\left(-1 - \frac{\kappa\rho^2\dot{\phi}^2}{2}\right)\dot{\phi} = U''[\phi]\cdot\dot{\phi}. \tag{7.5}$$

Compared to the case without the gravity, there is one extra term, $\kappa\rho^2\dot{\phi}^2/2$. If we assume the mode equation is given by the operator, '$-\Box + U''[\phi]$', as in the flat space case[4], the mode equation for a perturbative field $\phi \to \phi + \Phi_l(\xi)Y_l(\Omega)$ is

$$\left(-\Box + U''[\phi]\right)\Phi_l = \left[-\frac{d^2}{d\xi^2} - \frac{3\dot{\rho}}{\rho}\frac{d}{d\xi} + \frac{l(l+2)}{\rho^2} + U''[\phi]\right]\Phi_l = \lambda\Phi_l. \tag{7.6}$$

Let us test the case $\Phi_l(\xi) = \dot{\phi}(\xi)$. Then, the mode equation becomes

$$\left(\frac{l(l+2)-3}{\rho^2} - \frac{3\kappa\dot{\phi}^2}{2}\right)\dot{\phi} = \lambda\dot{\phi}. \tag{7.7}$$

Because $\dot{\phi}$ is not constant on the wall, this cannot be an eigenmode. Although $\Phi = \dot{\phi}$ is not an eigenfunction, one can say there is at least one negative mode because the $l = 0$ case implies that

$$\int \rho^3\dot{\phi}\left(-\Box + U''[\phi]\right)\dot{\phi}d\xi = \int -3\rho\left(1 + \frac{\kappa\rho^2\dot{\phi}^2}{2}\right)\dot{\phi}^2 d\xi < 0. \tag{7.8}$$

[3] See Section 7.3.

[4] This assumption is approximately valid only in the weak gravity limit.

However, the action (7.8) is approximately right only in the weak gravity limit. Since this approach is based on the scalar field, it cannot explain the cases where the gravitational fields become dominant. Although this cannot cover the whole case of the gravity, this confirms there is at least one negative mode in the weak gravity and this also agrees with the analysis of the type A bounce as in Equation (4.27). In order to explain a complete behavior of perturbative fields, we need the perturbative expansions of the scalar field and the metric, as in Section 7.1.

7.1 The perturbative expansion of the CdL bounce

The thin-wall approximation is a good tool to see a semi-classical bounce solution of the vacuum tunneling. To describe the negative mode problem properly, we need to investigate the whole configuration space, which the thin-wall approximation cannot take into account. There are several attempts for decades to solve the negative mode problem of vacuum tunneling in the presence of the gravity[20, 27, 28, 30–36]. The most common way is the perturbative expansion of the Lagrangian. We have developed a gauge-independent approach which describes negative modes properly and gives a good point of view of the vacuum decay process.

7.1.1 The $O(4)$-symmetric case

Let us consider the $O(4)$-symmetric perturbations of the Coleman-de Luccia metric,

$$ds^2 = (1 + A(\xi))^2 d\xi^2 + \rho(\xi)^2 (1 + \Psi(\xi))^2 d\Omega_3^2, \tag{7.9}$$

and define the perturbative scalar field by

$$\phi(\xi) \to \phi(\xi) + \Phi(\xi). \tag{7.10}$$

In the $O(4)$-symmetric case, these three perturbative variables (A, Ψ and Φ) are the least number of variables, needed to describe the system properly. In the case of the higher angular momentum, we need two more extra perturbative terms. We will see this case in Section 7.1.2.

The background CdL action after integration by parts is given by (3.12)

$$S_E = 2\pi^2 \int d\xi \left[\rho^3 \left(\frac{1}{2}\dot{\phi}^2 + U \right) - \frac{3}{\kappa} \left(\rho\dot{\rho}^2 + \rho \right) \right]. \tag{7.11}$$

The background fields (ρ, ϕ) satisfy the constraint (3.9) and the field equation (3.10).

Now we expand the total action around the background solutions. Then, the first order of the action in perturbation vanishes by the constraint (3.9) and the field equation (3.10), and the quadratic action is given by

$$S_E^{(2)} = 2\pi^2 \int \mathcal{L}_E^{(2)}(\Phi, \Psi, A; \dot{\Phi}, \dot{\Psi}) d\xi \tag{7.12}$$

where

$$\begin{aligned}\mathcal{L}_E^{(2)}(\Phi, \Psi, A; \dot{\Phi}, \dot{\Psi}) = &-\frac{3}{\kappa}\rho^3\dot{\Psi}^2 + \frac{3}{\kappa}\rho\Psi^2 + \frac{1}{2}\rho^3\dot{\Phi}^2 + \frac{1}{2}\rho^3 U''\Phi^2 - 3\rho^3\dot{\phi}\dot{\Psi}\Phi \\ &+ \left(-\rho^3\dot{\phi}\dot{\Phi} + \rho^3 U'\Phi + \frac{6}{\kappa}\dot{\rho}\rho^2\dot{\Psi} + \frac{6}{\kappa}\rho\Psi\right) A - \frac{3}{\kappa}\rho\dot{\rho}^2 Q A^2\end{aligned} \tag{7.13}$$

with

$$Q = 1 - \frac{\kappa\rho^2\dot{\phi}^2}{6\dot{\rho}^2}. \tag{7.14}$$

The fact that the second order Lagrangian ($\mathcal{L}_E^{(2)}$) doesn't contain a ξ-derivative of A implies the existence of a constraint ($C^{(1)} = \delta\mathcal{L}_E^{(2)}/\delta A$) in the second order Lagrangian. Since varying A is re-parameterizing the Euclidean time (ξ), this is the same as the Einstein equation ($G_{00} = -\kappa T_{00}$) which gives the constraint equation for the background fields. It implies this constraint is the first order expansion of the constraint of the background fields,

$$C^{(1)} : \frac{\kappa\rho^2}{6}\left(\dot{\phi}\dot{\Phi} - U'\Phi\right) - \left(\rho\dot{\rho}\dot{\Psi} + \Psi\right) + \dot{\rho}^2 Q A = 0. \tag{7.15}$$

The set of these perturbative fields has a gauge freedom as the set of the background fields does. Under the transformation $\xi \to \xi + \alpha(\xi)$, the system is invariant under the following gauge transformations

$$\delta_G\Phi = \dot{\phi}\alpha, \quad \delta_G\Psi = \frac{\dot{\rho}}{\rho}\alpha, \quad \delta_G A = \dot{\alpha}. \tag{7.16}$$

In other words, the second order Lagrangian is invariant under the gauge transformation,

$$\begin{aligned}\delta_G\mathcal{L}_E^{(2)} &= -\frac{3}{\kappa}\rho^3(\delta_G\dot{\Psi})^2 + \frac{3}{\kappa}\rho(\delta_G\Psi)^2 + \frac{1}{2}\rho^3(\delta_G\dot{\Phi})^2 + \frac{1}{2}U''\rho^3(\delta_G\Phi)^2 - 3\rho^3\dot{\phi}(\delta_G\dot{\Psi})(\delta_G\Phi) \\ &+ \left(-\rho^3\dot{\phi}(\delta_G\dot{\Phi}) + \rho^3 U'(\delta_G\Phi) + \frac{6}{\kappa}\dot{\rho}\rho^2(\delta_G\dot{\Psi}) + \frac{6}{\kappa}\rho(\delta_G\Psi)\right)(\delta_G A) - \frac{3}{\kappa}\rho\dot{\rho}^2 Q(\delta_G A)^2 \\ &= 0 + (\text{total derivative term})\end{aligned} \tag{7.17}$$

and the constraint is also gauge invariant,

$$\delta_G C^{(1)} = \frac{\kappa\rho^2}{6}\left(\dot{\phi}(\delta_G\dot{\Phi}) - U'(\delta_G\Phi)\right) - \left(\rho\dot{\rho}(\delta_G\dot{\Psi}) + (\delta_G\Psi)\right) + \dot{\rho}^2 Q(\delta_G A) = 0. \tag{7.18}$$

The second order Lagrangian has three variables (Φ, Ψ and A), a constraint ($C^{(1)}$) and a gauge condition which we have not imposed yet. If we eliminate A by using the constraint, the Lagrangian has only two variables and a gauge condition. As the result, the Lagrangian (7.13) is written by

$$\begin{aligned}\mathcal{L}_E^{(2)}(\Phi,\Psi;\dot{\Phi},\dot{\Psi}) &= \frac{\rho^3}{2Q}\left(\dot{\Phi}-\frac{\rho\dot{\phi}}{\dot{\rho}}\dot{\Psi}\right)^2 + W[\Phi,\Psi,\dot{\Psi}] - \frac{3}{\kappa}\frac{\rho}{\dot{\rho}^2 Q}(C^{(1)})^2 \\ &= \frac{\rho^3}{2Q}\left(\dot{\Phi}-\frac{\rho\dot{\phi}}{\dot{\rho}}\dot{\Psi}\right)^2 + W[\Phi,\Psi,\dot{\Psi}]. \end{aligned} \tag{7.19}$$

The first term is the euclidean kinetic energy term and W is the sum of the first order time derivative terms and the potential terms as

$$\begin{aligned} W &= \frac{\rho^3}{Q}\frac{d}{d\xi}\left(\frac{\rho\dot{\phi}}{\dot{\rho}}\right)\dot{\Psi}\Phi + \frac{\rho^3}{\dot{\rho}^2 Q}\left(2U' - \frac{2\dot{\phi}\ddot{\rho}}{\dot{\rho}} - \frac{\dot{\phi}\dot{Q}}{Q}\right)\Phi\Psi + \frac{3\rho^2}{\kappa\dot{\rho}^2 Q}\left(-\frac{2\kappa\rho\dot{\phi}^2}{3} + \frac{\dot{\rho}\dot{Q}}{Q}\right)\Psi^2 \\ &+ \frac{\rho^3}{2Q}\left[U'' + \frac{\kappa\rho^2 U'^2}{3\dot{\rho}^2 Q} + \frac{\kappa\rho\dot{\phi}U'}{3\dot{\rho}^3 Q}\right]\Phi^2. \end{aligned} \tag{7.20}$$

This new form of Lagrangian is still gauge invariant since the constraint which we used to eliminate A term is also gauge invariant. This fact implies that it is possible to write the second order Lagrangian in terms of gauge invariant variables.

Let us define a gauge invariant variable $\chi(\xi)$,

$$\chi \equiv \Phi - \frac{\rho\dot{\phi}}{\dot{\rho}}\Psi, \tag{7.21}$$

then the derivative of χ is given by

$$\dot{\chi} = \dot{\Phi} - \frac{\rho\dot{\phi}}{\dot{\rho}}\dot{\Psi} - \frac{d}{d\xi}\left(\frac{\rho\dot{\phi}}{\dot{\rho}}\right)\Psi. \tag{7.22}$$

The kinetic term in terms of χ should be

$$\begin{aligned}\frac{\rho^3}{2Q}\dot{\chi}^2 &= \frac{\rho^3}{2Q}\left\{\dot{\Phi} - \frac{\rho\dot{\phi}}{\dot{\rho}}\dot{\Psi} - \frac{d}{d\xi}\left(\frac{\rho\dot{\phi}}{\dot{\rho}}\right)\Psi\right\}^2 \\ &= \frac{\rho^3}{2Q}\left(\dot{\Phi}-\frac{\rho\dot{\phi}}{\dot{\rho}}\dot{\Psi}\right)^2 - \frac{\rho^3}{Q}\frac{d}{d\xi}\left(\frac{\rho\dot{\phi}}{\dot{\rho}}\right)\dot{\Phi}\Psi + \frac{\rho^3}{Q}\frac{\rho\dot{\phi}}{\dot{\rho}}\frac{d}{d\xi}\left(\frac{\rho\dot{\phi}}{\dot{\rho}}\right)\Psi\dot{\Psi} + \frac{\rho^3}{2Q}\left\{\frac{d}{d\xi}\left(\frac{\rho\dot{\phi}}{\dot{\rho}}\right)\right\}^2\Psi^2. \end{aligned} \tag{7.23}$$

The first order in ξ derivative term($\dot{\Phi}\Psi$) has the same coefficient as the first order term($\Phi\dot{\Psi}$) in W. This means we can get rid of the first order terms by integration by part, so the kinetic term

of the gauge invariant Lagrangian has to be proportional to $\dot{\chi}^2$. Without ξ-derivatives, χ is the only possible gauge invariant linear combination of Ψ and Φ. Since the remaining terms have no time derivatives, the potential term of the gauge invariant Lagrangian should be proportional to χ^2. Thus, the following form is the only way to write the gauge invariant form of the Lagrangian.

$$\boxed{\mathcal{L}_E^{(2)}(\chi;\dot{\chi}) = \frac{\rho^3}{2Q}\dot{\chi}^2 + \frac{\rho^3}{2Q}f(\rho,\phi)\chi^2.} \tag{7.24}$$

To verify the Lagrangian can be written as (7.24), we need to check whether the following equation combined by Equations (7.19), (7.20), (7.23) and (7.24) holds

$$\begin{aligned}
\frac{\rho^3}{2Q}f(\rho,\phi)\chi^2 &= \frac{\rho^3}{Q}\frac{d}{d\xi}\left(\frac{\rho\dot{\phi}}{\dot{\rho}}\right)\dot{\Phi}\Psi - \frac{\rho^3}{Q}\frac{\rho\dot{\phi}}{\dot{\rho}}\frac{d}{d\xi}\left(\frac{\rho\dot{\phi}}{\dot{\rho}}\right)\Psi\dot{\Psi} - \frac{\rho^3}{2Q}\left\{\frac{d}{d\xi}\left(\frac{\rho\dot{\phi}}{\dot{\rho}}\right)\right\}^2\Psi^2 \\
&\quad + \frac{\rho^3}{Q}\frac{d}{d\xi}\left(\frac{\rho\dot{\phi}}{\dot{\rho}}\right)\dot{\Psi}\Phi + \frac{\rho^3}{\dot{\rho}^2Q}\left(2U' - \frac{2\dot{\phi}\ddot{\rho}}{\dot{\rho}} - \frac{\dot{\phi}\dot{Q}}{Q}\right)\Phi\Psi + \frac{3\rho^2}{\kappa\dot{\rho}^2Q}\left(-\frac{2\kappa\rho\dot{\phi}^2}{3} + \frac{\dot{\rho}\dot{Q}}{Q}\right)\Psi^2 \\
&\quad + \frac{\rho^3}{2Q}\left[U'' + \frac{\kappa\rho^2U'^2}{3\dot{\rho}^2Q} + \frac{\kappa\rho\dot{\phi}U'}{3\dot{\rho}^3Q}\right]\Phi^2 + (\text{total derivative term}) \qquad (7.25) \\
&= \frac{\rho^3}{2Q}\left[U'' + \frac{\kappa\rho^2U'^2}{3\dot{\rho}^2Q} + \frac{\kappa\rho\dot{\phi}U'}{3\dot{\rho}^3Q}\right]\Phi^2 \\
&\quad + \left[-\frac{d}{d\xi}\left\{\frac{\rho^3}{Q}\frac{d}{d\xi}\left(\frac{\rho\dot{\phi}}{\dot{\rho}}\right)\right\} + \frac{\rho^3}{\dot{\rho}^2Q}\left(2U' - \frac{2\dot{\phi}\ddot{\rho}}{\dot{\rho}} - \frac{\dot{\phi}\dot{Q}}{Q}\right)\right]\Phi\Psi \\
&\quad + \left[\frac{1}{2}\frac{d}{d\xi}\left\{\frac{\rho^3}{Q}\frac{\rho\dot{\phi}}{\dot{\rho}}\frac{d}{d\xi}\left(\frac{\rho\dot{\phi}}{\dot{\rho}}\right)\right\} + \frac{3\rho^2}{\kappa\dot{\rho}^2Q}\left(-\frac{2\kappa\rho\dot{\phi}^2}{3} + \frac{\dot{\rho}\dot{Q}}{Q}\right)\right]\Psi^2 + (\text{total derivative term}). \qquad (7.26)
\end{aligned}$$

By using the identities,

$$\begin{aligned}
\frac{\rho^3}{2Q}\left[U'' + \frac{\kappa\rho^2U'^2}{3\dot{\rho}^2Q} + \frac{\kappa\rho\dot{\phi}U'}{3\dot{\rho}^3Q}\right] &= -\frac{\dot{\rho}}{2\rho\dot{\phi}}\left[-\frac{d}{d\xi}\left\{\frac{\rho^3}{Q}\frac{d}{d\xi}\left(\frac{\rho\dot{\phi}}{\dot{\rho}}\right)\right\} + \frac{\rho^3}{\dot{\rho}^2Q}\left(2U' - \frac{2\dot{\phi}\ddot{\rho}}{\dot{\rho}} - \frac{\dot{\phi}\dot{Q}}{Q}\right)\right] \\
&= \left(\frac{\dot{\rho}}{\rho\dot{\phi}}\right)^2\left[\frac{1}{2}\frac{d}{d\xi}\left\{\frac{\rho^3}{Q}\frac{\rho\dot{\phi}}{\dot{\rho}}\frac{d}{d\xi}\left(\frac{\rho\dot{\phi}}{\dot{\rho}}\right)\right\} + \frac{3\rho^2}{\kappa\dot{\rho}^2Q}\left(-\frac{2\kappa\rho\dot{\phi}^2}{3} + \frac{\dot{\rho}\dot{Q}}{Q}\right)\right], \qquad (7.27)
\end{aligned}$$

the equation (7.26) becomes the form we required

$$\frac{\rho^3}{2Q}f(\rho,\phi)\chi^2 = \frac{\rho^3}{2Q}\left[U'' + \frac{\kappa\rho^2U'^2}{3\dot{\rho}^2Q} + \frac{\kappa\rho\dot{\phi}U'}{3\dot{\rho}^3Q}\right]\left(\Phi - \frac{\rho\dot{\phi}}{\dot{\rho}}\Psi\right)^2 + (\text{total derivative term}). \tag{7.28}$$

This means the second order Lagrangian is written as Equation (7.24) and $f(\rho,\phi)$ is given by

$$f(\rho,\phi) = U'' + \frac{\kappa\rho^2U'^2}{3\dot{\rho}^2Q} + \frac{\kappa\rho\dot{\phi}U'}{3\dot{\rho}^3Q}$$

$$= \frac{\dddot{\phi}}{\dot{\phi}} + \frac{\kappa\rho^2\ddot{\phi}^2}{3\dot{\rho}^2 Q} + \frac{\dot{\rho}\ddot{\phi}}{\rho\dot{\phi}Q}\left(3 + \frac{\kappa\rho^2\dot{\phi}^2}{3\dot{\rho}^4} + \frac{3\kappa\rho^2\dot{\phi}^2}{2\dot{\rho}^2}\right) + \frac{1}{\dot{\rho}^2 Q}\left[-\frac{3}{\rho^2} + \frac{5\kappa\dot{\phi}^2}{2} + \frac{\kappa^2\rho^2\dot{\phi}^4}{2} + \kappa U\left(1 - \frac{\kappa\rho^2\dot{\phi}^2}{2}\right)\right]. \tag{7.29}$$

We can see that the sign of the kinetic term of this Lagrangian only depends on the sign of Q. It means if Q becomes negative in some regions, we can lower the action arbitrarily by varying fields rapidly there. We will check that every CdL bounce in a de Sitter background has a negative Q region, in Section 7.2. This means that every CdL bounce in a de Sitter space has infinitely many negative modes. Actually, these negative kinetic regions were found before by Lavrelashvili, Rubakov and Tinyakov[27] but the difference is that they claimed this only for the special gauge choice ($\Psi = 0$). Meanwhile, our approach is gauge-independent so this argument is valid for all possible physical gauges. In other words, every CdL bounce has an infinite number of negative modes regardless of a gauge choice, and it has to be true since the physical property does not depend on the gauge choice. Of course, it is easy to check the second order Lagrangian becomes LRT's Lagrangian (7.1) by choosing $\Psi = 0$ gauge.

We studied the boundary conditions (3.20), (3.21) and (3.22) for background fields in a closed manifold are given by

$$\begin{aligned} \rho(0) = \rho(\xi_{\max}) = 0, \\ \dot{\rho}(0) = 1, \quad \dot{\rho}(\xi_{\max}) = -1, \\ \dot{\phi}(0) = \dot{\phi}(\xi_{\max}) = 0. \end{aligned} \tag{7.30}$$

Because the perturbations of background fields can shift the end point of the coordinate, $\xi_{\max}$ can be also shifted. This means that there is a subtlety in dealing with the perturbative fields around $\xi_{\max}$.

Let us find out how to solve this issue. For a convenience, we define a new notation, '˜', for the actual variables including the perturbative term. Up to the first order in perturbation, the actual fields are written by

$$\tilde{\phi} = \phi + \Phi, \quad \tilde{\rho} = \rho + \delta\rho. \tag{7.31}$$

These actual fields also satisfy the same boundary conditions but the end point of ξ can be moved to $\xi_{\max} \to \tilde{\xi}_{\max}$ as

$$\tilde{\rho}(0) = \tilde{\rho}(\tilde{\xi}_{\max}) = 0$$

$$\dot{\tilde{\rho}}(0) = 1, \quad \dot{\tilde{\rho}}(\tilde{\xi}_{\max}) = -1$$
$$\dot{\tilde{\phi}}(0) = \dot{\tilde{\phi}}(\tilde{\xi}_{\max}) = 0. \tag{7.32}$$

The proper length (l) of ξ is gauge independent since it is a physical quantity,

$$l = \int_0^{\tilde{\xi}_{\max}} (1 + A) d\xi. \tag{7.33}$$

To avoid the end point problem, we can choose the gauge such that

$$\tilde{\xi}_{\max} = \xi_{\max}. \tag{7.34}$$

By the definition of the end point, we find

$$\int_0^{\tilde{\xi}_{\max}} \dot{\rho} d\xi = 0, \quad \int_0^{\tilde{\xi}_{\max}} (\dot{\delta\rho}) d\xi = 0. \tag{7.35}$$

The geometrical boundary condition (3.21) at the both ends implies that

$$\frac{d(\rho + \delta\rho)}{(1 + A)d\xi} = \frac{d\rho}{d\xi} + \frac{d\delta\rho}{d\xi} - \frac{d\rho}{d\xi} A = \frac{d\rho}{d\xi} \quad (\text{at } \rho = 0,\ \dot{\rho} = \pm 1), \tag{7.36}$$

$$A = \frac{1}{\dot{\rho}} \dot{\delta\rho} = \dot{\rho}(\dot{\delta\rho}). \tag{7.37}$$

We can also get this boundary condition from the constraint

$$C^{(2)}|_{\rho=0} = \dot{\rho}\dot{\delta\rho} - A = 0. \quad \left(\because \Psi + \rho\dot{\rho}\dot{\Psi} = \dot{\rho}\dot{\delta\rho} \quad \text{at } \rho = 0.\right) \tag{7.38}$$

It is always possible to find the fields which obey the condition (7.37) in a closed manifold so the gauge condition (7.34) is a valid condition. Because physical properties do not depends on the gauge choice, the effect of moving the end point ($\xi_{\max}$) does not give any significant contribution even for some gauges which do not fix the end point ($\xi_{\max}$).

Types	Scalar	Vector	Tensor
Fields	A, B, Ψ, C	B_a, E_a	$E_{(ab)}$
Divergenceless ?	N/A	Yes	Yes
Traceless ?	N/A	N/A	Yes
Number of fields	4	4(=6-2)	2(=6-1-3)
Gauge freedoms	2	2(=3-1)	0
Constraints	2	2(=3-1)	0

Table 7.1: Vector type perturbative fields are divergenceless ($\nabla_a B^a = \nabla_a E^a = 0$) and a tensor type perturbative field is divergenceless ($\nabla_a E^{ab} = 0$) and traceless ($E^a{}_a = 0$). The divergence and the trace of the whole perturbative fields contribute to the scalar type perturbation.

7.1.2 Including Angular Momentum

In the $O(4)$-symmetric case, we need two perturbative fields (A and Ψ) in the metric. To describe more generic cases, more perturbative fields are required. We can write the perturbation of the metric by performing a scalar-vector-tensor decomposition[37]. At linear order, the metric has the form,

$$\begin{aligned} ds^2 &= (1+2A)d\xi^2 + (B_a + \nabla_a B)d\xi da \\ &\quad +\rho(\xi)^2\left[\bar{g}_{ab}(1+2\Psi) + 2\nabla_a\nabla_b C + \nabla_{(a}E_{b)} + E_{(ab)}\right] dadb. \end{aligned} \tag{7.39}$$

There are three types of perturbative fields. The properties of these fields are summarized in Table 7.1. By convention, ∇_a means a covariant derivative with respect to the three-dimensional spatial metric $\bar{g}_{ab}$.

Since we do not deal with vector matter fields, B_a and E_a do not couple to matter fields. There are four vector type perturbative fields but the actual number of degrees of freedom is zero because of two constraints and two gauge conditions. The vector fields are invariant under the gauge transformation, $a \to a + \beta_a$, where β_a is also divergenceless. The tensor fields $E_{(ab)}$ also has two degrees of freedom. These give two modes of gravitational waves. They do contribute to the action but do not couple to the scalar matter perturbation so they are not relevant for negative modes. It means that only the scalar type perturbation matters in the vacuum decay process.

Let us consider the scalar type perturbation only. Each perturbative field can be decomposed into the part which depends on ξ and the three-dimensional spherical harmonics ($Y_{lmn}(\Omega)$). Then, the metric given by[5]

$$\begin{aligned} ds^2 &= (1+2A_l(\xi)Y_l(\Omega))d\xi^2 + B_l(\xi)\nabla_a Y_l(\Omega)d\xi da \\ &\quad +\rho(\xi)^2\left[\bar{g}_{ab}(1+2\Psi_l(\xi)Y_l(\Omega)) + 2C_l(\xi)(k^{-2}\nabla_a\nabla_b + \bar{g}_{ab}/3)Y_l(\Omega)\right] dadb \end{aligned} \tag{7.40}$$

where $\bar{g}_{ab}$ is the three-dimensional spatial metric. The $Y_l(\Omega)$'s are eigenfunctions of the three-dimensional Laplacian,

$$\Delta Y_l(\Omega) = -l(l+2)\cdot Y_l(\Omega) = -k^2\cdot Y_l(\Omega) \tag{7.41}$$

For the simplicity, we set $k^2 = l(l+2)$ and we will omit the angular momentum index l in the perturbative fields.

For the $l=1$ case, $C(\xi)$ is a redundant field and we can set it equal to zero. In other words, the identity for the $l=1$ mode,

$$\nabla_a\nabla_b Y_{1mn}(\Omega) = -\bar{g}_{ab}Y_{1mn}(\Omega), \tag{7.42}$$

reduces one degree of freedom of the perturbative fields.

From the perturbative metric, we can find the second order Lagrangian including angular momentum as

$$\begin{aligned} \mathcal{L}_E^{(2)} &= -\frac{3}{\kappa}\rho^3\dot{\Psi}^2 - \frac{\rho}{\kappa}(k^2-3)\Psi^2 + \frac{1}{2}\rho^3\dot{\Phi}^2 + \frac{1}{2}\left(k^2\rho + \rho^3U''\right)\Phi^2 - 3\rho^3\dot{\phi}\dot{\Psi}\Phi \\ &\quad +\frac{\rho^3}{3\kappa}\left(\frac{k^2-3}{k^2}\right)\dot{C}^2 - \frac{\rho}{9\kappa}(k^2-3)C^2 - \frac{2\rho}{3\kappa}(k^2-3)\Psi C \\ &\quad +\left[-\rho^3\dot{\phi}\dot{\Phi} + \rho^3U'\Phi + \frac{6}{\kappa}\dot{\rho}\rho^2\dot{\Psi} + \frac{6}{\kappa}(1-k^2/3)\rho\Psi + \frac{2}{\kappa}(1-k^2/3)\rho C\right]A - \frac{3}{\kappa}\rho\dot{\rho}^2QA^2 \\ &\quad +\frac{2\dot{\rho}k^2}{\kappa}AB - \left[\frac{2\rho}{\kappa}\dot{\Psi} + \frac{2\rho}{3\kappa}\left(\frac{k^2-3}{k^2}\right)\dot{C} + \rho\dot{\phi}\Phi\right]k^2B - \frac{k^2}{\kappa\rho}B^2. \end{aligned} \tag{7.43}$$

This Lagrangian is also invariant under the following gauge transformation,

$$\xi \rightarrow \xi + \alpha(\xi)Y(\Omega) \tag{7.44}$$

$$a \rightarrow a + \beta(\xi)\partial_a Y(\Omega). \tag{7.45}$$

[5]The Ψ and C fields are different from (7.39). This metric is defined so to make C vanish at $l=1$.

and the gauge transformation rule are given by

$$\delta_G\Phi = \dot{\phi}\alpha, \quad \delta_G\Psi = \frac{\dot{\rho}}{\rho}\alpha - \frac{k^2}{3}\beta, \quad \delta_G A = \dot{\alpha}, \quad \delta_G B = \alpha + \rho^2\dot{\beta}, \quad \delta_G C = k^2\beta. \tag{7.46}$$

Since there are two different gauge parameters (α, β), we also need two gauge fixing conditions. Furthermore, this implies that there are two constraints in the system. One comes from the G_{00} equation, corresponding to α, and the other one comes from the G_{0i} equation which is related with β. As we expect, there are no derivatives of the perturbative fields A and B in the Lagrangian. We can treat A and B as Lagrange multipliers and those constraints can be found by taking derivatives with respect to A and B, respectively.

$$C_A^{(1)} : \frac{\kappa\rho^2}{6}\left(\dot{\phi}\dot{\Phi} - U'\Phi\right) - \left[\rho\dot{\rho}\dot{\Psi} + \left(1 - \frac{k^2}{3}\right)\left(\Psi + \frac{C}{3}\right) + \frac{\dot{\rho}k^2}{3\rho}B\right] + \dot{\rho}^2 QA = 0. \tag{7.47}$$

$$C_B^{(1)} : \dot{\Psi} + \frac{k^2 - 3}{3k^2}\dot{C} + \frac{\kappa\dot{\phi}}{2}\Phi - \frac{\dot{\rho}}{\rho}A + \frac{1}{\rho^2}B = 0. \tag{7.48}$$

We can check that the second order Lagrangian and both constraints are also gauge invariant.

$$\delta_G\mathcal{L}_E^{(2)} = 0, \quad \delta_G C_A^{(1)} = \delta_G C_B^{(1)} = 0. \tag{7.49}$$

This fact motivates us again to find a gauge independent form of the Lagrangian. There is only one possible gauge independent linear combination of perturbative fields

$$\chi \equiv \Phi - \frac{\rho\dot{\phi}}{\dot{\rho}}\Psi - \frac{\rho\dot{\phi}}{3\dot{\rho}}C. \tag{7.50}$$

We can eliminate two Lagrange multipliers (A, B) by using the identity,

$$\alpha A + \beta B + \gamma AB + \delta A^2 + \epsilon B^2 = \frac{\epsilon\alpha^2 + \delta\beta^2 - \gamma\alpha\beta}{\gamma^2 - 4\delta\epsilon}. \tag{7.51}$$

This gives

$$\begin{aligned}
(7.51) \;=\; & \left\{ -\frac{3}{\kappa}\rho\dot{\rho}^2 Q\cdot k^4\left[\frac{2\rho}{\kappa}\dot{\Psi} + \frac{2\rho}{3\kappa}\left(\frac{k^2-3}{k^2}\right)\dot{C} + \rho\dot{\phi}\Phi\right]^2 \right. \\
& -\frac{k^2}{\kappa\rho}\cdot\left[-\rho^3\dot{\phi}\dot{\Phi} + \rho^3 U'\Phi + \frac{6}{\kappa}\dot{\rho}\rho^2\dot{\Psi} + \frac{6}{\kappa}(1-k^2/3)\rho\Psi + \frac{2}{\kappa}(1-k^2/3)\rho C\right]^2 \\
& +\frac{2\dot{\rho}k^2}{\kappa}\cdot k^2\left[-\rho^3\dot{\phi}\dot{\Phi} + \rho^3 U'\Phi + \frac{6}{\kappa}\dot{\rho}\rho^2\dot{\Psi} + \frac{6}{\kappa}(1-k^2/3)\rho\Psi + \frac{2}{\kappa}(1-k^2/3)\rho C\right] \\
& \left.\cdot\left[\frac{2\rho}{\kappa}\dot{\Psi} + \frac{2\rho}{3\kappa}\left(\frac{k^2-3}{k^2}\right)\dot{C} + \rho\dot{\phi}\Phi\right]\right\} \Bigg/ \left\{\left(\frac{2\dot{\rho}k^2}{\kappa}\right)^2 - 4\cdot\frac{3}{\kappa}\rho\dot{\rho}^2 Q\cdot\frac{k^2}{\kappa\rho}\right\}.
\end{aligned} \tag{7.52}$$

The kinetic terms in (7.52) are given by

$$\frac{\rho^3}{2(Q-k^2/3)}\left[\frac{2}{\kappa}(3-2k^2+k^2Q)\dot{\Phi}^2+\frac{2}{9}\frac{Q}{\kappa}\frac{(k^2-3)^2}{k^2}\dot{C}^2+\frac{\kappa\rho^2\dot{\phi}^2}{6}\dot{\Phi}^2\right.$$
$$\left.-\frac{4}{3}\frac{k^2-3}{\kappa}(1-Q)\dot{\Psi}\dot{C}+\frac{2}{9}(k^2-3)\frac{\rho\dot{\phi}}{\dot{\rho}}\dot{\Phi}\dot{C}+\frac{2}{3}(k^2-3)\frac{\rho\dot{\phi}}{\dot{\rho}}\dot{\Phi}\dot{\Psi}\right]. \tag{7.53}$$

By combining with the kinetic terms in the Lagrangian (7.43), we obtain the kinetic terms of the Lagrangian after eliminating Lagrange multipliers,

$$\frac{\rho^3(1-k^2/3)}{2(Q-k^2/3)}\cdot\left(\dot{\Phi}-\frac{\rho\dot{\phi}}{\dot{\rho}}\dot{\Psi}-\frac{\rho\dot{\phi}}{3\dot{\rho}}\dot{C}\right)^2. \tag{7.54}$$

This is proportional to the kinetic part of $\dot{\chi}^2$,

$$\dot{\chi}^2=\left(\dot{\Phi}-\frac{\rho\dot{\phi}}{\dot{\rho}}\dot{\Psi}-\frac{\rho\dot{\phi}}{3\dot{\rho}}\dot{C}\right)^2+(\text{non-kinetic terms}). \tag{7.55}$$

We found the kinetic terms can be written in terms of $\dot{\chi}^2$. It implies the potential terms should be proportional to χ^2 because χ is the only gauge invariant linear combination of fields. After following the same steps we made in the $O(4)$ symmetric case, we can find a gauge independent form of the Lagrangian,

$$\boxed{\mathcal{L}_E^{(2)}=\frac{\rho^3(1-k^2/3)}{2(Q-k^2/3)}\dot{\chi}^2+\frac{\rho^3(1-k^2/3)}{2(Q-k^2/3)}f(\rho,\phi,k^2)\chi^2,} \tag{7.56}$$

where

$$\begin{aligned}f &= U''+\frac{k^2}{\rho^2}+\frac{\kappa}{3\dot{\rho}^3(Q-k^2/3)}\left\{\dot{\rho}\rho^2U'^2+\rho\dot{\phi}U'-k^2\left[2\rho\dot{\rho}^2\dot{\phi}U'-3\dot{\rho}^3\dot{\phi}^2Q+\dot{\rho}\dot{\phi}^2\right]\right\}\\ &= \frac{\dddot{\phi}}{\dot{\phi}}+\frac{\kappa\rho^2\ddot{\phi}^2}{3\dot{\rho}^2(Q-k^2/3)}+\frac{\dot{\rho}\ddot{\phi}}{\rho\dot{\phi}(Q-k^2/3)}\left[\left(3+\frac{\kappa\rho^2\dot{\phi}^2}{3\dot{\rho}^4}+\frac{3\kappa\rho^2\dot{\phi}^2}{2\dot{\rho}^2}\right)-k^2\left(1+\frac{2\kappa\rho^2\dot{\phi}^2}{3\dot{\rho}^2}\right)\right]\\ &\quad+\frac{1}{(Q-k^2/3)}\left\{\left[-\frac{3}{\rho^2}(Q-k^2/3)+\frac{\kappa\dot{\phi}^2}{\dot{\rho}^2}\left(1+3\dot{\rho}^2\left(1-\frac{Q}{2}\right)\right)\right](1-k^2/3)-k^2\frac{\kappa^2\rho^2\dot{\phi}^4}{12\dot{\rho}^2}\right\}\end{aligned} \tag{7.57}$$

We can see that the $l=1$ case do not contribute to the action. The kinetic terms cannot be negative since both $(1-k^2/3)$ and $(Q-k^2/3)$ are negative if $l\geq 2$. We can still see the Q dependence of the Lagrangian but the sign of Q does not determine the sign of the kinetic term. This also reproduces the $O(4)$ symmetric case if $l=0$. The highest order of k^2 in f is $\frac{-k^4}{3\rho^2(Q-k^2/3)}$. This term is positive definite and diverges as k goes to infinity.

	$l = 0$	$l = 1$	$l \geq 2$
Physical variables	Φ, Ψ, A	Φ, Ψ, A, B	Φ, Ψ, A, B, C
Number of variables	3	4	5
Number of Constraints	1 ($C_A^{(1)}$)	2 ($C_A^{(1)}$, $C_B^{(1)}$)	2 ($C_A^{(1)}$, $C_B^{(1)}$)
Number of Gauge freedom	1 (α)	2 (α, β)	2 (α, β)
Degrees of freedom	1	0	1
	neg. Q regions exist	N/A	no neg. kinetic region

Table 7.2: For $l = 1$ ($k^2 = 3$), there are four variables(Φ, Ψ, A and B), two constraints and two gauge conditions. Thus, there are no physical degrees of freedom. The Lagrangian vanishes identically in this case ($1 - k^2/3 = 0$). For $l \geq 2$, the kinetic term is positive definite because both $(1 - k^2/3)$ and $(Q - k^2/3)$ are negative, so there are no negative kinetic regions.

The result for the $l \geq 2$ modes is somewhat similar with the result of Sasaki and Tanaka[28]. Their second order Lagrangian is also proportional to $(1 - k^2/3)$ and has positive definite kinetic terms for $l \geq 2$. However, it is hard to see the Q dependence in their action. Especially for the $O(4)$ symmetric case, the number of degree of freedom is inappropriate. Meanwhile, with the gauge independent approach, we find that the $O(4)$ symmetric mode can have an infinite number of negative modes and higher angular momentum modes($l \geq 2$) cannot. This is true regardless of a gauge choice, and this property has to be gauge independent because physical properties do not depend on the gauge.

7.2 Properties of negative Q regions

We showed that the vacuum decay process in curved space can have a negative kinetic region which gives an infinite number of negative modes. In this section, we will show there are two different kinds of negative Q regions and that a CdL bounce in a de Sitter space always has a negative Q region. After that, we will discuss more details about negative Q regions for small type A bounces, large type A bounces and type B bounces.

7.2.1 Two kinds of negative Q regions

There are two different types of negative Q regions. The first one is found on the wall if the height of the scalar potential is sufficiently high. The other case is a negative Q region around the maximum of ρ ($\dot{\rho} = 0$). Because every CdL bounce in the de-Sitter background has a maximum of $\rho(\rho_M)$, the latter one is an inevitable case.

Let us define $\tilde{Q}$, which has the same sign as Q,

$$\tilde{Q} \equiv \dot{\rho}^2 Q = 1 - \frac{\kappa \rho^2 U}{3}. \tag{7.58}$$

The negative Q region on the wall exists if the height of the scalar potential is high enough to satisfy

$$\tilde{Q} = 1 - \frac{\kappa \rho^2 U}{3} < 0. \tag{7.59}$$

The above condition is valid regardless of the thickness of the wall. With the thin-wall approximation, we can rewrite this as

$$1 - \frac{\kappa \bar{\rho}^2 U_{\rm top}}{3} < 0 \tag{7.60}$$

where $\bar{\rho}$ is the size of a bubble with the thin-wall approximation.

Here, $U_{\rm top}$ is the top of the potential. Since the scalar field stays at $U_{\rm top}$ in the case of the HM solution, the radius of the HM solution is determined by the value of the top of the potential. Although this negative Q region on the wall is not directly related to the HM solution, we can find the above condition is the same as

$$\frac{\bar{\rho}}{\Lambda_{\rm top}} > 1, \quad \left(\Lambda_{\rm top} = \Lambda_{\rm HM} = \sqrt{\frac{3}{\kappa U_{\rm top}}} \right). \tag{7.61}$$

Since the size of the HM solution is always smaller than that of the CdL solution ($\Lambda_{\rm HM} < \Lambda_f$), this negative Q region on the wall starts to appear before the wall reaches the type B solution as

$\bar{\rho}$ is monotonically increased. For small bounces($\bar{\rho} \ll \Lambda_f$), the size of bounce barely depends on the gravitational effects and the scale of the potential also has to be much smaller than the Planck mass scale so $\bar{\rho}$ is smaller than $\Lambda_{\rm HM}$ in most cases. This means it is hard to find a negative Q region on the wall in the case of small bounces. We will discuss more details in Section 7.2.2.

Let us study the second case of the negative Q region. We can always find negative Q regions around the maximum of $\rho(\rho_M)$. At the maximum of ρ, the term $\dot{\phi}^2$ is exponentially small but never gets to exactly zero while $\dot{\rho}$ is zero. This means that the second term in Q goes to negative infinity as ρ goes to its maximum, so Q has to be negative there. We can also see this result in $\tilde{Q}$ (7.59). The size($\sqrt{\frac{3}{\kappa U(\rho_M)}}$) of de Sitter horizon given by $U[\phi(\rho_M)]$ has to be ρ_M if the wall is perfectly thin($\dot{\phi} = 0$ outside the wall). However, if we see the small difference due to the infinitesimally small $\dot{\phi}$, $\sqrt{\frac{3}{\kappa U(\rho_M)}}$ should be smaller than the maximum value of ρ (ρ_M) since ρ increases faster than in the static case($\dot{\phi} = 0$).

$$\sqrt{\frac{3}{\kappa U[\phi(\rho_M)]}} < \rho_M \tag{7.62}$$

$$\because \dot{\rho}^2 = 1 + \frac{\kappa\rho^2}{3}\left(\dot{\phi}^2 - U\right) > 1 - \frac{\kappa\rho^2}{3}U, \quad \rho \text{ increases faster.} \tag{7.63}$$

Thus, $\tilde{Q}$ is always negative at the maximum of ρ. We will also study some categories of the negative Q region around the maximum of ρ in Section 7.2.2.

Because every CdL bounce in de Sitter background has unavoidable negative Q regions which corresponds to negative kinetic terms, it has infinite number of negative modes. Since it is well-known that gravitational fields have negative kinetic terms in general, it would be related to gravitational effects. We can easily check the negative kinetic terms due to gravity from the fact that the kinetic term in terms of Ψ at the second order Lagrangian is $-\frac{3}{\kappa}\rho^3\dot{\Psi}^2$, which should be the same as the kinetic terms of pure gravitational cases. On the contrary, we can see the scalar fields have a positive kinetic term in the second order Lagrangian. This implies that when we describe the system in terms of the gauge invariant variable(χ), the kinetic term becomes negative where the gravitational effect dominates while it becomes positive where the fields effect gets stronger. The sign of Q determines which one is stronger in the system and negative Q regions are the area

where the gravitational field dominates.

$$Q = 1 - \frac{\kappa\rho^2\dot{\phi}^2}{6\dot{\rho}^2} = \frac{1}{\dot{\rho}^2}\left(1 - \frac{\kappa\rho^2 U}{3}\right). \tag{7.64}$$

We can see that Q decreases as κ, $\dot{\phi}^2$, $U(\phi)$ or ρ increases. Recall also that $\dot{\rho}^2$ decreases as ρ increases. Larger κ means stronger gravity and larger $\dot{\phi}^2$ or U implies a higher mass density which causes stronger gravitational field. When the bubble nucleates, the metric outside the bubble barely changes so it is approximately same as in the pure false vacuum case. This means the gravitational field outside the bubble increases linearly with the radius before or after the nucleation in Newtonian gravity. Beyond Newtonian gravity, it is not linear anymore but it still has to increase as ρ increases. To sum up, Q decreases as the gravitational effects gets stronger.

The above explanation cannot show why there must be a negative Q region around $\dot{\rho} = 0$. In order to understand this, let us think about the case where ρ is constant ($\dot{\rho} = 0$) in a certain region as the following

$$ds^2 = (1 + A(\xi))^2 d\xi^2 + \rho^2(1 + \Psi(\xi)^2)d\Omega_3^2. \tag{7.65}$$

This is a Euclidean cylinder which effectively behaves as a one dimensional case at the background level. Since ρ doesn't change at all when the fields vary, the gravitational field and the scalar field are decoupled completely in this case.

The second order Lagrangian on this Euclidean cylinder is given by

$$\begin{aligned}\mathcal{L}_E^{(2)}(\Phi, \Psi, A; \dot{\Phi}, \dot{\Psi}) = &-\frac{3}{\kappa}\rho^3\dot{\Psi}^2 + \frac{3}{\kappa}\rho\Psi^2 + \frac{1}{2}\rho^3\dot{\Phi}^2 + \frac{1}{2}\rho^3 U''\Phi^2 - 3\rho^3\dot{\phi}\dot{\Psi}\Phi \\ &+ \left(-\rho^3\dot{\phi}\dot{\Phi} + \rho^3 U'\Phi + \frac{6}{\kappa}\rho\Psi\right)A + \frac{\rho^3\dot{\phi}^2}{2}A^2.\end{aligned} \tag{7.66}$$

After eliminating A, we can find the second order Lagrangian, which only depends on Ψ,

$$\mathcal{L}_E^{(2)}(\Psi; \dot{\Psi}) = -\frac{3}{\kappa}\rho^3\dot{\Psi}^2 - \frac{18}{\kappa^2\rho\dot{\phi}^2}\left(1 - \frac{\kappa\rho^2\dot{\phi}^2}{6}\right)\Psi^2. \tag{7.67}$$

It does not depend on Φ anymore if $\dot{\rho} = 0$. This also shows that these two fields are decoupled. Even though the Lagrangian does not depend on Φ, Φ still exists and has any configuration that does not violate the constraint $C^{(1)}$.

$$C^{(1)} : \frac{\kappa\rho^2}{6}\left(\dot{\phi}\dot{\Phi} - U'\Phi\right) - \Psi - \frac{\kappa\rho^2\dot{\phi}^2}{6}A = 0. \tag{7.68}$$

However, Φ does not contribute to the Lagrangian since A in the constraint always cancels out the contribution from Φ. More precisely, we can write the second order Lagrangian as following,

$$\mathcal{L}_E^{(2)} = -\frac{3}{\kappa}\rho^3\dot{\Psi}^2 - \frac{18}{\kappa^2\rho\dot{\phi}^2}\left(1 - \frac{\kappa\rho^2\dot{\phi}^2}{6}\right)\Psi^2 + \frac{18}{\kappa^2\rho\dot{\phi}^2}\left[C^{(1)}(\Phi, \dot{\Phi}, \Psi, A)\right]^2 + (\text{surface term}). \quad (7.69)$$

The constraint ($C^{(1)}$) is the Einstein equation ($G_{00}^{(1)} = -\kappa T_{00}^{(1)}$) which is equivalent to the conservation of the energy density. In this effective one dimensional case, there is no friction term to decrease the energy. Thus, no possible configuration of Φ and A can change the energy due to the scalar field so the Lagrangian does not depend on them. Where $\dot{\rho} = 0$, the scalar field effects are ruled out and only the gravitational effects remain. This is why there is always negative Q region near the maximum of ρ. Of course, although $\dot{\rho} = 0$ is only at the maximum of ρ in the CdL bounces, this argument is approximately applicable to the case near the maximum of ρ ($|\dot{\rho}| \ll 1$). In this case, the fields are barely coupled to each other and the scalar field effect is almost negligible.

7.2.2 Negative Q regions for various types of bounces

We checked that there are two different kinds of negative Q regions. In this section, we investigate the relationship between the energy condition and the width of a negative Q region for small bounces, large bounces and type B bounces. We consider the condition, '$(\Delta\phi)^4 \sim (\Delta U) \sim (S_1)^{4/3} \sim U_{\rm top} \sim m^4$', with the thin-wall approximation, as in Chapter 4. The energy condition and the width of a negative Q region for each type of bounces are listed in Table 7.3.

First of all, let us investigate the negative Q regions on the wall. The width of the negative Q region is roughly

$$\Delta\xi = \int d\xi \sim \int_{\bar{\phi}_1}^{\bar{\phi}_2} d\phi \frac{1}{\sqrt{2(U - U_f)}} \sim \frac{\Delta\bar{\phi}}{\sqrt{\Delta U}} \sim \frac{1}{m}, \quad \left(U(\bar{\phi}_{1,2}) \equiv \frac{3\bar{\rho}^2}{\kappa}\right). \quad (7.70)$$

Unless Q barely touches zero, the width of a negative Q region is comparable with the width of the wall. In other words, the width of a negative Q region is greater than the Planck length if the mass scale of the potential (m) is smaller than the Planck scale ($m_{\rm pl}$), but it is smaller than the Planck length if $m > m_{\rm pl}$.

For small bounces ($\bar{\rho} \ll \Lambda_f$), it is possible to have negative Q regions only if the scale of the potential is greater than the Planck scale. The size of bounce is approximately same as the size

	Energy Condition	The width($\Delta\xi$) of negative Q region	
		Wall	ρ_M ($\dot{\rho}=0$)
Small bounces	$m/\alpha < m_{\rm pl}$	None	$\Delta\xi \ll \frac{1}{m_{\rm pl}}$
	$m/\alpha \gtrsim m_{\rm pl} \gg U_f^{1/4}$	$\Delta\xi \lesssim \frac{1}{\alpha m_{\rm pl}}$	$\Delta\xi \ll \frac{1}{m_{\rm pl}}$
Large bounces	$m < m_{\rm pl}$	$\Delta\xi > \frac{1}{m_{\rm pl}}$	$\Delta\xi < \frac{1}{m_{\rm pl}}$
	$m \gtrsim m_{\rm pl}$	$\Delta\xi \lesssim \frac{1}{m_{\rm pl}}$	$\Delta\xi \gtrsim \frac{1}{m_{\rm pl}}$
Type B	$m < m_{\rm pl}$	$\Delta\xi > \frac{1}{m_{\rm pl}}$	
	$m \gtrsim m_{\rm pl}$	$\Delta\xi \lesssim \frac{1}{m_{\rm pl}}$	

Table 7.3: As in Chapter 4, we consider '$m \sim (\Delta\phi)^4 \sim (\Delta U) \sim (S_1)^{4/3} \sim U_{\rm top} \sim \epsilon/\alpha$'. In the case of small bounces, the width of negative Q region is always smaller than the Planck length. There is no restriction of the range of the scalar potential for large bounces and the width depends on the scale of the potential but negative Q regions on the wall exist only if $\bar{\rho} > \Lambda_{\rm top}$. Type B essentially becomes either the wall case or the maximum of ρ case but the width of the negative Q region is the same as the wall case. For type B bounces, it is not necessary to be a sufficiently high potential to find a negative Q region since there is always a negative Q region around the maximum of ρ. If the width of negative Q region is smaller than the Planck length, negative modes would not exist physically.

without gravity

$$\bar{\rho} \approx \frac{3S_1}{\epsilon} \sim \frac{1}{\alpha m}, \tag{7.71}$$

where $\alpha = \epsilon/m < 1$. To have a negative Q region,

$$\frac{\kappa\bar{\rho}^2 U_{\rm top}}{3} \sim \frac{m^2}{\alpha^2 m_{\rm pl}^2} \gtrsim 1. \tag{7.72}$$

If $m \gtrsim \alpha m_{\rm pl}$, there is a negative Q region on the wall. According to Table 4.1, if the mass scale of the potential is comparable with the Planck mass ($m \sim m_{\rm pl}$), small bounces ($\bar{\rho} \ll \Lambda_f$) can exist where $U_f \ll m^4 \sim m_{\rm pl}^4$.

For large bounces ($\bar{\rho} \lesssim \Lambda_f$), the condition to have a negative Q region does not depend on the scale of the potential so a negative Q region on the wall can exist with any scale if the potential satisfies the condition (7.60),

$$1 < \frac{\kappa\bar{\rho}^2 U_{\rm top}}{3} \quad \rightarrow \quad \frac{\bar{\rho}}{\Lambda_{\rm top}} > 1 \tag{7.73}$$

In other words, if the size of the bubble gets larger than the horizon size of the HM solution, the negative Q region on the wall starts to appear.

Now let us investigate the width of the negative Q regions at the maximum of ρ. Consider the case where the mass scale of the potential (m) is much smaller than the Planck scale ($m \ll m_{\rm pl}$). Then, the width of the wall is approximately $1/m$, so the thin-wall approximation is valid for any kind of potential. Then, we can write each background fields near the maximum of ρ as

$$\begin{aligned} \phi &\sim me^{-m/H} \quad (m \gg H) \\ \dot{\phi} &\sim m^2 e^{-m/H} \\ \rho &\simeq 1/H \\ \dot{\rho} &\simeq \cos(H\delta) \end{aligned} \tag{7.74}$$

where δ is the displacement from the maximum of ρ and m is the mass scale of the scalar field. Then, we can find where Q becomes zero,

$$Q = 1 - \frac{\kappa\rho^2\dot{\phi}^2}{6\dot{\rho}^2} \sim 1 - \frac{\dot{\phi}^2}{m_{\rm pl}^2 H^2 \sin^2(H\delta_0)} = 0. \tag{7.75}$$

The size of the negative Q region($\Delta\xi$) is smaller than the Planck length

$$\Delta\xi = 2\delta_0 \sim \frac{\dot{\phi}}{m_{\rm pl} H^2} \ll \frac{1}{m_{\rm pl}}. \tag{7.76}$$

In the weak gravity limit, the size of bounce is much smaller than the horizon. In this case, the gravitational effect barely contributes to the tunneling process so the field configuration near the bounce is approximately the same as in the flat space. Thus, there is only one negative mode which dominates the tunneling as in flat space, and the infinite number of negative modes around the maximum of ρ would be physically meaningless because the negative Q region is less than the Planck scale.

If ϵ gets unusually small, the size of the bounce can be comparable to the horizon even in the weak gravity case ($m \ll m_{\rm pl}$). It's still the thin-wall case but $\dot{\phi}$ becomes larger than the small bounce case ($\dot{\phi} > m^2 e^{-m/H}$). The width of the negative region is roughly

$$\Delta\xi \sim \frac{\dot{\phi}}{m_{\rm pl}H^2} \sim \frac{m_{\rm pl}\dot{\phi}}{m^4}. \tag{7.77}$$

This is also smaller than the Planck length since $\dot{\phi}$ decreases exponentially outside the wall.

If the mass scale of the potential is much smaller than the Planck scale, type B bounces are found only if the size of bounce in flat space for a given potential is much larger than the horizon size or infinite ($\epsilon = 0$).

$$\bar{\rho}_{\rm flat} = \frac{3S_1}{\epsilon} > \frac{4}{\kappa S_1} \gg \Lambda \tag{7.78}$$

For type B solutions, Q becomes 0 when U satisfies

$$\frac{\kappa U}{3} = \frac{1}{\bar{\rho}^2} = \frac{1}{\Lambda_f^2} + \left(\frac{\kappa S_1}{4} - \frac{\epsilon}{3S_1}\right)^2, \tag{7.79}$$

$$\frac{\kappa(U - U_f)}{3} = \left(\frac{\kappa S_1}{4} - \frac{\epsilon}{3S_1}\right)^2 \lesssim \frac{m^6}{m_{\rm pl}^4}. \tag{7.80}$$

Since Q becomes 0 very near the false vacuum, the width of the negative Q region is almost the same as the width of the wall. The width is larger than the Planck length in this case.

Graphs	Neg. Q	Type	Orientation	A Slowly varying negative mode on the wall?
7.2	Not on wall	A-like	N/A	Yes
7.3	Not on wall	A-like	N/A	Yes
7.4	Not on wall	A-like	N/A	No
7.5	Wall	A-like	$\xi_{\rm top} < \xi_1 < \xi_{\rm min} < \xi_2$	No, maybe
7.6	Wall	A-like	$\xi_1 < \xi_{\rm top} < \xi_{\rm min} < \xi_2$	No
7.7	Mixed	A-like	$\xi_1 < \xi_{\rm top} < \xi_{\rm min} < \xi_M < \xi_2$	Don't know
7.8	ρ_M	A-like	$\xi_{\rm top} < \xi_1 < \xi_{\rm min} < \xi_M < \xi_2$	Yes
7.9	ρ_M	B-like	$\xi_1 < \xi_{\rm top} < \xi_{\rm min} = \xi_M < \xi_2$	No
7.10	ρ_M	B-like	$\xi_1 < \xi_{\rm top} = \xi_{\rm min} = \xi_M < \xi_2$	No
7.11	ρ_M	B-like	$\xi_1 < \xi_{\rm top} < \xi_{\rm min} = \xi_M < \xi_2$	No, but possible outside the wall

Table 7.4: The preview of examples of the potential term and negative modes. In Figure 7.4, we are able to see the ordinary negative mode turn into a positive mode as $Q \to 0$. For type B-like bounces, it is hard to see slowly varying negative modes on the wall. 'ξ_1, ξ_2, $\xi_{\rm top}$, $\xi_{\rm min}$ and ξ_M' are defined in Equation (7.90).

7.3 A slowly varying negative mode in curved space

As we studied in Chapter 6, there is one negative mode in flat space, corresponding to moving the wall back and forth. In this section, we investigate how the ordinary negative mode behaves as gravitational effects get stronger where Q on the wall approaches zero or becomes negative by using the Lagrangian (7.24).

The gauge invariant form of the Lagrangian (7.24) basically consists of a kinetic term and a potential term. The kinetic term becomes dominant for rapidly varying fields and it gives extra negative modes. On the contrary, the potential term can be comparable with the kinetic term for slowly varying fields. The ordinary negative mode from the U'' term as in flat space can be deformed where the gravitational terms dominate, but it is still a slowly varying mode. Table 7.4 shows how the potential term and the slowly varying mode behave in various cases.

To find negative modes on the wall, we can rewrite the second order Lagrangian (7.24) by taking $y = \chi/\sqrt{Q}$,

$$\mathcal{L}_E^{(2)}[y;\dot{y}] = \frac{\rho^3}{2}\dot{y}^2 + \frac{\rho^3}{2}\mathcal{V}y^2, \tag{7.81}$$

where

$$\begin{aligned}\mathcal{V} &= \left[U'' + \frac{\kappa\rho^2 U'^2}{3\dot{\rho}^2 Q} + \frac{\kappa\rho\dot{\phi}U'}{3\dot{\rho}^3 Q}\right] - \frac{3\dot{\rho}\dot{Q}}{2\rho Q} - \frac{\ddot{Q}}{2Q} + \frac{3\dot{Q}^2}{4Q^2} \\ &= \frac{U''}{Q} + \frac{\kappa\rho^2 U'^2}{2\dot{\rho}^2 Q^2} + \frac{\kappa\rho\dot{\phi}U'}{\dot{\rho}^3 Q^2}\cdot\left(1-\dot{\rho}^2 Q\right) + \frac{\kappa\dot{\phi}^2}{6\dot{\rho}^4 Q^2}\cdot\left(3 - 8\dot{\rho}^2 Q + 9\dot{\rho}^4 Q^2\right). \end{aligned} \tag{7.82}$$

The mode equation is given by

$$-\ddot{y} - \frac{3\dot{\rho}}{\rho}\dot{y} + \mathcal{V}y = \lambda y. \tag{7.83}$$

In this form of the Lagrangian, the potential $\mathcal{V}$ determines the existence of a negative mode if Q is positive everywhere. As $Q \to 0$, the dominant contribution diverges to $+\infty$ as

$$\lim_{Q\to 0}\mathcal{V} = \frac{1}{Q^2}\left(\frac{\kappa\rho^2 U'^2}{2\dot{\rho}^2} + \frac{\kappa\rho\dot{\phi}U'}{\dot{\rho}^3} + \frac{\kappa\dot{\phi}^2}{2\dot{\rho}^4}\right) = \frac{\kappa}{2\dot{\rho}^2 Q^2}\left(\rho U' + \frac{\dot{\phi}}{\dot{\rho}}\right)^2 \to +\infty. \tag{7.84}$$

The boundary conditions for y at the both ends are

$$y(0) = \Phi(0), \quad y(\xi_{\max}) = \Phi(\xi_{\max}), \quad \text{and} \quad \dot{y}(0) = \dot{y}(\xi_{\max}) = 0 \tag{7.85}$$

because the boundary conditions (7.30) and (7.32) give

$$\rho = 0, \quad \dot{\phi} = 0, \quad \text{and} \quad \dot{\Phi} = 0 \quad \text{ at both ends.} \tag{7.86}$$

For 'κ=0.01, 0.055, and 0.057', we found a mode which converges after passing the wall but it diverges at $Q = 0$ because $\mathcal{V}$ diverges where Q becomes 0 near the maximum of ρ. This would make a small error in the eigenvalue.

We can see how the potential term $\mathcal{V}$ changes for a given potential,

$$U[\phi] = \phi^2(\phi - 3)^2 + 0.5\phi^2 + 1.5, \tag{7.87}$$

as κ increases. First of all, in the case that Q on the wall is not much smaller than unity, the potential term ($\mathcal{V}$) behaves almost same as U'', as shown in Figure 7.2. We will see that the negative Q region on the wall starts to appear at $\kappa \approx 0.0575$. This means that the case shown in Figure 7.2 is neither a very small bounce nor a very weak gravity limit since $\bar{\rho} \approx \frac{1}{3}\rho_M$ and $\kappa = 0.01$

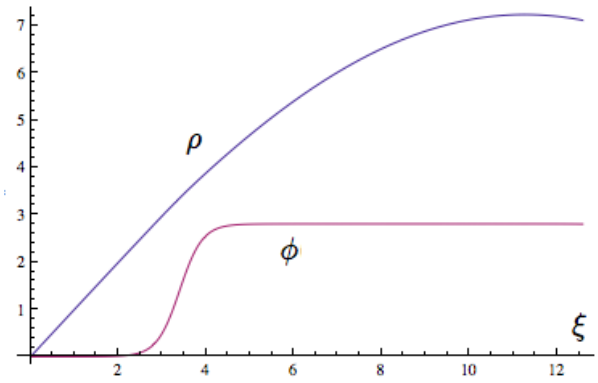

(a) ρ and ϕ

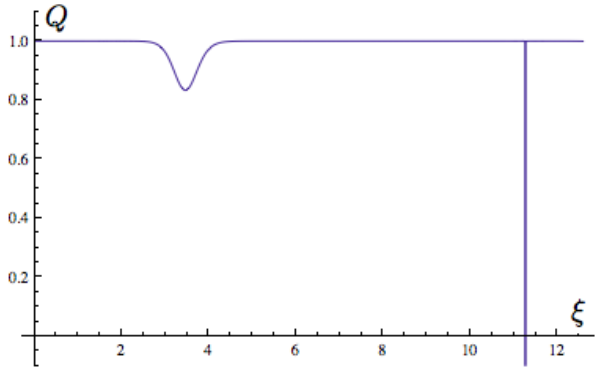

(b) Q, $Q_{\rm min}$=0.83

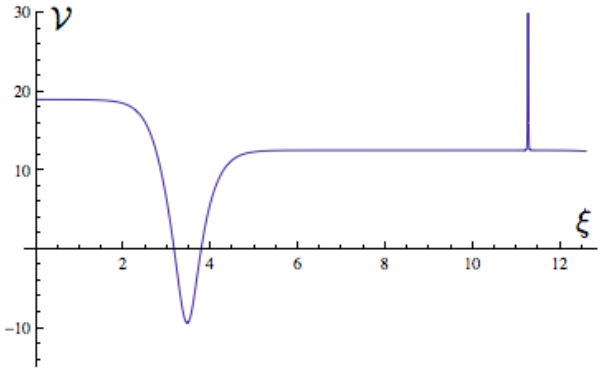

(c) $\mathcal{V}$

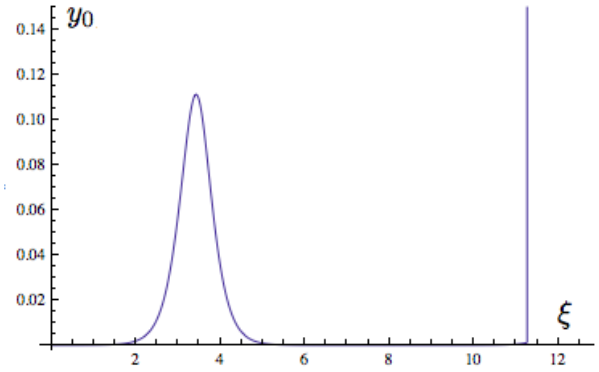

(d) The lowest mode(y_0), $\lambda_0 = -0.229$

Figure 7.2: $\kappa = 0.01$, $U[\phi]$ given by (7.87).

is approximately 1/6 of $\kappa \approx 0.0575$. Nevertheless, if $Q_{\rm min} = 0.83 \lesssim 1$, the U'' term is the only term which mainly contributes to $\mathcal{V}$ and there should be an ordinary negative mode which moves the wall back and forth. By using the Lagrangian (7.81), we can find the lowest mode (y_0) and its eigenvalue numerically as in Figure 7.2d. The lowest eigenvalue is $\lambda_0 = -0.229$ and the lowest mode looks almost the same as $\dot{\phi}$. The eigenvalue with the thin-wall approximation is '$-3/\bar{\rho}^2$' in flat space, as in Section 6.2. If we take $\bar{\rho} = 3.5$, then $-3/\bar{\rho}^2 = -0.244$, which is close to $\lambda_0 = -0.229$. This also suggests that the gravitational effects do not mainly contribute to the tunneling.

At $\kappa = 0.055$, Q is still positive on the wall but it is very close to zero ($Q_{\rm min} = 0.043 \ll 1$) as in Figure 7.3. The potential term $\mathcal{V}$ becomes deeper and negative in a narrower region than in the $\kappa = 0.01$ case so it looks quite different from the U'' term. We can also find the lowest mode from the Lagrangian (7.81). The lowest eigenvalue is $\lambda_0 = -0.0628$ and its eigenfunction (y_0) becomes

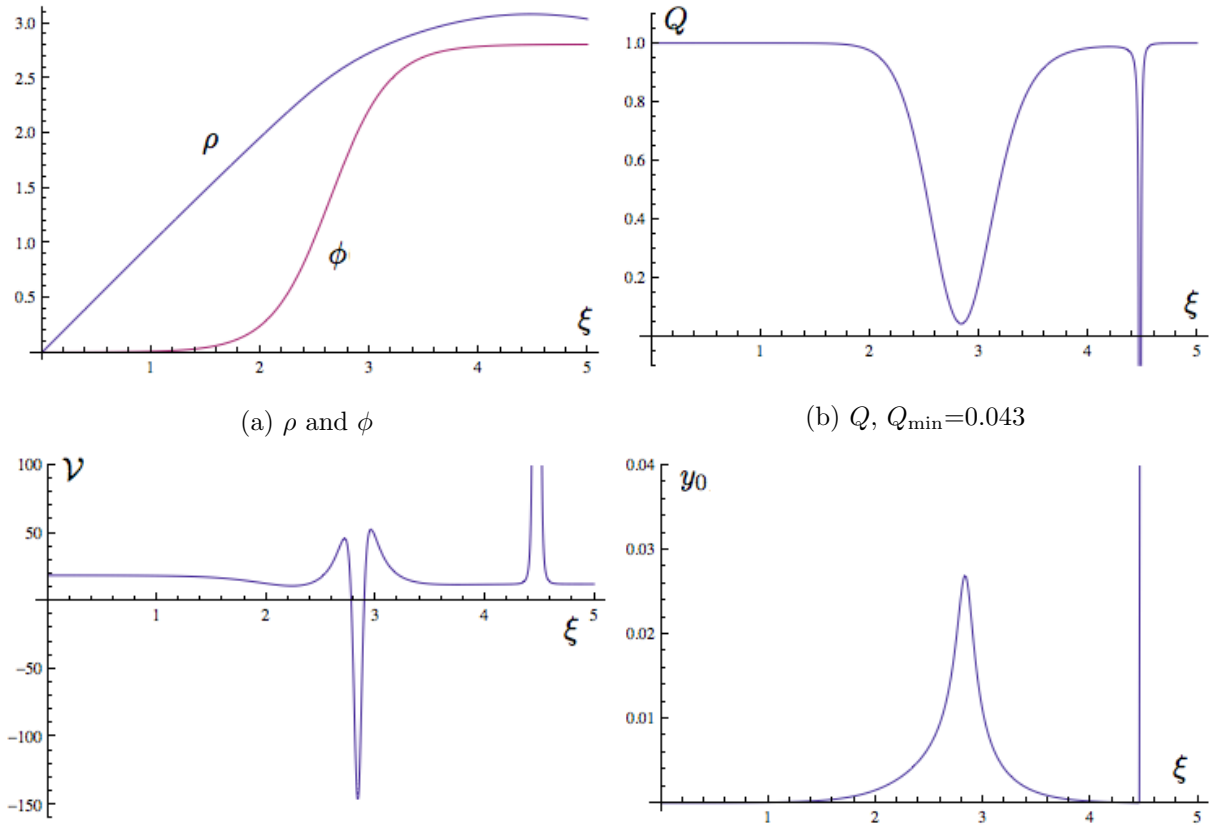

(a) ρ and ϕ

(b) Q, $Q_{\min}$=0.043

(c) $\mathcal{V}$

(d) The lowest mode(y_0), $\lambda_0 = -0.0628$

Figure 7.3: $\kappa = 0.055$, $U[\phi]$ given by (7.87).

sharper at the maximum as shown in Figure 7.3. The lowest eigenvalue becomes very close to zero but it is still negative. If we take $\bar{\rho} = 0.28$, then $-3/\bar{\rho}^2 = -0.383$, which is quite different from $\lambda_0 = -0.0628$.

At $\kappa = 0.057$, the minimum of Q is 0.0008 so it barely touches the zero line as in Figure 7.4. Since Q is smaller than in the $\kappa = 0.055$ case, the potential term $\mathcal{V}$ becomes deeper and it becomes negative in a narrower region. Although it does not look quite different from the $\kappa = 0.055$ case, the lowest eigenvalue is $\lambda_0 = +0.0769$, which is positive. We know that the lowest eigenvalue on the wall gets closer to zero as the minimum of Q gets smaller. More precisely, the eigenvalue becomes positive before the minimum of Q becomes negative.

The following cases (κ=0.0575, 0.07 and 0.09) have a negative Q region on the wall. If Q is negative, y becomes imaginary. To avoid a complex field, let us go back to the form of Lagrangian

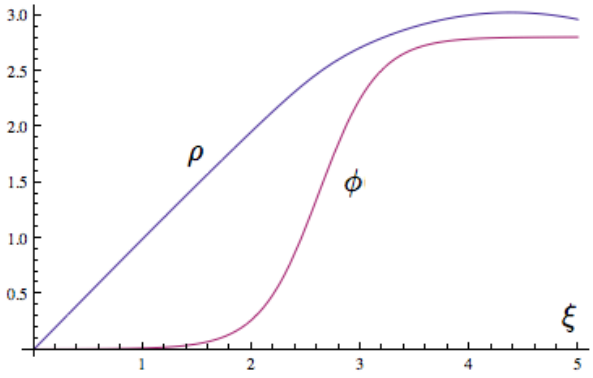

(a) ρ and ϕ

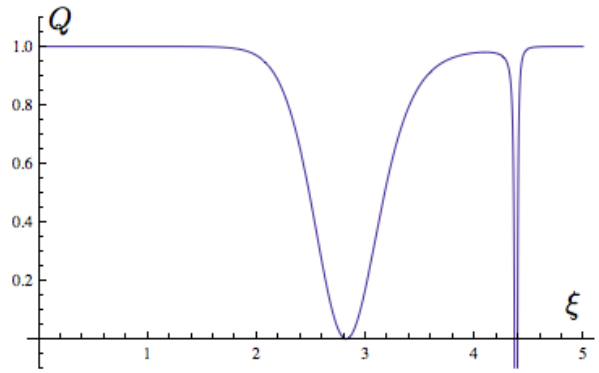

(b) Q, $Q_{\min}$=0.0008

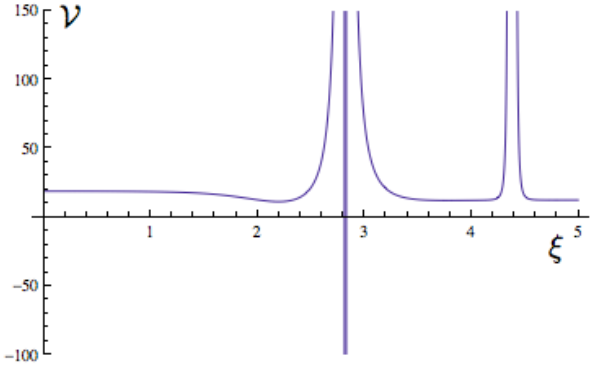

(c) $\mathcal{V}$

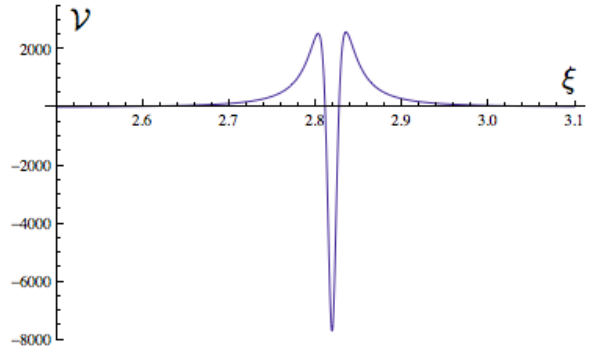

(d) Enlarged $\mathcal{V}$

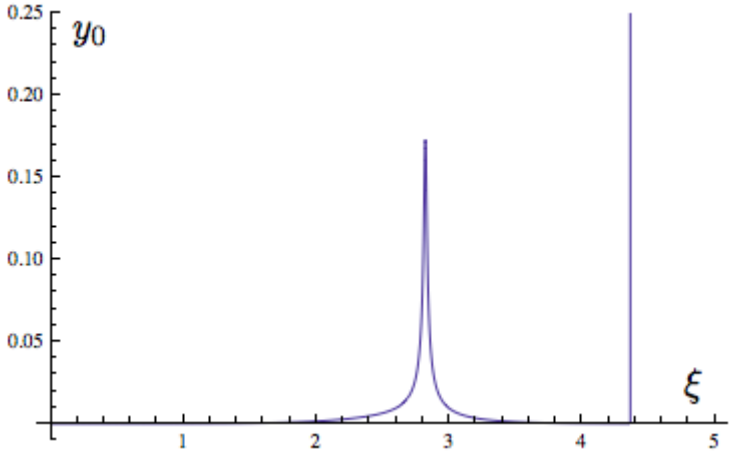

(e) The lowest mode(y_0), $\lambda_0 = +0.0769$

Figure 7.4: $\kappa = 0.057$, $U[\phi]$ given by (7.87).

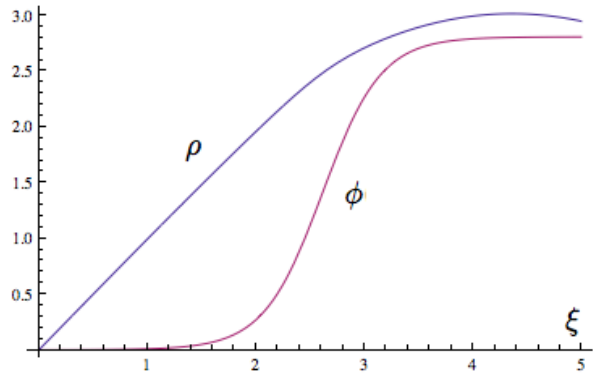

(a) ρ and ϕ

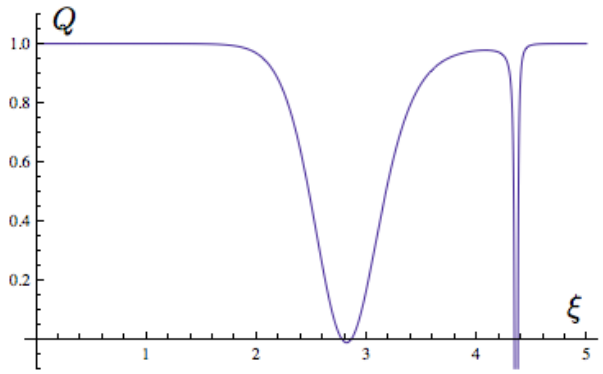

(b) Q

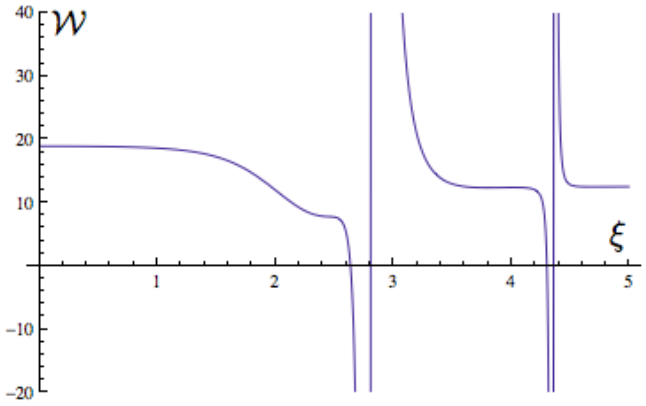

(c) $\mathcal{W} = f/Q$

Figure 7.5: $\kappa = 0.0575$, $U[\phi]$ given by (7.87).

in Equation (7.24) and introduce a potential term $\mathcal{W}$ as

$$\mathcal{L}_E^{(2)} = \frac{\rho^3}{2Q}\dot{\chi}^2 + \frac{\rho^3}{2}\mathcal{W}\chi^2 \tag{7.88}$$

where

$$\mathcal{W} = \frac{1}{Q}\left[U'' + \frac{\kappa\rho^2 U'^2}{3\dot{\rho}^2 Q} + \frac{\kappa\rho\dot{\phi}U'}{3\dot{\rho}^3 Q}\right]. \tag{7.89}$$

Because the kinetic energy term can be negative, there is no lower bound of the mode spectrum. Nevertheless, if the potential term ($\mathcal{W}$) is positive on the wall, then we do expect there is no slowly varying negative mode on the wall.

For a convenience, define ξ_{top}, ξ_{min}, ξ_M, ξ_1 and ξ_2 such that

$$\phi_{\text{top}} = \phi(\xi_{\text{top}}), \quad \dot{Q}(\xi_{\text{min}}) = 0, \quad \dot{\rho}(\xi_M) = 0,$$

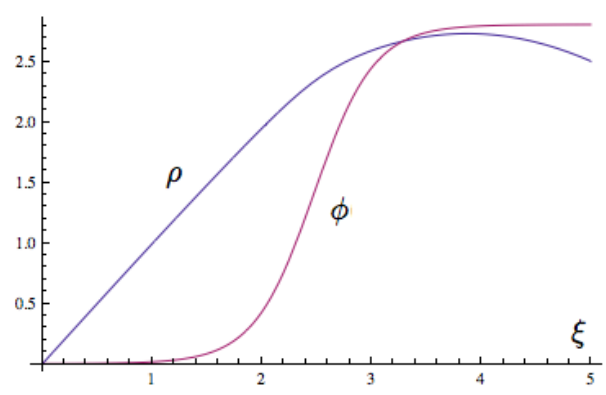

(a) ρ and ϕ

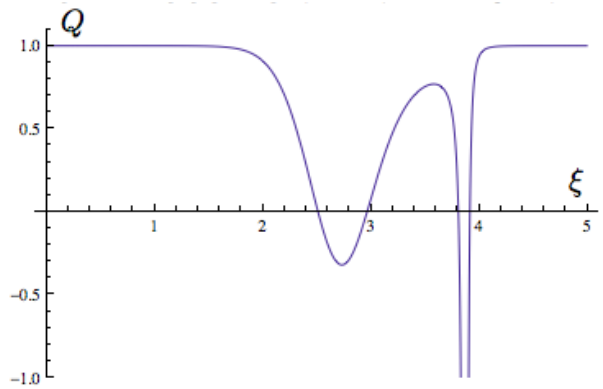

(b) Q

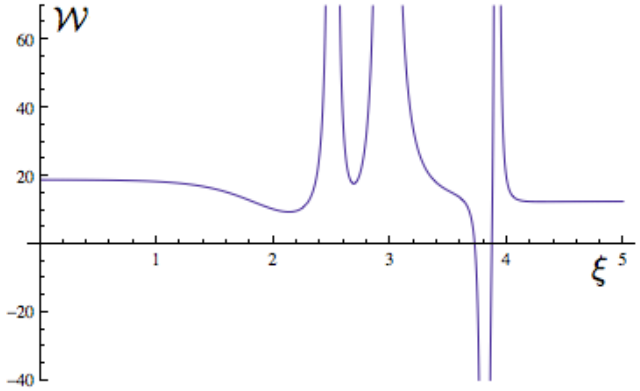

(c) $\mathcal{W} = f/Q$

Figure 7.6: $\kappa = 0.07$, $U[\phi]$ given by (7.87).

$$\text{and} \quad Q(\xi_1) = Q(\xi_2) = 0 \quad (\text{with } \xi_1 < \xi_2). \tag{7.90}$$

At $\kappa = 0.0575$, there is a very narrow negative Q region on the wall as in Figure 7.5. The potential term goes to $-\infty$ at $\xi = \xi_1$ and diverges to $+\infty$ at $\xi = \xi_2$. Because the potential is only negative in very narrow region, if the field is concentrated on the region, the kinetic energy term can be large enough to cancel the effect of the negative $\mathcal{W}$. We don't know yet about the existence of a slowly varying negative mode, but it seems not to exist since neither the previous case nor the next case has a negative mode.

At $\kappa = 0.07$, the width of the negative Q region becomes relatively wide as shown in Figure 7.6. The potential term goes to $+\infty$ at both $\xi = \xi_1$ and $\xi = \xi_2$ and it is always positive on the wall. We do not expect a slowly varying negative mode here.

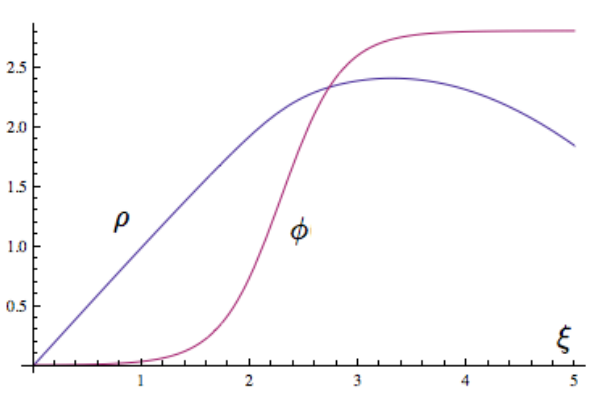

(a) ρ and ϕ

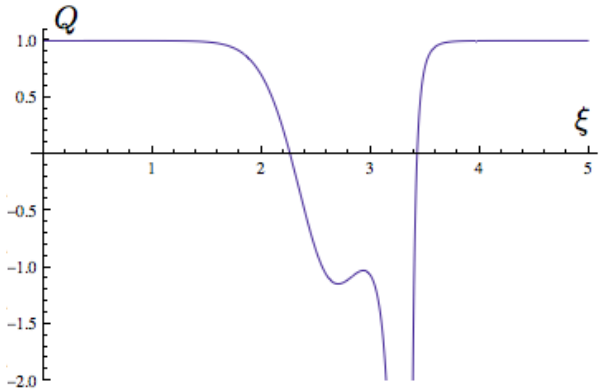

(b) Q

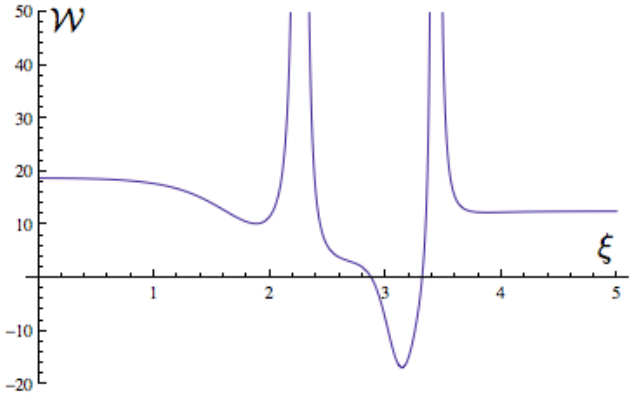

(c) $\mathcal{W} = f/Q$

Figure 7.7: $\kappa = 0.09$, $U[\phi]$ given by (7.87).

At $\kappa = 0.09$, Q becomes negative from a point in the wall to the maximum of ρ as in Figure 7.7. We expect that there could be a slowly varying negative mode in this wide region but we need a careful further investigation to check it.

Then, let us study why the potential term ($\mathcal{W}$) behaves from Figures 7.5 to Figures 7.7. If Q becomes negative in a region on the wall, the U''/Q term gives a positive contribution there. This means a slowly varying negative mode does not come from moving the wall but if it exists, it comes from the gravitational effects. In the limit of $Q \to 0$, the $\mathcal{W}$ term diverges to either $+\infty$ or $-\infty$. Let us define $\mathcal{U} \equiv \frac{\kappa\rho^2 U'}{3\dot{\rho}^2}\left(U' + \frac{\dot{\phi}}{\rho\dot{\rho}}\right) = Q^2\mathcal{W} - QU''$. The sign of $\mathcal{U}$ determines the behavior of $\mathcal{W}$

around the $Q = 0$ points. Its sign around $\phi = \phi_{\rm top}$ is given by

$$\mathcal{U} = \frac{\kappa\rho^2 U'}{3\dot{\rho}^2}\left(U' + \frac{\dot{\phi}}{\rho\dot{\rho}}\right)\begin{cases} > 0 & \text{if } U' > 0 \ (\xi < \xi_{\rm top}), \\ < 0 & \text{if } U' < 0 \ (\xi > \xi_{\rm top}). \end{cases} \tag{7.91}$$

The equation (7.91) implies that

$$\lim_{\xi\to\xi_1\pm 0}\mathcal{W} = \begin{cases} +\infty & \text{if } \xi_1 < \xi_{\rm top} \\ -\infty & \text{if } \xi_1 > \xi_{\rm top}. \end{cases} \tag{7.92}$$

In the thin-wall approximation, the minimum of Q is located at $U_{\rm top}$ ($\xi_{\rm min} = \xi_{\rm top}$). As this statement is only true within the approximation, we need to check more details without the approximation. The minimum of Q is found by

$$\dot{Q} = 0 \quad \Leftrightarrow \quad \frac{d}{d\xi}\left(\frac{\rho\dot{\phi}}{\dot{\rho}}\right) = 0 \quad \text{at } \xi = \xi_{\rm min}, \tag{7.93}$$

$$\frac{d}{d\xi}\left(\frac{\rho\dot{\phi}}{\dot{\rho}}\right) = \frac{1}{\dot{\rho}^2}\left[\left(\dot{\rho}^2 - \rho\ddot{\rho}\right)\dot{\phi} + \rho\dot{\rho}\ddot{\phi}\right] = \frac{1}{\dot{\rho}^2}\left[\left(1 - 3\dot{\rho}^2 Q\right)\dot{\phi} + \rho\dot{\rho}U'\right] = 0 \quad \text{at } \xi = \xi_{\rm min}. \tag{7.94}$$

This means $\frac{dU}{d\xi}\left(= \frac{U'}{\dot{\phi}}\right)$ is negative at $\xi = \xi_{\rm min}$ so the minimum of Q has to appear after passing the top of the potential all the time. In other words, it implies '$\xi_{\rm top} < \xi_{\rm min}$'. Let us say the coordinate of the second zero of $\mathcal{U}$ is $\xi = \xi_0$. We know the first zero is located at $\xi = \xi_{\rm top}$ and the second zero is found by '$U' + \frac{\dot{\phi}}{\rho\dot{\rho}} = 0$'. At $\xi = \xi_0$, the equation (7.94) becomes

$$\left.\frac{d}{d\xi}\left(\frac{\rho\dot{\phi}}{\dot{\rho}}\right)\right|_{\xi=\xi_0} = -3Q\dot{\phi} > 0. \quad \text{if } Q < 0 \text{ and } \dot{\phi} > 0. \tag{7.95}$$

This implies ξ_0 can be always found in $\xi_0 < \xi_{\rm min}$ but it cannot be found in $\xi_{\rm min} < \xi < \xi_2$ so the $\mathcal{U}$ term is always positive at $\xi = \xi_2$,

$$\lim_{\xi\to\xi_2\pm 0}\mathcal{W} = +\infty. \tag{7.96}$$

To sum up, there are two different cases of the behaviors of $\mathcal{W}$. If the width of the negative Q region is narrow enough to satisfy '$\xi_{\rm top} < \xi_1 < \xi_{\rm min} < \xi_2$', then $\mathcal{W}$ goes to '$-\infty$' at $\xi = \xi_1$ as in Figure 7.5. If the width of the negative Q region gets a bit wider, then the top of the potential is located inside the negative Q region as '$\xi_1 < \xi_{\rm top} < \xi_{\rm min} < \xi_2$'. In this case, $\mathcal{W}$ diverges to $+\infty$ at $\xi = \xi_1$ as in Figure 7.6. Since the potential term is positive around the wall, there cannot be

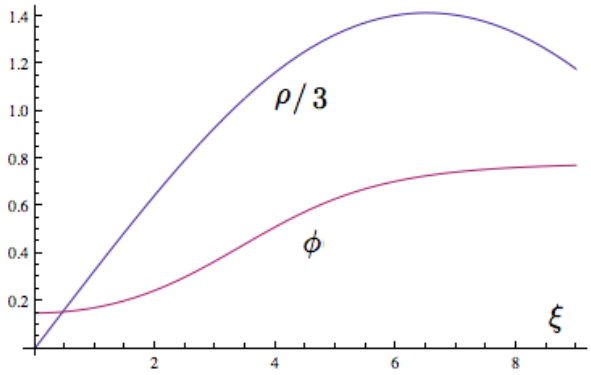

(a) ρ and ϕ

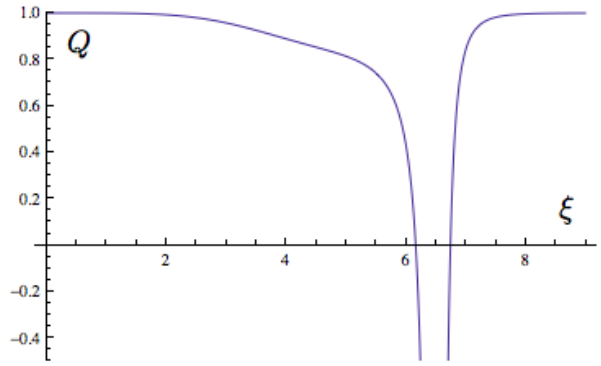

(b) Q

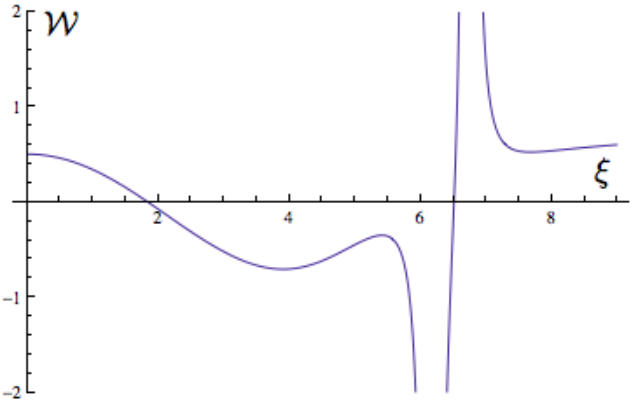

(c) $\mathcal{W} = f/Q$

Figure 7.8: Negative Q region for a type A. $\kappa = 1$, $U = \phi^2(\phi - 1)^2 + 0.1\phi^4 + 0.1$.

a negative mode by concentrating perturbative fields near the wall. However, we can still find a slowly varying negative mode around the maximum of ρ because $\mathcal{W}$ goes to $-\infty$ there.

As the wall gets larger and thicker, the negative Q region on the wall can meet the negative Q region on the maximum of ρ as in Figure 7.7. In this case, these two negative Q regions mix, so the potential term becomes negative in a wide region from a point of the wall to the maximum of ρ.

Let us move to the negative Q region at the maximum of ρ. Each case from Figure 7.8 to Figure 7.11 has a different potential $U[\phi]$, respectively. In Figure 7.8, we can see a negative Q region around the maximum of ρ. This is a type A case because the wall is far away from the negative Q region. The potential term $\mathcal{W}$ behaves somewhat similar with Figure 7.5. It goes to $-\infty$ at $\xi = \xi_1$ and then diverges to $+\infty$ at $\xi = \xi_2$ because the top of the potential is located outside the negative Q region ($\xi_{\rm top} < \xi_1$) as we checked in the case of a negative Q region on the wall.

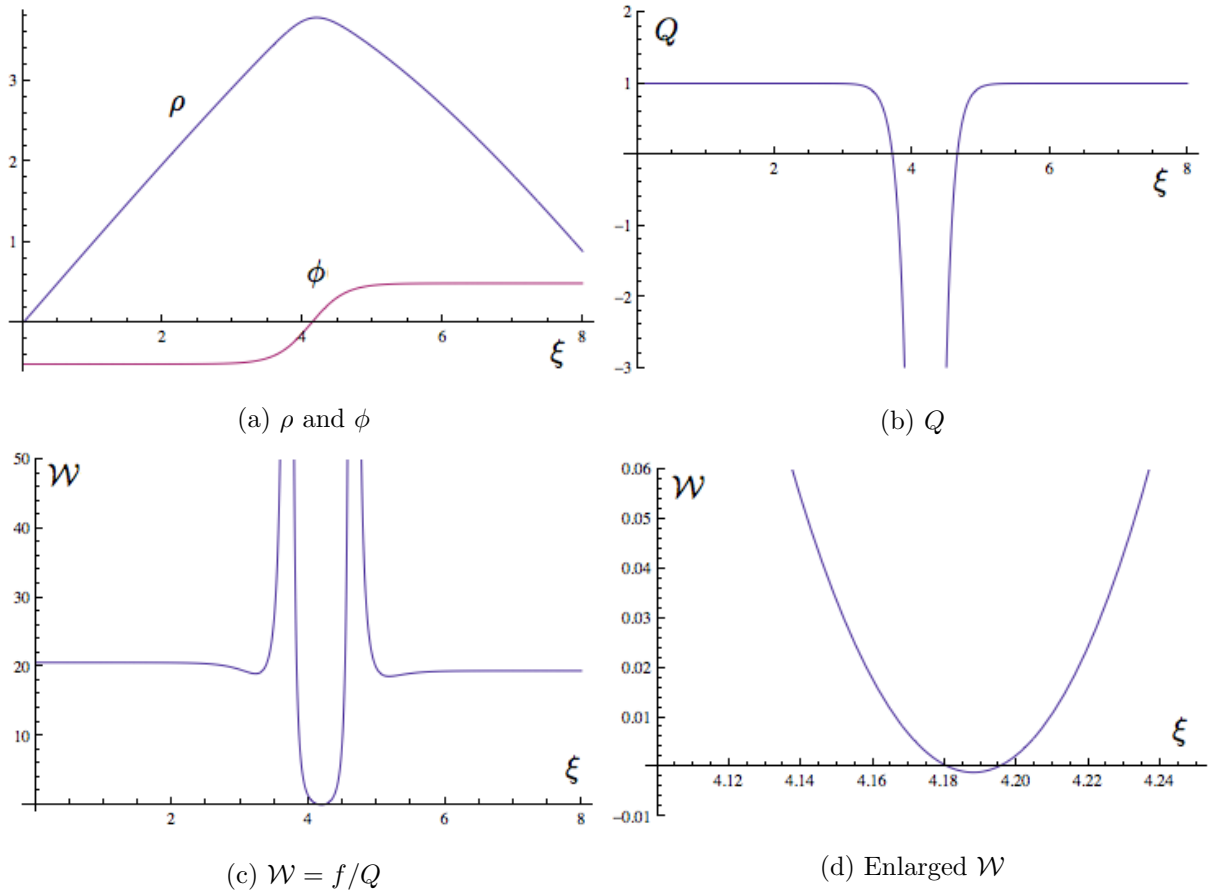

(a) ρ and ϕ

(b) Q

(c) $\mathcal{W} = f/Q$

(d) Enlarged $\mathcal{W}$

Figure 7.9: Negative Q region for a type B. $\kappa = 1$, $U = 10(\phi - 0.5)^2(\phi + 0.5)^2 + 0.1\phi + 0.1$.

In Figure 7.9, the top of the potential is located inside the negative Q region so the potential term $\mathcal{W}$ diverges to $+\infty$ at $\xi = \xi_1$ and $\xi = \xi_2$. Just before reaching ξ_M, there is a tiny region whose potential term is negative with a very small value.

In Figure 7.10, a symmetric potential is described. It looks very similar to Figure 7.9 but the potential term is always positive because it is totally symmetric.

In Figure 7.11, the field at $\xi = 0$ is quite closed to the top of the potential so U'' is always negative. The potential term behaves similarly with Figure 7.9 on the wall but it is negative outside the wall. A slowly varying negative mode does not exist on the wall but it can exist outside the wall.

Then, let us investigate why the potential behaves as described. The top of the potential can be placed either outside or inside the negative Q region. The former case satisfies that '$\xi_{\rm top} <$

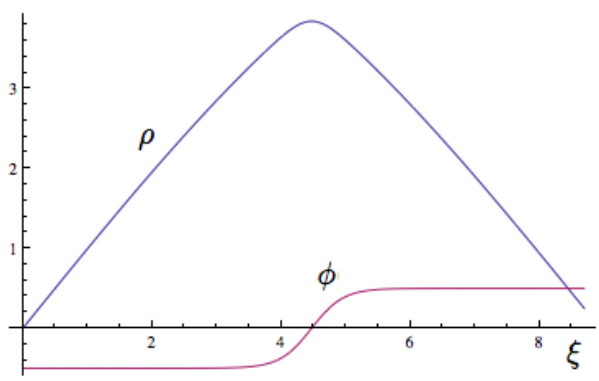

(a) ρ and ϕ

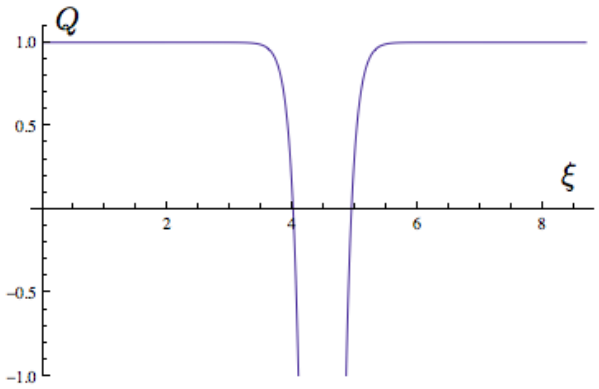

(b) Q

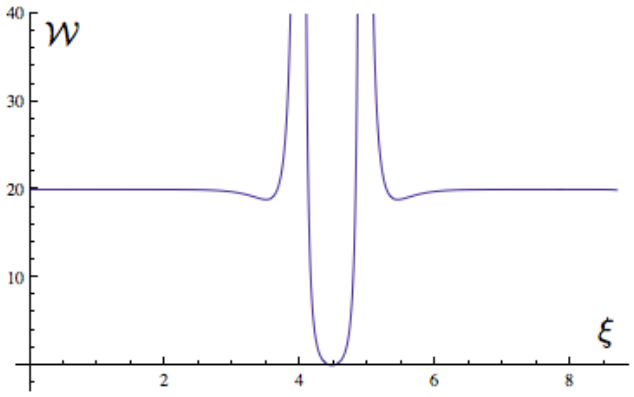

(c) $\mathcal{W} = f/Q$, $\mathcal{W}_{\min} = 0$

Figure 7.10: Negative Q region for a symmetric type B. $\kappa = 1$, $U = 10(\phi - 0.5)^2(\phi + 0.5)^2 + 0.1$.

$\xi_1 < \xi_{\min} = \xi_M < \xi_2$' and this is a type A-like bounce as in Figure 7.8. The latter one obeys that '$\xi_1 < \xi_{\text{top}} < \xi_{\min} = \xi_M < \xi_2$' which is a type B-like bounce. If and only if the potential is totally symmetric, the coordinates become '$\xi_1 < \xi_{\text{top}} = \xi_{\min} = \xi_M < \xi_2$'.

Since Q diverges at $\xi = \xi_M$, the potential term vanishes there ($\mathcal{W} = 0$, at $\xi = \xi_{\min} = \xi_M$). By using the same approach in the case of the wall, we can find the potential behaves

$$\lim_{\xi \to \xi_1 \pm 0} \mathcal{W} = \begin{cases} +\infty & \text{if } \xi_1 < \xi_{\text{top}} \\ -\infty & \text{if } \xi_1 > \xi_{\text{top}}. \end{cases} \tag{7.97}$$

The second zero of $\mathcal{U}$ still satisfies $\xi_0 < \xi_{\min} = \xi_M$ but it is very close to $\xi_{\min}$ because of the $1/\dot{\rho}$ term. There is no longer a zero of $\mathcal{U}$ since both terms in $\mathcal{U}$ are positive if $\dot{\rho} < 0$. This fact gives

$$\lim_{\xi \to \xi_2 \pm 0} \mathcal{W} = +\infty. \tag{7.98}$$

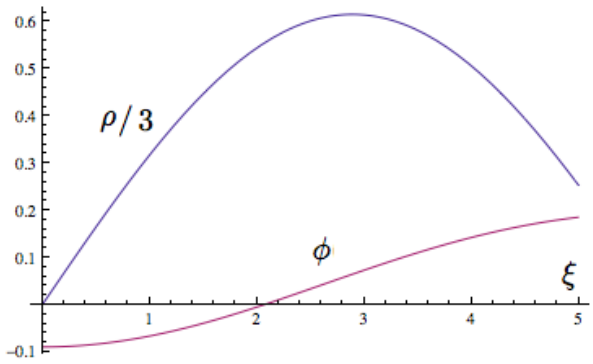

(a) ρ and ϕ

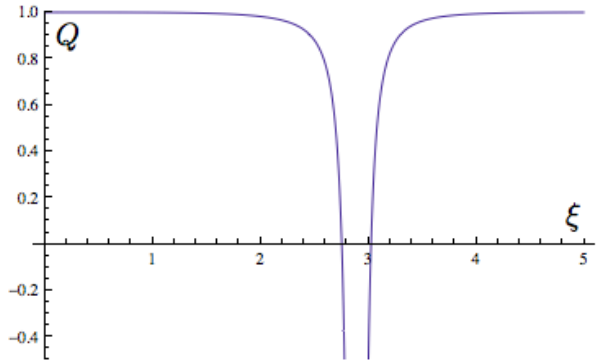

(b) Q

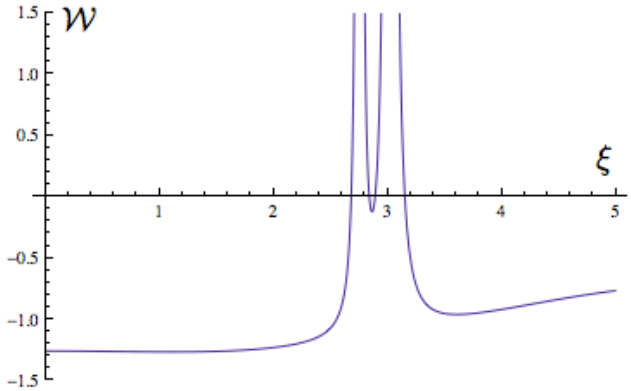

(c) $\mathcal{W} = f/Q$

Figure 7.11: Negative Q region for a thick type B. $\kappa = 1.6$, $U = (\phi - 0.5)^2(\phi + 0.5)^2 + 0.1(\phi - 0.5)^3 + 0.5$.

In the range $\xi_{\text{top}} < \xi < \xi_0$, the $\mathcal{U}$ term is negative. Since U''/Q is positive there, the whole potential term($\mathcal{W}$) is negative only in the region smaller than $\xi_{\text{top}} < \xi < \xi_M$. In other words, $\mathcal{W}(\xi) < 0$ if $\xi_{\text{top}} < \xi^* < \xi < \xi_M$ where $\mathcal{W} = 0$ at $\xi = \xi^*$ and $\xi = \xi_M$. The absolute value of $\mathcal{W}$ is much smaller than U'' outside the wall because the leading order of $\dot{\rho}$ in $\mathcal{W}$ around $\xi = \xi_M$ is the $O(\dot{\rho})$ term. This implies the potential term is negative only in a very small region with a small value as in Figure 7.9 and this kind of a type B-like bounce would not have a slowly varying negative mode.

If the potential is totally symmetric, $\mathcal{W}$ becomes zero only at $\xi = \xi_{\text{top}} = \xi_{\text{min}} = \xi_M$ so $\mathcal{W}$ cannot be negative as in Figure 7.10 and a slowly varying negative mode does not exist. If the wall gets thick enough, the field at $\xi = 0$ has a negative U'' as in Figure 7.11. Then, we expect a

slowly varying negative mode outside the negative Q region. The potential term outside the wall is approximately U'' but inside the wall behaves as like a type B-like bounce.

In this section, we showed how the lowest mode on the wall is deformed from an ordinary negative mode from the U'' term as the minimum of Q approaches zero. Especially, we checked that the lowest eigenvalue becomes positive before the minimum of Q becomes negative. In most cases where a negative Q region appear, we do not expect a slowly varying negative mode there, but we need further investigations for the cases of Figure 7.5 and Figure 7.7. These results showed that a slowly varying mode is no longer the main channel of vacuum decay as the gravitational effects get stronger.

7.4 Interpretation of negative modes

We saw that the existence of negative Q regions gave an infinite number of rapidly varying negative modes in any kinds of CdL bounces. Since these modes still exist in the weak gravity limit, it looks as if there is a discontinuity between the flat space case and the space which barely has gravitational effects. In this section, let us check how they are connected to each other.

7.4.1 Negative modes with multiple bubbles

We found that if there is one bubble in de Sitter background, there are an infinite number of negative modes. Let us consider multiple bounces and less symmetric cases.

The first step is investigating two bubbles in the $O(4)$ symmetric case. This is a special case of the oscillating bounces solution[38]. The scalar field and the metric factor 'ρ' are exactly symmetric with respect to the maximum of ρ, respectively. At the maximum of ρ, both $\dot{\rho}$ and $\dot{\phi}$ are zero ($\dot{\phi}_M = \dot{\rho}_M = 0$) so it is better to see the behavior of $\tilde{Q}$ instead of Q. At the maximum of ρ, $\tilde{Q}$ is zero but the sign of $\tilde{Q}$ around the maximum of ρ depends on the size of the bubbles.

$$\tilde{Q}_M = 1 - \frac{\kappa\rho_M^2 U_M}{3} = 1 + \frac{\kappa\rho_M^2}{3}\left(\frac{1}{2}\dot{\phi}_M^2 - U_M\right) = \dot{\rho}_M^2 = 0 \tag{7.99}$$

By using the expansions

$$\rho(\xi_M + \delta\xi) = \rho_M + \dot{\rho}_M\delta\xi + \frac{1}{2}\ddot{\rho}_M(\delta\xi)^2 = \rho_M + \frac{1}{2}\ddot{\rho}_M(\delta\xi)^2, \tag{7.100}$$

$$\phi(\xi_M + \delta\xi) = \phi_M + \dot{\phi}_M\delta\xi + \frac{1}{2}\ddot{\phi}_M(\delta\xi)^2 = \phi_M + \frac{1}{2}\ddot{\phi}_M(\delta\xi)^2, \tag{7.101}$$

we can expand $\tilde{Q}$ near the top as

$$\tilde{Q}(\xi_M \pm \delta\xi) = \tilde{Q}_M + \frac{1}{\rho_M^2}\left(1 - \frac{\kappa\rho_M^4 (U'_M)^2}{6}\right)(\delta\xi)^2 = \frac{1}{\rho_M^2}\left(1 - \frac{3(U'_M)^2}{2\kappa U_M^2}\right)(\delta\xi)^2. \tag{7.102}$$

If $1 - \frac{\kappa\rho_M^4 (U'_M)^2}{6} < 0$, negative Q regions exist around the maximum of ρ. If two bubbles are large bounces, the potential at $\rho = \rho_M$ is a bit higher than the potential at the false vacuum so there can be a negative Q region around the maximum of ρ. Meanwhile, if the size of each bubble is much smaller than the horizon size or the field configuration is close to the HM solution, the potential at $\rho = \rho_M$ is very close to the false vacuum or the top of the potential, respectively, so the potential increases slow enough to make Q negative when ρ decreases around the maximum of ρ. In other words, Q cannot be negative if Q is the local minimum at $\rho = \rho_M$.

Now let us break the $O(4)$ symmetry of the background fields. The maximum number of bubbles in the $O(4)$ symmetric case is two but there is no limit on the number of bubbles in less symmetric cases unless their total volume exceeds the size of the de Sitter space. The expected number of bubbles is given by the tunneling rate (Γ) times the four dimensional volume of de Sitter space. With the $O(4)$ symmetric background fields, negative kinetic energy regions exist only if the perturbative fields are $O(4)$ symmetric. However, this argument is no longer valid after breaking the symmetry of the background fields. Since we are interested in finding negative kinetic regions in less symmetric cases, $\tilde{Q} = 1 - \frac{\kappa\rho^2 U}{3}$ can be a good tool to verify them but we need to find appropriate variables which are equivalent to ξ and ρ. In order to investigate the negative kinetic energy regions, we need to extend the Lagrangian to generic cases. Instead of calculating directly, we are going to make some qualitative arguments.

In the $O(4)$ symmetric case, there can be only one or two bubbles as we studied. There is a negative Q region around the maximum of ρ since it is a Euclidian cylinder which locally decouples each perturbative field, as in Section 7.2.1. If we find such a Euclidian cylinder in less symmetric cases, the region around the cylinder can be the negative kinetic region that implies an infinite number of negative modes. However, it does not guarantee that a negative kinetic energy region always implies the existence of a local Euclidean cylinder. For instance, the negative Q region on the wall is not the case. In other words, showing that there is no Euclidean cylinder in the space-time does not mean that there is no negative kinetic energy region since the former is just a necessary condition. Our main goal here is proving that there are no extra negative modes in the

case of many bubbles. In order to make a sufficient condition, we need to restrict some conditions.

We assume the potential is less than the Planck scale ($U < m_{\rm pl}^4$). Then, the negative Q region on the wall appears only for large bounce cases. Let us forget about large bounces for a moment so we consider only small bounces here.

In the $O(4)$ symmetric case, negative kinetic regions exist only where $\dot{\rho} = 0$ with the width ($\Delta\xi < 1/m_{\rm pl}$). At $\dot{\rho} = 0$, the perturbation of the scalar field (Φ) does not contribute to the second order Lagrangian, and it can be interpreted as a pure gravitational perturbation around. Since a Euclidean cylinder effectively makes a one dimensional case, there is no damping term for the scalar field and the constraint which implies the conservation of the energy always cancels out the perturbation of the scalar field. However, if $\dot{\phi}$ vanishes on that region as in the case of two bubbles, this explanation is no longer valid and the kinetic energy terms of the perturbative fields are ill-defined.

In the $O(4)$ symmetric case, the curvature is given by,

$$\begin{aligned} R_4 &= -\frac{\rho\ddot{\rho} + \dot{\rho}^2 - 1}{6\rho^2} = \frac{1}{6}\left(\frac{2\kappa U(\phi)}{3} + \frac{\kappa\dot{\phi}^2}{6}\right) \\ &= \frac{1}{3}\left(\frac{1}{\Lambda(\phi)^2} + \frac{\kappa\dot{\phi}^2}{12}\right). \end{aligned} \tag{7.103}$$

We can neglect $\dot{\phi}^2$ terms since we are considering only small bounces. Then, we can write

$$R_4 \approx \frac{1}{3\Lambda(\phi)^2}. \tag{7.104}$$

The notation '$\approx$' in this section means '$=$' without $\dot{\phi}^2$ terms. Imagine the three dimensional subspace which is perpendicular to the ξ direction(or the direction of $\vec{\nabla}\phi$), then the curvature of the hyperspace is approximately

$$R_3 \approx \frac{1}{3\rho^2}. \tag{7.105}$$

The three-curvature R_3 cannot exceed the four-curvature R_4. If $R_3 \approx R_4$, R_3 gets its maximum and it points out where a Euclidean cylinder is. As we showed before, the width of the negative Q region ($\Delta\xi$) is less than the Planck length for small bounces. More precisely, the width is given by

$$(\Delta\xi) \sim \Lambda^2\sqrt{\kappa\dot{\phi}^2} \tag{7.106}$$

because it is satisfied where $Q = 0$ that

$$\kappa\dot{\phi}^2 = \frac{6\dot{\rho}^2}{\rho^2} \sim \frac{6\sin^2\left(\frac{(\Delta\xi)}{2\Lambda}\right)}{\Lambda^2} \sim \frac{(\Delta\xi)^2}{\Lambda^4}. \tag{7.107}$$

The width of the area (Δx) which satisfies $R_3 \approx R_4$ is found by

$$\frac{1}{\Lambda^2} \sim \frac{1}{[\Lambda + (\Delta x)]^2} + \kappa\dot{\phi}^2, \tag{7.108}$$

and it satisfies

$$(\Delta x) \sim \Lambda^3 \cdot \kappa\dot{\phi}^2 \sim \Lambda\sqrt{\kappa\dot{\phi}^2} \cdot (\Delta\xi) \ll (\Delta\xi). \tag{7.109}$$

Although both (Δx) and $(\Delta\xi)$ are less than the Planck length, (Δx) is even much smaller than $(\Delta\xi)$. This means that the approximation which neglects the $\kappa\dot{\phi}^2$ terms to find a local Euclidean cylinder is totally fine and the negative kinetic region around it also covers the area near the Euclidean cylinder with the width $(\Delta\xi)$.

Now, we think about less symmetric cases. If there is effectively a one-dimensional geometry, there must be a negative kinetic energy region around it unless the gradient of ϕ vanishes there. However, it is not sure if there is a different case of a negative kinetic region. Because we are considering small bubbles, the scalar field outside bubbles are almost constant. This means that the geometry outside bubbles is not very different from in the $O(4)$-symmetry case. If we define R_3 as the curvature of three dimensional hyperspace which is perpendicular to the direction of $\vec{\nabla}\phi$, it is impossible to a find negative kinetic region far away from a $R_3 \approx R_4$ region since the geometry is slightly different from the $O(4)$ symmetric case. R_3 mostly depends on the distance from the closest bubble and Thus, there cannot be a negative kinetic regions except effectively a one-dimensional area.

The fact that the whole geometry is approximately the same as the $O(4)$ symmetric case allows us to define ρ_3 in less symmetric cases.

$$\rho_3 \approx \sqrt{\frac{1}{3R_3}}. \tag{7.110}$$

If ξ_3 is defined to be a parameter which moves along the gradient of ϕ, ρ_3 approximately satisfies

$$\dot{\rho}_3^2 = 1 + \frac{\kappa(\rho_3)^2}{3}\left(\frac{1}{2}\dot{\phi}^2 - U\right). \tag{7.111}$$

We can calculate ρ_3 by integrating 7.111 outside the bubbles

$$d\rho_3 = \pm\sqrt{1 + \frac{\kappa(\rho_3)^2}{3}\left(\frac{1}{2}\dot{\phi}^2 - U\right)}d\xi_3. \tag{7.112}$$

Since the physical variables (ρ_3, R_3) do not depend on rescaling ξ_3, ρ_3 is uniquely determined by the above integration. Each bubble center is the point $\rho_3 = 0$ and the integration path is unique

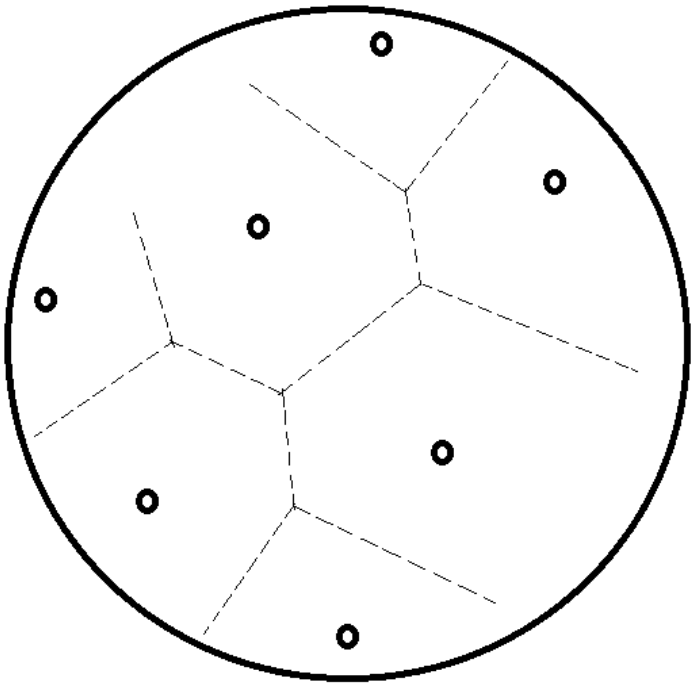

Figure 7.12: Many small bubbles in Euclidean de Sitter space. The junctions of three dashed line is the local maximum of ρ_3 where ρ_3 is defined by the integration (7.112). If there are many bubbles distributed, the maximum of ρ_3 is less than the horizon size(Λ) so negative kinetic energy regions do not show up.

except at the points $\vec{\nabla}\phi = 0$. At the points where $\vec{\nabla}\phi$ vanishes, the path would not be unique but ρ_3 still does not depend on the path we choose. We expect that if there is one closest bubble, ρ_3 is similar to the distance from the closet bubble. In the region that there are two or many closest bubbles, ρ_3 increases more slowly than in one closest bubble case so ρ_3 is little bit smaller than the distance from the closest bubble as we saw in the case of two bubbles.

As in the $O(4)$ symmetric case, a negative kinetic energy region can exist around the points where $R_3 \approx R_4$. In order to make $R_3 \approx R_4$, the distance from the closest bubble has to be approximately a horizon size (Λ). Since the width of the negative Q region is less than the Planck length and the variation of the geometry from the $O(4)$ symmetric case is also small, it is not guaranteed that every $R_3 \approx R_4$ point gives negative kinetic energy regions but $R_3 \approx R_4$ is a necessary condition to find a negative kinetic energy region. To sum up, if there is a negative

kinetic energy region in less symmetric cases, it should be approximately a horizon distance (Λ) from the closest bubble. This result teaches us that if there are a few bubbles, the existence of negative kinetic regions depends on how they are located. We cannot say that there is always infinite number of negative modes for the few bubble cases. The expected number of bubbles in de Sitter background is given by $N = \gamma \cdot VT \sim \frac{\gamma}{H^4}$ where $\gamma = \Gamma/V$. If $N \gg 1$, there are many bubbles distributed randomly. Then, there cannot be negative kinetic energy regions because negative Q regions given by one bubble are always interfered by another bubble. Each bubble has its own slowly varying negative mode but there are no longer extra negative modes from the negative kinetic energy regions.

In the case of large bubbles, most of the approaches for small bounces do not work anymore since scalar fields outside bubbles are not almost constant any more. There cannot be many bubbles because the background de Sitter space does not have enough space to fill them in.

7.4.2 Interpretation of multiple bubbles in a de Sitter background

In Section 7.4.1, we found that the infinite number of negative modes does not appear if many bubbles are nucleated in a de Sitter space. Now, let us investigate how to evaluate path integrals in the presence of gravity.

In the limit of zero temperature ($\beta \to \infty$) in a de Sitter space, the range of the Euclidean time (T) of the tunneling also goes to the infinity. Within an infinitely large spacetime, the path integral is given by summing all possible numbers of bubbles so it becomes an exponential. Thus, the result is the same as the flat space case (2.58).

$$I = I_0 \sum_{n=0} \frac{1}{n!} \left(iKe^{-B}VT\right)^n = I_0 \exp\left[iKe^{-B}VT\right]. \tag{7.113}$$

At finite temperature, T is finite so the volume of the spacetime is also finite. Furthermore, the lowest energy state is not the only state contributing to the path integral as like the equation (2.32),

$$I(T) = \sum_i c_i e^{-E_i T} \neq e^{-E_0 T}, \quad \text{if } T \text{ is finite.} \tag{7.114}$$

To keep the dominance of the lowest state, we need the condition,

$$\Delta E \cdot T \gg 1. \tag{7.115}$$

By Equation (2.40), ΔE is given by $\Delta E \approx \omega = \sqrt{U_f''}$. The condition (7.115) turns out to be

$$\Delta E \cdot T \sim \frac{\sqrt{U_f''}}{\sqrt{\kappa U_f}} \sim \frac{1}{\sqrt{\kappa} \cdot m_f} \gg 1 \quad \rightarrow \quad m_f \ll m_{\rm pl}. \tag{7.116}$$

Here, we assume $U_f = m_f^4 \sim (U_f'')^2$. In other words, if $m_f \ll m_{\rm pl}$, we can write the path integral as

$$I = \sum_{n=0} c_n e^{-E_n T} \approx c_0 e^{-E_0 T}. \tag{7.117}$$

There is no ambiguity in defining the lowest eigenvalue (E_0) even in the case where there are many negative modes because the real part of E_0 is defined without the tunneling process. Then, the decay rate per unit volume is given by

$$\gamma = \Gamma/V \approx 2 \cdot \frac{\mathrm{Im}(\ln I(T))}{VT}. \tag{7.118}$$

As we mentioned in Section 6.3.2, the dominant terms in the expansion of an exponential ($\exp[\alpha] = 1 + \alpha + \frac{1}{2}\alpha^2 + ... + \frac{1}{n!}\alpha^n + ...$) come from $n \approx \alpha$. Then, the expected number of bubbles in a Euclidean de Sitter space (N), where $\Delta E \cdot T \gg 1$, is

$$N \sim \begin{cases} \frac{\gamma}{H^4} \sim K e^{-B} VT & \text{if } \frac{\gamma}{H^4} \gtrsim 1, \\ 1 & \text{if } \frac{\gamma}{H^4} \lesssim 1. \end{cases} \tag{7.119}$$

Let us consider the case of small bounces. Small bounces always satisfy the $\Delta E \cdot T \gg 1$ condition, $m_f \ll m_{\rm pl}$. There are two regimes, as in the example of three vacua in Section 6.3.2. If $\frac{\gamma}{H^4} \lesssim 1$, we expect that there is one bubble in a Euclidean de Sitter space. Only the one bubble term contributes to the path integral. Because there are '$1 + \infty$' negative modes, we would rather write the path integral as

$$I/I_0 = \sum_n \frac{1}{n!} \left(iKe^{-B}VT\right)^n \approx 1 + iKe^{-B}VT = 1 + i^\infty i\tilde{K}e^{-B}VT. \tag{7.120}$$

Although there are infinitely many negative modes in the system, those oscillating modes are concentrated around the horizon with respect to the bubble. If we consider the local behavior of the bubble, it is not very different from the behavior of a bubble in flat space. In other words, the infinite number of oscillating modes could affect global properties of the system but they do not contribute to the true vacuum bubble for the case of one small bubble. Those rapidly varying

negative modes would give a interesting behavior around the horizon, but we are not able to see it around a bubble so the decay rate could be well-defined despite of the infinitely many negative modes. It is also possible to remove those negative modes by introducing a proper cutoff such as the Planck mass because the width of a negative kinetic energy region is smaller than the Planck length, as in Table 7.3. Then, the decay rate is approximately

$$\gamma \approx 2Ke^{-B} \tag{7.121}$$

instead of $\tilde{K}$ in Equation (7.120), where K is real and has a similar analogy in flat space.

These two regimes could be also understood by considering the nature of the phase transition in a de Sitter space. According to [11], the system of bubbles percolates if the condition '$\gamma/H^4 \gtrsim 1$' is satisfied.[6] In the one bubble case ($\gamma/H^4 \lesssim 1$), the cosmic expansion rate is larger than the rate of the bubble nucleation so the true vacuum does not percolate. This implies that the false vacuum persists and inflation turns out to be eternal.

If $\frac{\gamma}{H^4} \gtrsim 1$, there can be many bubbles in a Euclidean de Sitter space. Then, the path integral is approximated by an exponential as

$$\begin{aligned} I/I_0 = \sum_n \frac{1}{n!} \left(iKe^{-B}VT\right)^n &\approx 1 + i^\infty i\tilde{K}e^{-B}VT + \frac{1}{2}\left(iKe^{-B}VT\right)^2 + ... \\ &\approx \exp\left[iKe^{-B}VT\right]. \end{aligned} \tag{7.122}$$

The size of the spacetime is restricted by $T \sim \frac{1}{N^{1/4}H} < \frac{1}{H}$. This means that the volume for each bubble is not large enough to have a negative kinetic region. Thus, there are no extra negative modes. This means K is real and the decay rate is

$$\gamma \approx \frac{2\,\mathrm{Im}(\ln I)}{VT} \approx 2Ke^{-B}. \tag{7.123}$$

In this case, the system of bubbles does percolate and the false vacuum is unstable. The instability of the false vacuum does not come from many rapidly varying negative modes but from the negative modes on the bubble walls.

Let us think about a large type A bounce. For these bounces, ϵ has to be sufficiently small if $m_f \ll m_{\rm pl}$, so the condition $\Delta E \cdot T \gg 1$ is not necessarily satisfied. It means that the decay rate

[6] The condition for percolation is not exactly unity but order of unity.

	One small bubble	Many small bubbles	Large type A bubble
Conditions	$\frac{\gamma}{H^4} \lesssim 1$	$\frac{\gamma}{H^4} \gtrsim 1$	$N \lesssim 1$
Negative modes	$1 + \infty$	1 for each bubble	(1 or 0) $+ \infty$
Path integral	$1 + i^{\infty} i\tilde{K} e^{-B} VT$	$\exp\left[iKe^{-B}VT\right]$	$1 + i^{\infty} i\tilde{K} e^{-B} VT$
False Vacuum	Persists	Unstable	Persists
Percolation?	No	Yes	No
Eternal Inflation?	Yes	No	Yes

Table 7.5: The summary of three different cases of vacuum decay in a de Sitter background.

is not given by Equation (7.118) if $m_f \gtrsim m_{\rm pl}$. The path integral is given by Equation (7.120) as in one small bounce and the expected number of bubbles (N) is just $Ke^{-B}VT$. If $\epsilon \ll m \ll m_{\rm pl}$,

$$N \sim Ke^{-B}VT \sim B^2 \cdot m^4 \cdot e^{-B} \cdot \Lambda^4 \sim \left(\frac{m_{\rm pl}}{m}\right)^{10} e^{-\left(m_{\rm pl}/m\right)^3} \ll 1 \tag{7.124}$$

because of the conditions $\Lambda \sim \frac{m_{\rm pl}}{m^2}$ and $B \sim \left(\frac{m_{\rm pl}}{m}\right)^3$ for a large type A bounce. If $m \sim m_{\rm pl}$,

$$N \sim Ke^{-B}VT \sim 1. \tag{7.125}$$

Thus, the number of bubbles is $N \lesssim 1$ for a large type A bounce. Even though the size of a bubble is comparable with the size of the horizon initially, it does not percolate and inflation is eternal.

Let us speculate about the connection between these results and the flat space case. We have studied the vacuum decay in flat space and it can be solved perfectly. When we turn on gravity, there are an unavoidable infinite number of negative modes in a closed manifold, which is totally different from in the flat space case. Nevertheless, those negative modes do not really contribute to the path integral in the weak gravity limit because the negative modes disappeared if there are many bubbles and the dominant term comes from a large number of bubbles. In the flat space limit, there must be many bubbles in a de Sitter space because the size of the horizon goes to $+\infty$ so it is always $\frac{\gamma}{H^4} \gtrsim 1$. As the gravitational effect gets stronger, the size of a bubble gets larger and the expected number of bubbles decreases. Then, the negative modes arise in reality and it should be understood in the context of quantum gravity.

Chapter 8

Conclusion

I discussed various topics of negative modes in the vacuum decay over this thesis. The existence of a negative mode implies the false vacuum is unstable and it may cause the tunneling process. There is only one negative mode in flat space. On the contrary, there can be an infinite number of negative modes in a de Sitter space background. In the weak gravity limit, we can see they barely contribute to the physical properties, so it can be smoothly connected to the flat space case. However, there is still lots of room for speculation about those negative modes if the gravitational effects get stronger.

In Chapter 2, I described quantum tunneling in flat space. I started with tunneling in quantum mechanics and then generalized it to a field theory. The decay rate is given by Ae^{-B} where B is the Euclidean action of the classical path. By successfully evaluating the path integral, we found the complete form of the decay rate.

In Chapter 3, I reviewed the vacuum decay process in curved space. In the presence of gravity, not only scalar matter fields but also gravitational fields become dynamic variables. I discussed some aspects of the system such as gauge invariance, boundary conditions and topologies of solutions.

In Chapter 4, I introduced the thin-wall approximation which is the only way to find analytic solutions. I discussed the validity of the approximation, which is given by Table 4.1. There are two types of solutions in curved space. The type A case is found where the size of a bubble is smaller than the horizon. This has an analogy in flat space. The type B bounce exists where the wall is located at the maximum of the metric factor as a consequence of strong gravity.

In Chapter 5, I dealt with the thermal approach of the vacuum tunneling. We checked that the

nature of the tunneling has both thermal and quantum aspects. It also gave a good interpretation of the horizon and a type B bounce in curved space.

In Chapter 6, I showed there is one and only one negative mode in the vacuum tunneling in flat space. I introduced an approach to find eigenmodes analytically with the thin-wall approximation. We analyzed the negative modes for one- or two-field potentials with three vacua.

In Chapter 7, I discussed negative modes in curved space. I showed a gauge independent approach of the second order Lagrangian. By using the approach, we saw how gravitational effects affect the mode structure of the vacuum decay process. We showed that an ordinary negative mode disappears as the gravitational effects get stronger. This means that a slowly varying mode is no longer the main channel of vacuum decay if the gravitational effects dominate. We checked that there exists a region which has a negative kinetic energy where the top of the potential is sufficiently high or where the the metric factor becomes the maximum. This region implies the existence of an infinite number of negative modes. There are two regimes that take account of these modes by considering the nature of the phase transition. In the regime in the weak gravity limit, the system successfully matches with an analogy in flat space.

Bibliography

[1] A. Guth, *The Inflationary Universe: A possible solution to the horizon and flatness problems*, Phys. Rev. D **23** (1981) 347.

[2] A. Linde, *A new inflationary universe scenario: A possible solution of the horizon, flatness, homogeneity, isotropy and primordial monople problems*, Phys. Lett. B **108** (1982) 389.

[3] A. Albrecht and P. Steinhardt, *Cosmology for grand unified theories with radiatively induced symmetry breaking*, Phys. Rev. Lett. **48** (1982) 1220.

[4] S. Coleman, *The Fate of the False Vacuum. 1. Semiclassical Theory*, Phys. Rev. D **15** (1977) 2929.

[5] C. G. Callan and S. Coleman, *The Fate of the false Vacuum. 2. First Quantum Correction*, Phys. Rev. D **16** (1977) 1762.

[6] S. Coleman, *Quantum Tunneling and Negative Eigenvalues*, Nucl. Phys. B **298** (1988) 178.

[7] S. Coleman and F. D. Luccia, *Gravitational Effects on and of Vacuum Decay*, Phys. Rev. D **21** (1980) 044014.

[8] BICEP2 Collaboration, *BICEP2 I: Detection of B-mode polarization at degree angular scales*, `arXiv:1403.3985`.

[9] BICEP2 Collaboration, *BICEP2 II: Experiment and three-year data set*, `arXiv:1403.4302`.

[10] S. W. Hawking, I. G. Moss, and J. M. Stewart, *Bubble collisions in the very early universe*, Phys. Rev. D **26** (1982) 2681.

[11] A. Guth and E. J. Weinberg, *Could the Universe have recovered from a slow first order phase transition?*, Nucl. Phys. B **212** (1983) 321.

[12] S. Coleman, V. Glaser, and A. Martin, *Action Minima Among Solutions to a Class of Euclidean Scalar Field Equations*, Commun. Math. Phys. **58** (1978) 211.

[13] A. Kusenko, K. Lee, and E. J. Weinberg, *Vacuum decay and internal symmetries*, Phys. Rev. D **55** (1997) 4903–4909.

[14] A. Masoumi and E. J. Weinberg, *Bounces with $O(3) \times O(2)$ symmetry*, Phys. Rev. D **86** (2012) 104029.

[15] J. Garriga and A. Megevand, *Decay of de Sitter vacua by thermal activation*, Int. J. Theor. Phys. **43** (2004) 883–904.

[16] S. W. Hawking and I. G. Moss, *Supercooled Phase Transitions in the Very Early Universe*, Phys. Lett. B **110** (1982) 35.

[17] G. W. Gibbons and S. W. Hawking, *Cosmological Event Horizons, Thermodynamics, and Particle Creation*, Phys. Rev. D **15** (1977) 2738.

[18] K. Lee and E. J. Weinberg, *Decay of the False Vacuum in Curved Space-time*, Phys. Rev. D **36** (1987) 1088.

[19] S. Coleman and P. Steinhardt, *Gravitational Effects on and of Vacuum Decay*, unpublished.

[20] K. Marvel and N. Turok, *Horizons and Tunneling in the Euclidean False Vacuum*, `arXiv:0712.2719`.

[21] A. Brown, *Hubble, Bubble, Toil and Trouble: Vacuum Decay in the Early Universe*. PhD thesis, Columbia University, 2009.

[22] A. Brown and E. J. Weinberg, *Thermal derivation of the Coleman-De Luccia tunneling prescription*, Phys. Rev. D **76** (2007) 064003.

[23] R. M. Wald, *General Relativity*. The University of Chicago Press, 1984.

[24] S.-H. Tye and D. Wohns, *Resonant Tunneling in Scalar Quantum Field Theory*, `arXiv:0910.1088`.

[25] V. Balasubramanian, B. Czech, K. Larjo, and T. S. Levi, *Vacuum decay in multidimensional field landscapes: thin, thick and intersecting walls*, Phys. Rev. D **84** (2011) 025019.

[26] B. Czech, *A novel channel for vacuum decay*, Phys. Lett. B **713** (2012) 331–334.

[27] G. V. Lavrelashvili, V. A. Rubakov, and P. Tinyakov, *Tunneling Transitions With Gravitation: Breaking Of The Quasiclassical Approximation*, Phys. Lett. B **161** (1985) 280–284.

[28] T. Tanaka and M. Sasaki, *False vacuum decay with gravity: Negative mode problem*, Prog. Theor. Phys. **88** (1992) 503–528.

[29] H. Lee and E. J. Weinberg. publishing soon.

[30] T. Tanaka, *The no-negative mode theorem in false vacuum decay with gravity*, Nucl. Phys. B **556** (1999) 373.

[31] A. Khvedelidze, G. V. Lavrelashvili, and T. Tanaka, *On cosmological perturbations in closed FRW model with scalar field and false vacuum decay*, Phys. Rev. D **62** (2000) 083501.

[32] G. V. Lavrelashvili, *Negative mode problem in false vacuum decay with gravity*, Nucl. Phys. Proc. Suppl. **88** (2000) 75–82.

[33] S. Gratton and N. Turok, *Homogeneous modes of cosmological instantons*, Phys. Rev. D **63** (2001) 123514.

[34] K. Marvel and D. Wesley, *Tunnling with negative tension*, JHEP **0812** (2008) 034.

[35] L. Battarra, G. Lavrelashvili, and J.-L. Lehners, *Negative modes of oscillating instantons*, Phys. Rev. D **86** (2012) 124001.

[36] I.-S. Yang, *Recovering the negative mode for type B Coleman-de Luccia instantons*, Phys. Rev. D **87** (2013) 084026.

[37] P. Peter and J.-P. Uzan, *Primordial Cosmology*. Oxford University Press, 2009.

[38] J. C. Hackworth and E. J. Weinberg, *Oscillating bounce solutions and vacuum tunneling in de Sitter spacetime*, Phys. Rev. D **71** (2005) .